

U.S.

ADA 037244

Final Report
**STUDY OF A SEISMIC
MORTAR LOCATION TECHNIQUE**

FRED J. TANIS
Infrared and Optics Division

MARCH 1976

D B C
MAR 21 1977
C

Naval Regional Procurement Office
Long Beach, California 90801

Contract No. N00123-74-C-0761

**ENVIRONMENTAL
RESEARCH INSTITUTE OF MICHIGAN**
FORMERLY WILLOW RUN LABORATORIES, THE UNIVERSITY OF MICHIGAN
BOX 618 • ANN ARBOR • MICHIGAN 48107

DISTRIBUTION STATEMENT A
Approved for public release
Distribution Unlimited

Reproduced From
Best Available Copy

SECURITY CLASSIFICATION OF THIS PAGE (When Data Entered)

REPORT DOCUMENTATION PAGE		READ INSTRUCTIONS BEFORE COMPLETING FORM	
1. REPORT NUMBER 14/ERINA 196809-6-F	2. GOVT ACCESSION NO.	3. RECIPIENT'S CATALOG NUMBER (9)	4. TYPE OF REPORT & PERIOD COVERED Final Report - 26 November 1973 15 December 1975
4. TITLE (and Subtitle) (6) Study of a Seismic Mortar Location Technique		5. PERFORMING ORG. REPORT NUMBER	6. CONTRACT OR GRANT NUMBER(s) (15) N00123-74-C-0761
7. AUTHOR(s) (10) Fred J. Tanis		10. PROGRAM ELEMENT, PROJECT, TASK AREA & WORK UNIT NUMBERS	
9. PERFORMING ORGANIZATION NAME AND ADDRESS Environmental Research Institute of Michigan Infrared and Optics Division, P.O. Box 618 Ann Arbor, Michigan 48107		11. CONTROLLING OFFICE NAME AND ADDRESS	
11. CONTROLLING OFFICE NAME AND ADDRESS		12. REPORT DATE (11) January 1976	
14. MONITORING AGENCY NAME AND ADDRESS (if different from Controlling Office) Naval Regional Procurement Office Long Beach, California 90801		13. NUMBER OF PAGES (12) 1520	
16. DISTRIBUTION STATEMENT (of this Report)		15. SECURITY CLASS (of this report) Unclassified	
17. DISTRIBUTION STATEMENT (of the abstract entered in Block 20, if different from Report)		15a. DECLASSIFICATION/DOWNGRADING SCHEDULE	
18. SUPPLEMENTARY NOTES Project Monitor was Mr. John Hoffman, Naval Electronics Laboratory Center, San Diego, California 92152			
19. KEY WORDS (Continue on reverse side if necessary and identify by block number) seismics, acoustics, mortar location, location algorithms, Rayleigh waves, system design			
20. ABSTRACT (Continue on reverse side if necessary and identify by block number) A light weight, man packed seismic system has been investigated as a means for hostile mortar location. Developed location algorithms, utilizing seismic signals from both hostile and directed fire, were evaluated against field measurement data which simulated battlefield conditions.			

408 259

DD FORM 1473 1 JAN 73 EDITION OF 1 NOV 65 IS OBSOLETE

UNCLASSIFIED

SECURITY CLASSIFICATION OF THIS PAGE (When Data Entered)

DISTRIBUTION STATEMENT A
Approved for public release
Distribution Unlimited

100

PREFACE

The research reported herein was conducted by the Geophysics Group of the Infrared and Optics Division of the Environmental Research Institute of Michigan.

This work was sponsored by the Naval Regional Procurement Office Long Beach, California under Contract N00123-74-C-0761 and monitored by the Naval Electronic Laboratory Center (NELC). The period of research extended from 26 November 1973 to 15 December 1975. Project monitor on this contract was John G. Hoffman (NELC).

The principal investigator was Fred J. Tanis with important contributions to the technical program made by J. Adams. This research was guided by Mr. R.R. Legault, Director of the Infrared and Optics Division. The Institute report number is 106800-5-F.

ACCESSION - 104

NTIS White Section
D'C Buff Section

UNANNOUNCED

JUSTIFICATION *For 500 file*

BY _____

DISTRIBUTION/AVAILABILITY CODES

Dist. AVAIL. and/or SPECIAL

A



SUMMARY

This contract was directed toward development of a seismic mortar location system. The concept envisions a small, low-cost, man packed computer, and hand-implaced sensors with data telemetry. The system operator acts as a forward observer calling fire on enemy gun positions. The sensor packages would have threshold detection, pass band filtering, A/D conversion, discrimination logic, and data transmission capabilities. Target positioning calculations and signal analysis would be performed in a small computer. Operator input includes sensor and calibration shot coordinates. Output consists of status indicators and enemy gun location estimates which can be transmitted to fire control. This system would also be applied to locate large artillery and other targets with impulsive seismic signatures.

The principal advantages of a seismic system over the sound ranging approach are (1) the use of velocities which are not time dependent allowing adaptive location, (2) terrain features will not mask the seismic signals as with acoustics, and (3) seismic signals allow direct discrimination of multiple events and signal identification through match comparisons. The principal disadvantages of a seismic locator as with all passive systems is a noise limited range. This study found that further effort must be directed towards signal enhancement.

Seismic surface waves constitute the largest signal at the ranges under consideration and were, therefore, used as a basis for developing a location technique.

Two location algorithms were derived to utilize seismic data. The first was similar to hyperbolic location but used a Kalman filter to correct for individual path velocities. The second technique compared signals from enemy recoil with those of directed return fire in a "seismic on seismic" location estimate. Computer simulation of derived location algorithms was found useful to obtain capabilities in terms of error characteristics.

A field measurement program was initiated to provide a data base for further evaluation. Seismic data recordings were made of mortar recoils and explosives at Twenty Nine Palms and Camp Pendleton Marine bases.

The Camp Pendleton data were of a poor quality because of local noise problems and as such did not produce useful results when applied to the location problem. The Twenty Nine Palms experiment on the other hand produced good data. While observations were made at ranges less than 2.0 kilometers, it is felt that seismic recoil signals without enhancement would be useful under quiet conditions to at least 3.0 kilometers. Signal enhancement processing could double the effective range.

Location accuracies produced by windless acoustic data (an ideal condition) were generally better than those from corresponding seismic data. Because of the higher seismic velocities seismic results were more sensitive to timing errors. Significant advances must be made in the methods of observing seismic wave time delays before the advantages of a seismic location system can be realized. Adaptive processing of seismic signals could also reduce noise without any intervention by the operator.

CONTENTS

PREFACE.	iii
SUMMARY.	v
LIST OF FIGURES.	ix
LIST OF TABLES	xi
1. INTRODUCTION.	1
2. SEISMIC MORTAR SIGNATURE CHARACTERISTICS.	3
2.1 Analysis of the Air Wave	4
2.2 Direction Finding with Acoustic Waves	5
2.3 Use of Seismic Surface Waves	5
2.4 Delay Time Analysis	6
2.5 Sensor Requirement	10
2.6 Signature Discrimination Problem	12
2.7 Dispersion of Surface Waves	16
3. DEVELOPMENT OF A LOCATION ALGORITHM	21
3.1 Hyperbolic Location	22
3.2 Method of Relative Time Difference	26
3.3 Simulation of Location Algorithms	29
3.4 Direction Analysis Method for Acoustic Arrivals	41
4. SYSTEM DESIGN CONSIDERATIONS.	47
4.1 Power Consumption	52
5. FIELD MEASUREMENTS PROGRAMS	55
5.1 Field Measurement Program-Twenty Nine Palms Marine Base	56
5.1.2 Instrumentation	56
5.1.3 Data Collection	63
5.1.4 Data Quality	64
5.2 Field Measurement Program-Cam Pendleton, California	64

5.2.1	Data Collection	67
5.2.2	Data Quality	67
6.	DATA ANALYSIS AND RESULTS.	68
6.1	Results of Visual Examination	68
6.2	Travel Time Calculations	69
6.3	Source Direction Determinations	73
6.4	Correlation Analysis	76
6.5	Calculation of Location Estimates	81
6.6	Discussion of Results	89
7.	CONCLUSIONS AND RECOMMENDATIONS.	92
7.1	General Conclusion	92
7.2	Specific Conclusions	92
7.3	General Recommendation	94
7.4	Specific Recommendations	94
	REFERENCES.	95
	APPENDIX A.	97
	APPENDIX B.	115

FIGURES

1.	Comparison of Three Component Seismic Signatures from A TNT Shot at Two Sites Separated by 382.7 m., Fort Sill, Oklahoma, 1971.	7
2.	Comparison of Three Component Seismic Mortar Signatures Separated by 382.7 m., Fort Sill, Oklahoma, 1971.	8
3.	Comparison of Three Component Seismic Mortar Signatures Separated by 382.7 m., Fort Sill, Oklahoma, 1971.	9
4.	Comparison of Three Component Seismic Signatures from INT Shot with a Mortar Recoil, Fort Sill, Oklahoma, 1971.	11
5.	105 mm Shell Impact Recorded at Fort Sill, 11/11/73, Site 4 @ 736.	14
6.	105 mm Shell Impact Recorded at Fort Sill, 11/9/73, Site 4 @ 736.	15
7.	Theoretical Rayleigh and Love Surface Wave Dispersion Curves for Layer/Half-Space Model I	18
8.	Theoretical Rayleigh and Love Surface Wave Dispersion Curves for Layer/Half-Space Model II.	19
9.	Geometric Construction of Seismic Ranging Algorithm	27
10.	Simulation Program for A Hyperbolic Fixing Location Algorithm.	30
11.	Simulation Program for A Seismic Ranging Location Algorithm	31
12.	Convergence of Mean Path Velocity Errors Using Kalman Filter Simulation Program	34
13.	Error in Source Location Estimate After Eight Impact Vs. Average Velocity Error for Various σ_T Values.	36
14.	Histograms From Ranging Location Simulation. Initial Location Error Equals 200 m. A Baseline of Five Sensors was Used	37
15.	Histograms From Ranging Location Simulation. $\sigma_T = 10$ ms, $\sigma_S = 10$ m. Five Sensors	38
16.	Histograms From Ranging Location Simulation. $\sigma_T = 5$ ms, $\sigma_S = 5$ m. Initial Location Estimate Error Equals 500 m.	39

17.	Histograms From Ranging Location Simulation. $\sigma_T = 10$ ms, $\sigma_S = 10$ m.	40
18.	Seismic Mortar Location System	48
19.	Response Curve for Sparton Seismometer	50
20.	Field Measurement Site, Twenty Nine Palms, California.	57
21.	Field Geometry and Sensor Placement at Twenty Nine Palms Marine Base.	58
22.	Digital Recording Instrumentation.	59
23.	Typical Response of Geospace Model HS-10 as Calibrated on ERIM's Shaketable: Damping Factor of Approximately 0.64.	61
24.	Anti-Alias Filter Response. Output Voltage is dB relative to OdB input	62
25.	Field Measurement Site, Camp Pendleton, California	65
26.	Field Geometry and Sensor Plaqement at Camp Pendleton.	66
27.	Selected Vertical Component Passbands for Explosion Event 07, Twenty Nine Palms Site	70
28.	Three Component Seismograms from Twenty Nine Palms Site.	71
29.	Vertical Axis Seismics From Three Explosions Separated by 125 Meters Between Fach Shot	72
30.	Plot of the Time Varying Angular Deflections as Determined by the Computer Algorithm from the Acoustic Signature. Shot 307. Twenty Nine Palms	74
31.	Overlay of Seismic Correlation Functions Showing Changes in Alignment for Selected Sensor Positions. Top Tract EV. 22 with EV. 64. Bottom Trace EV. 22 with EV. 65. Separation of EV. 65 and EV. 64 Approximately 25 Meters.	77
32.	Overlay of Seismic Correlation Functions from Recoil and Explosion Events Recorded at the Same Position. Top Trace EV. 11 (EXPLOSION) with EV. 11, Middle EV. 38 (Recoil) with EV. 11. Bottom EV. 37 (Recoil) with EV. 11	78
33.	Overlay of Seismic Correlation Functions Showing Changes in Alignment for Selected Sensor Positions	79
34.	Overlay of Seismic Correlation Functions Showing Changes in Alignment for Selected Sensor Positions	80

TABLES

1. Simulation Input Parameters	32
2. Source Estimate Errors (m) Associated with Ordered Sequences for Various σ_S and σ_T Impacts Followed by Recoils	35
3. Estimated Component Volume, Weight, and Cost of the Seismic Mortar Location System	54
4. Approximate Angular Deflections (Degrees) as Estimated. From the Muzzle Blast.	75
5. Location Estimates from Seismic and Acoustic Data - Twenty Nine Palms, 1.0 km Site.	82
6. Location Estimate for Twenty Nine Palms Data - 1.5 km Site	83
7. Location Estimated from Seismic and Acoustic Data - Camp Pendleton 108, 108A Sites.	84
8. Comparison of Location Errors With and Without Simulated Sensor Position and Return Fire Errors	85
9. Location Errors Using Correlation Data Which has Been Perturbated, Twenty Nine Palms, 1.5 km Site.	86
10. Location Estimates From Seismic Data With Smoothing - Twenty Nine Palms Site, 1.0 km Site	87
11. Location Estimates From Seismic Data With Smoothing - Twenty Nine Palms Site, 1.5 km Site	88

INTRODUCTION

The problem of enemy mortar location has not been solved for a small forward base of company size. The cost and logistics of using radar for this purpose are, to date, prohibitively expensive. This exploratory work as part of the U.S. Marine Corps HOWLS (Hostile-Weapons-Location-System) program has been directed toward development of a seismic mortar location system. This concept envisions development of a small, low cost, man-packed computer, and hand-implaced sensors with data telemetry capability. The system operator will function as a forward observer calling fire for calibration and on enemy gun positions. Unlike the radar in-flight projectile approach, this program concentrates on the propagation of seismic energy resulting from the impulse of the firing weapon and could provide 360° surveillance cover. The sensor packages which would probably be expendable are envisioned to have threshold detection, passband filtering, A/D conversion, a small amount of digital storage, limited discrimination logic, and data transmission capability. All target positioning calculation and signal analysis will be performed in a small computer. Operator input will include sensor and calibration shot position information. Output will consist of status indicator and enemy position information which can be transmitted to fire control.

One of the principal advantages of the seismic system over the conventional sound ranging system is the use of seismic velocities which are not time dependent. This feature allows the location to take on an adaptive character. With repetition of recoils and impacts more knowledge of media path velocities is obtained with which the position of enemy fire can be progressively estimated. Because a seismometer has some capability as a microphone, acoustic muzzle blast signals can also be utilized, if needed, for location.

Terrain features will not mask the seismic signal from a muzzle blast as they will for acoustics. As return fire is ranged upon the enemy's gun the signatures from friendly impact and enemy recoil will look similar and can be incorporated into a "seismic on seismic" location estimate. Thus we will know convincingly when the enemy fire has been neutralized. The practical use of these techniques in a mortar location algorithm has been investigated.

Discrimination of seismic recoil signals from shell impact signals is necessary when multiple events occur with rapid succession. The seismic mortar recoil signals are repeatable which allows signal identification through successive match comparisons. In addition, directionality of the acoustic wave could possibly discriminate signals from improbable azimuths.

As with all passive systems a seismic mortar locator will be noise limited. If noise conditions are very local then perhaps the problem can be relieved by ignoring one or more sensors. A generally high battlefield noise condition will reduce the effective range.

The approach taken to investigate the feasibility of a seismic mortar location system included the following program steps.

1. Utilizing existing data examine possible mortar generated signals and characteristics which could be exploited in a mortar location scheme with attention to problems of detection, discrimination, and location.
2. Develop a mortar location algorithm which could be used in a light weight man-packed system. Simulate location algorithms and evaluate their expected performance on assumed input errors.
3. Conduct a field measurements program to collect data which can be used to evaluate the algorithms.
4. Process the seismic field data, analyze its characteristics and utilize it as much as possible to obtain locations of mortar fire.

SEISMIC MORTAR SIGNATURE CHARACTERISTICS

A mortar firing generates four signals which will be recorded by the seismometer. These include seismic waves generated by recoil, the air wave from the muzzle blast, the seismic waves from the explosive shell impact, and the air wave from the shell burst.

A shell burst event (an explosion) generates seismic energy which penetrates the surface layers and propagates to the sensor as a compressional wave (P wave) or simply as sound in earth. Also generated, and perhaps, with the greatest amount of energy, are surface waves (Rayleigh wave). From such an event very little seismic shear wave energy is observed. In contrast, mortar recoil will generate shear energies confined to Love modes (surface confined shear waves) and shear body modes which can be polarized in both the horizontal (SH) and vertical (SV). Observed polarization will be partly determined by azimuth to the mortar location.

Seismic signal from mortar recoil has been shown to be highly repeatable. Signals received from explosions, on the other hand, while showing a great deal of correlation, do not show the same degree of repeatability unless they are small explosions and detonated at the same position. It is not the kind of event but rather its degree of similarity which determines repeatability. When explosions or impacts are scattered about due to range and deflection errors they exhibit less correlation. Such tendencies seem reasonable since shells explode at different distances and azimuths from the sensor.

Such a discriminant could be implemented by storing a known recoil signal from enemy mortar along with its auto-correlation function. A second signal would then be compared to the first by ratioing the cross-correlation peaks with the stored auto-correlation function. A constant ratio would indicate a recoil from the same

source. Conversely, a variable ratio would indicate recoil from another source or shell burst.

There is very little visual difference in the nature of the air wave train as recorded from a shell burst or a muzzle blast. In addition, the acoustic spectra of these air waves are much the same. Thus using only the acoustic air waves, it may be difficult if not impossible to directly discriminate a muzzle blast from a shell burst. In this case, one is left to sorting out all the arrivals in a large computer in order to eliminate all false locations. On the other hand, the seismic waves from an explosion and a recoil may differ substantially in terms of signal level on each of the three-component seismometers.

2.1 ANALYSIS OF THE AIR WAVE

The air wave portion of the muzzle blast seismogram will be the largest signal on the trace and could be very useful in determining azimuth to the mortar location. Two modes of seismic signal are possible. First, the sound wave may couple directly into the seismometer housing or immediate ground area as structural borne sound. Second, the sound may couple into the ground continuously as it propagates to the seismometer reinforcing a Rayleigh wave which propagates at the velocity of sound. This wave is often called the air-coupled Rayleigh wave. The recorded signal can be dominated by either one of these air-coupling phenomenon. The prominence of an air-coupled Rayleigh wave will depend on whether such a wave can be supported by the ground media. If the layered structure in the earth will support such a wave in the frequency band of the acoustic air wave then the air-coupled Rayleigh wave will dominate.

The two horizontal seismometers of a three-component package can be used to obtain direction such as one might with a pair of directional microphones, i.e., by the ratio of signal levels or by timing the waves

to separated stations. If the shape of the acoustic wavefront becomes distorted by the presence of foliage, and atmospheric conditions, good azimuth resolution may be impossible. The seismic direct-coupled acoustic wave would indicate a comparable degree of distortion. Thus in the case of wave distortion, using the seismometer as a microphone will not improve azimuth resolution. The air-coupled Rayleigh wave will be less likely distorted because its energy is coupled to the ground over the entire wave path. Azimuthal information from the acoustic wave could be used as (1) an initial rough location estimate, and (2) an event discriminant for unlikely azimuths.

2.2 DIRECTION FINDING WITH ACOUSTIC WAVES

The investigation has been made of using two horizontal seismometers to obtain direction, such as might be done with directional microphones. A general direction can be found from the acoustic waves accompanying a muzzle blast. Further analysis could be performed to refine angle estimates and identify major causes of error. It has not been ascertained, for example, whether ripples in the sound front in the atmosphere appear in the Rayleigh wave front in the earth. If these ripples do not appear in the ground then a major source of acoustic direction finding error will be eliminated [1]. Analyses which have been completed for this study are reported in Section 4.

2.3 USE OF SEISMIC SURFACE WAVES

The seismic surface waves generated by recoils and impacts may be the largest signal on the seismogram outside of the air wave. Body waves will generally attenuate rapidly because of their high frequency character and spherical spreading.

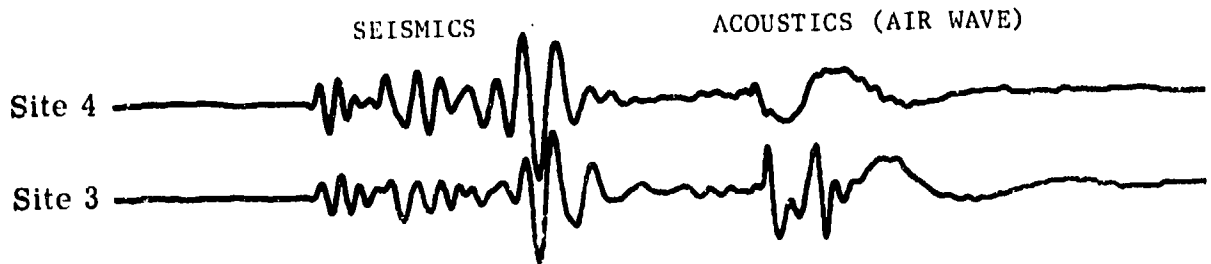
As with the acoustic waves these surface waves may be used to locate enemy fire by observing the arrival time difference (ΔT 's) at

three or more stations. However, accurate hyperbolic fixes will require knowledge of the path velocities. The Rayleigh and Love wave velocities can be expected to change, not only with area of deployment, but also to a lesser extent within the actual deployment area itself. The approximate range and azimuth of all return rounds will be known and the seismic waves generated by these impacts and recoils can be used to more accurately re-estimate the surface velocities. Thus a seismic mortar location system, once deployed, will improve in effectiveness as the position is defended.

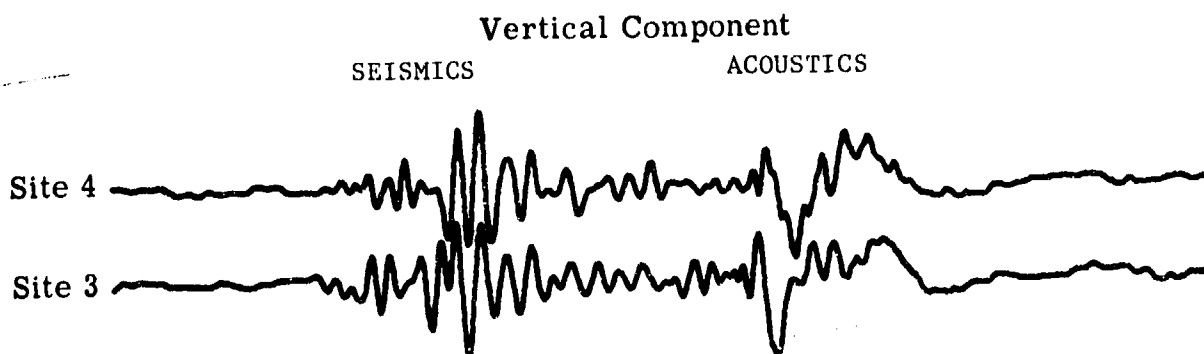
2.4 DELAY TIME ANALYSIS

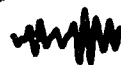
Efforts were made to evaluate some existing seismic mortar data for the use of correlation for ΔT determinations. Analog mortar and explosion data used were recorded at Ft. Sill, Oklahoma under Army contract DAAK02-73-C-0230. Selected records were filtered and digitized. A simple correlation program was written to perform the necessary computations.

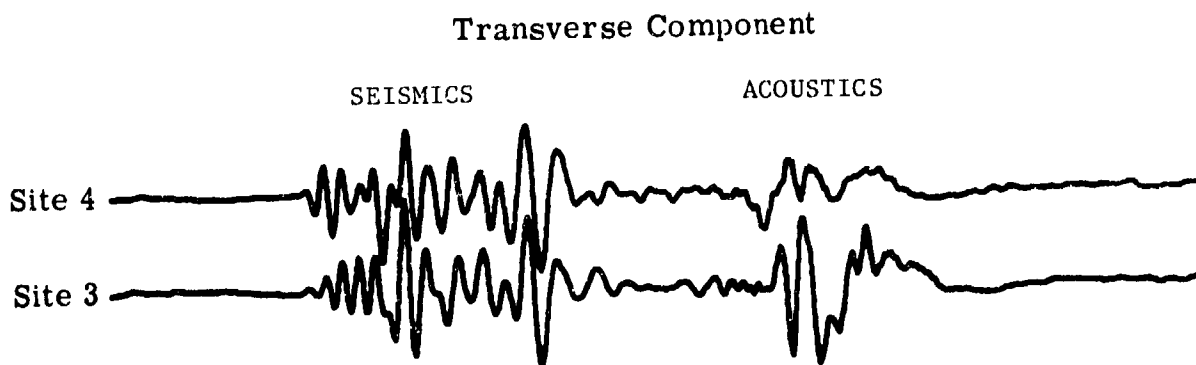
Figure 1 shows a comparison of three-component records of an explosion recorded at two 0.5 km sites which are separated by 382.7 m. The peak of each correlation function was determined so that the lag time from zero time alignment could be determined. This quantity has been labeled peak error and assumes path velocities are identical. In the figure Rayleigh waves which appear on the vertical and radial channels appear to have similar path effects. The Love waves which appear on the transverse channel correlate poorly and produce a large alignment error. Additional records examined at the same site indicated that Rayleigh waves which had travelled along substantially different paths remained well correlated. The results from another site at Ft. Sill were not as encouraging. Figures 2 and 3 show the same type of comparison for a mortar signature. The results were generally unacceptable which may be due to the presence of special



Correlation Function  Peak Error 6ms



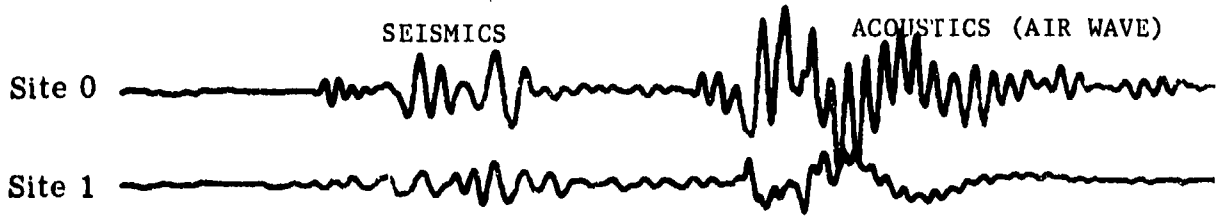
Correlation Function  Peak Error 87ms



Correlation Function  Peak Error 9ms

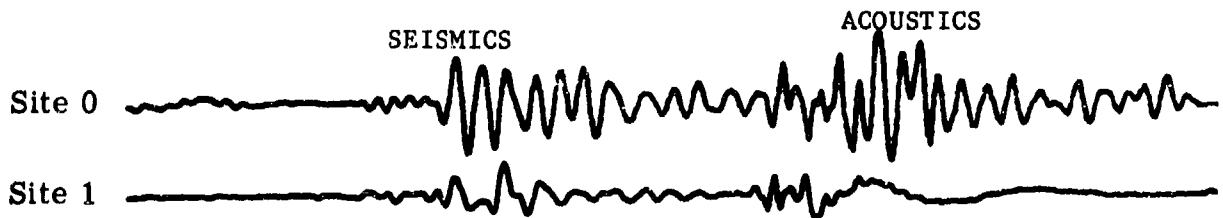
Radial Component

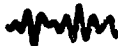
FIGURE 1. COMPARISON OF THREE COMPONENT SEISMIC SIGNATURES FROM A TNT SHOT AT TWO SITES SEPARATED BY 382.7 m., Fort Sill, Oklahoma, 1971



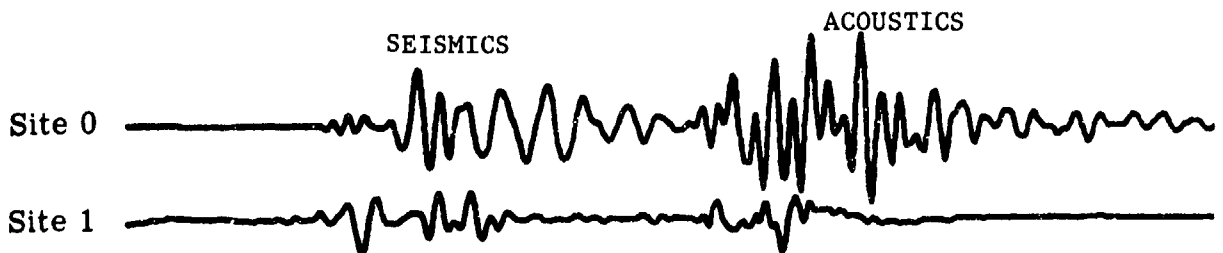
Correlation Function  Peak Error 18ms

Vertical Component



Correlation Function  Peak Error 90ms

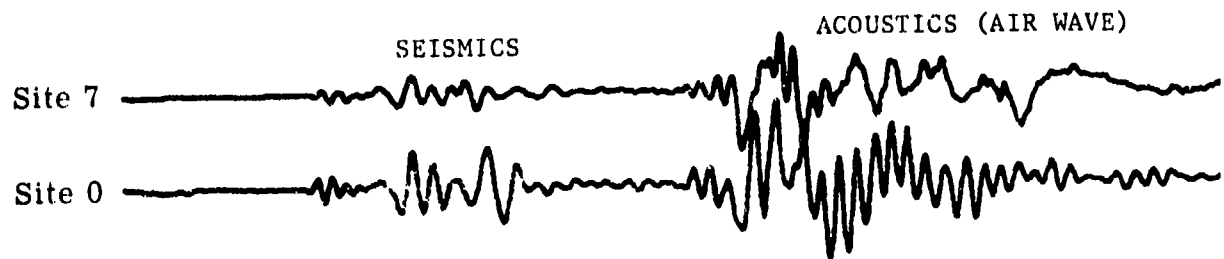
Transverse Component



Correlation Function  Peak Error 97ms

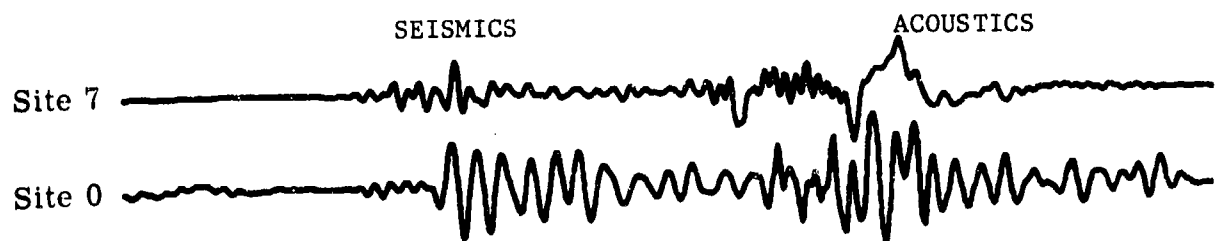
Radial Component

FIGURE 2. COMPARISON OF THREE COMPONENT SEISMIC MORTAR SIGNATURES SEPARATED BY 382.7 m., Fort Sill, Oklahoma, 1971



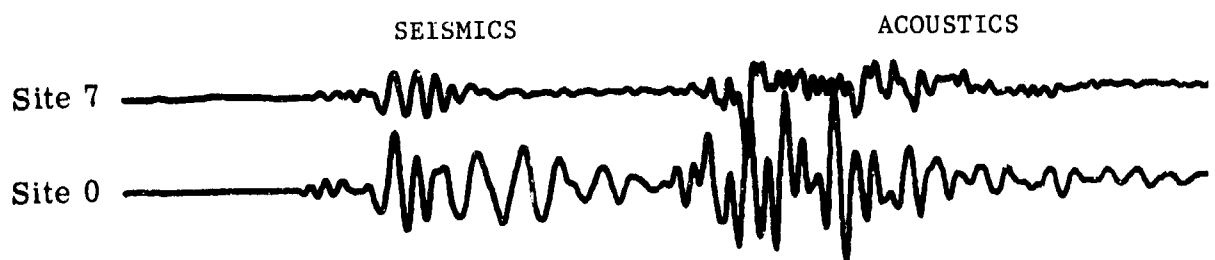
Correlation Function  Peak Error 27ms

Vertical Component



Correlation Function  Peak Error 66ms

Transverse Component



Correlation Function  Peak Error 57ms

Radial Component

FIGURE 3. COMPARISON OF THREE COMPONENT SEISMIC MORTAR SIGNATURES SEPARATED BY 382.7 m., Fort Sill, Oklahoma, 1971

geologic features. Seismic record comparison of a mortar recoil with an explosion detonated at the firing position are shown in Figure 4. Again, excellent correlation alignment was achieved on the vertical and radial channels (due to Rayleigh waves) but remained poorly correlated on transverse channels. In addition, it is evident that the recoil generates much larger Love waves than from the explosion. This large difference may account for the large peak lag error.

2.5 SENSOR REQUIREMENT

In considering deployment of the seismic mortar location system for point defense one may ask how many sensors are required for 360° coverage. If each sensor has a reliable detection range of r_{\max} and it is desired to locate enemy fire from a radius of R around the point defense than the sensor packages would optimally be placed uniformly on a circle of some radius a . Sensors on the opposite side from the enemy mortar will be out of detection range for radii greater than $R_{\max} - a$. Suppose, further, that we require a minimum of k sensors to detect the enemy mortar recoil. Since the k sensors will all lie on a circular arc, the requirement reduces to having the two end positions at maximum range. Of the arc subtends an angle ϕ then $N > 2\pi k/\phi$ sensors are required. The relationship between N and R_{\max} is easily derived as

$$N = \pi(k-1)/\arccos [(R^2 + a^2 - r_{\max}^2)/2Ra]$$

Under this formulation N is very sensitive to r_{\max} . A more useful relation is

$$r_{\max} = \sqrt{(R - a \cos \frac{\pi(k-1)}{N})^2 + a^2 \sin^2 \frac{\pi(k-1)}{N}}$$

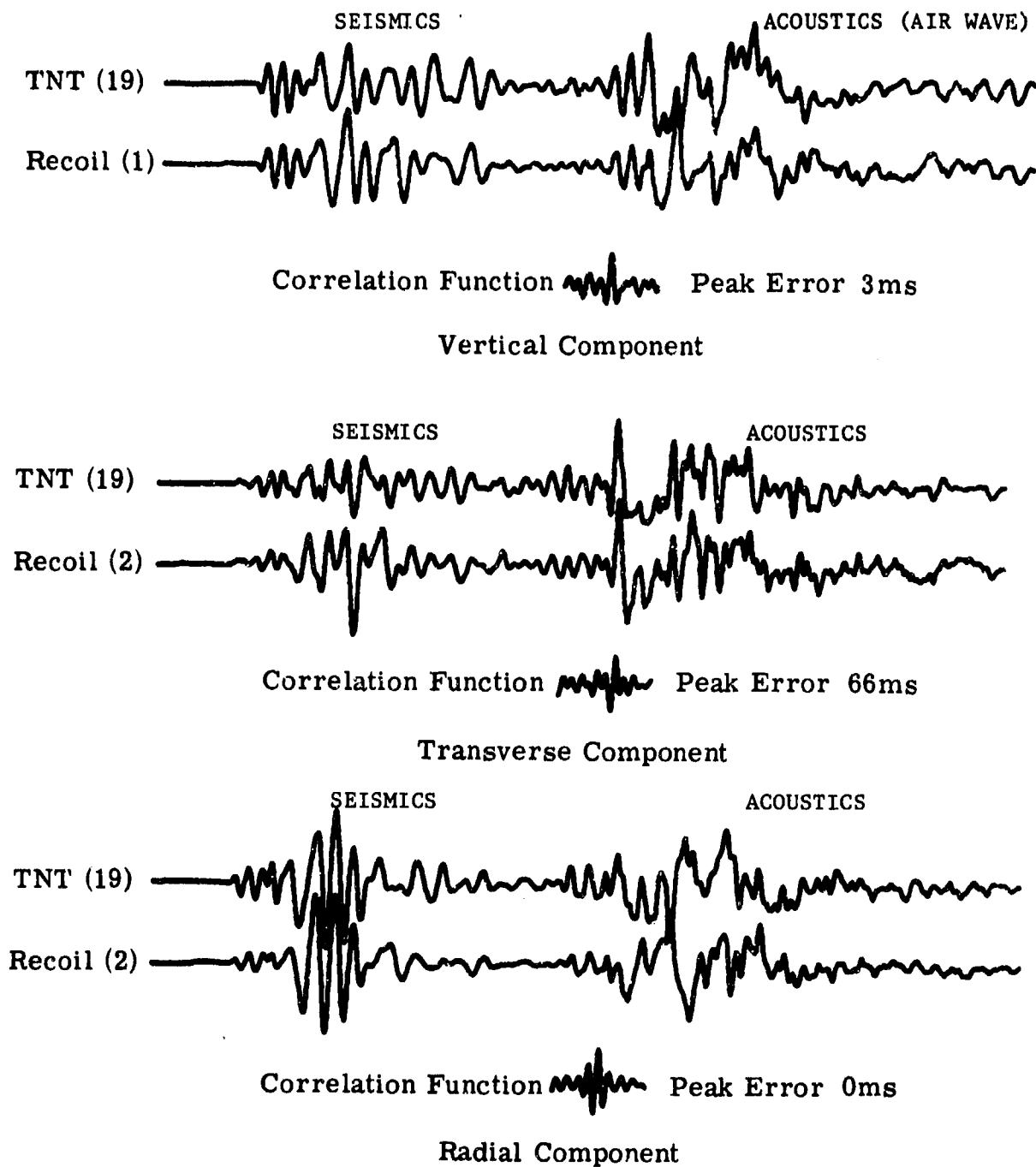


FIGURE 4. COMPARISON OF THREE COMPONENT SEISMIC SIGNATURES FROM TNT SHOT WITH A MORTAR RECOIL. Fort Sill, Oklahoma, 1971

If unlimited numbers of sensors were available then by the above equation

$$r_{\max} = R - a$$

Thus we can examine N such that r_{\max} begins to deviate rapidly from $R-a$. Using a value of 0.5 and 1.0 km, an R value of 3.0 km, and $k = 3$ the point of ten percent departure from $R - a = 2.0$ lies between 8 and 10 sensors. For a k value of 4 these numbers increase to 12 and 15 sensors respectively.

Examination of this circular criterion for sensor placement leads under practical considerations to a conclusion that a minimum of 10 sensors are needed for 360° coverage.

2.6 SIGNATURE DISCRIMINATION PROBLEM

As indicated previously discrimination of seismic recoil signals from impact signals may be crucial to effective operation of a mortar location system. A discrimination capability is especially necessary during periods of rapid exchange of fire. Lack of such capability necessitates a lengthy and, perhaps, complex sorting problem.

Examination of seismic data collected at Ft. Sill during November 1973 and under this project suggest three possible approaches for seismic discrimination of mortar recoil and impact signatures.

Results from this study have suggested three potential discriminants.

1. Seismic signal for mortar recoil has been shown to be highly repeatable. Signals received from explosions, on the other hand, while showing a great deal of correlation, do not show the same degree of repeatability unless they are small explosions and detonated at one position. When explosions or impacts are scattered about due to range and deflection errors they exhibit less correlation.

Such tendencies seem reasonable since shells explode at different distances and azimuths from the sensor. Figures 5 and 6 show a 105 mm shell impact signature as recorded at 0.5 km distance. While some of the surface waves show correlation the general repeatability of the record is much less than in the case of recoil. Thus repeatability of the signal shows promise as a signal discriminant.

2. Explosive sources tend to produce relatively stronger body wave energy than recoil sources. A body wave/surface ratio is then a potential discriminant between these two sources. The discriminant ratio may be enhanced by comparing signals from selected narrow band filters. While this discriminant may work well for close distances where body wave signals from mortar can be observed, there are obvious difficulties at the far distances where they are highly attenuated and difficult to measure.

3. Since surface waves attenuate less rapidly than body waves they can be observed at greater distances. Thus a surface wave discriminant would have more potential use for the mortar location problem. A procedure was developed to look at the sum of squares of the longitudinal and vertical components. Strong phase correlation was observed for surface waves recorded beyond 1 km from explosions at about 25 Hz. For surface waves from mortar recoil phase correlation was observed to vary little from 2 Hz to 50 Hz. The presence or absence of such phase correlation could potentially be used to discriminate recoils from impacts.

It was first thought that recoil seismics produced less energy on the vertical component than explosions. If this were the case, an energy ratio between components could be used as a discriminant. However, when tested this discriminant was found to be unreliable. Of the discriminants considered repeatability appears to be the most practical approach. Such a discriminant could be implemented by storing a known recoil signal from enemy mortar along with its

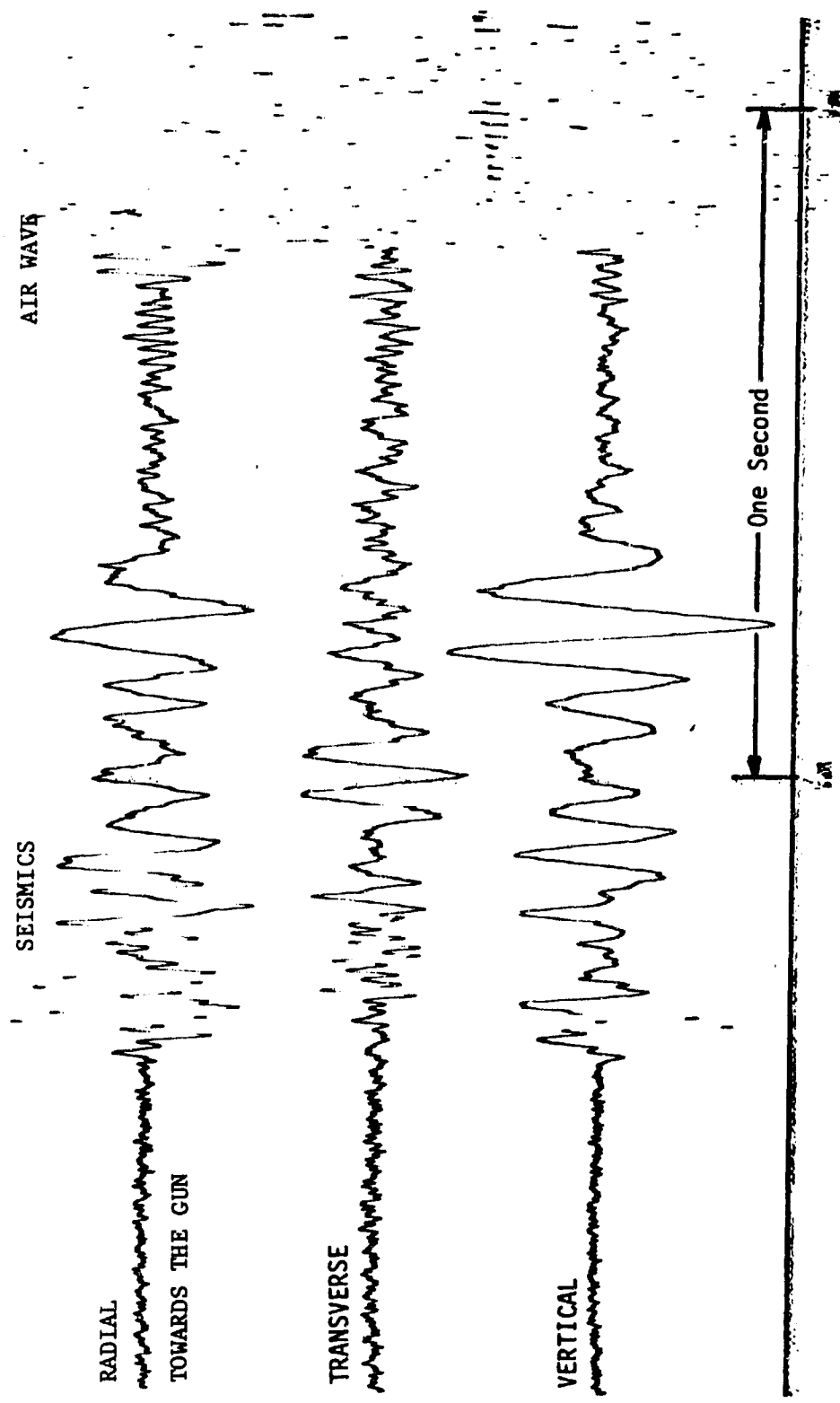


Figure 5. Three Component Seismic Signatures, 105 mm Shell Impact, Recorded at Ft. Sill, 11/11/73, Site 4 @ 736.

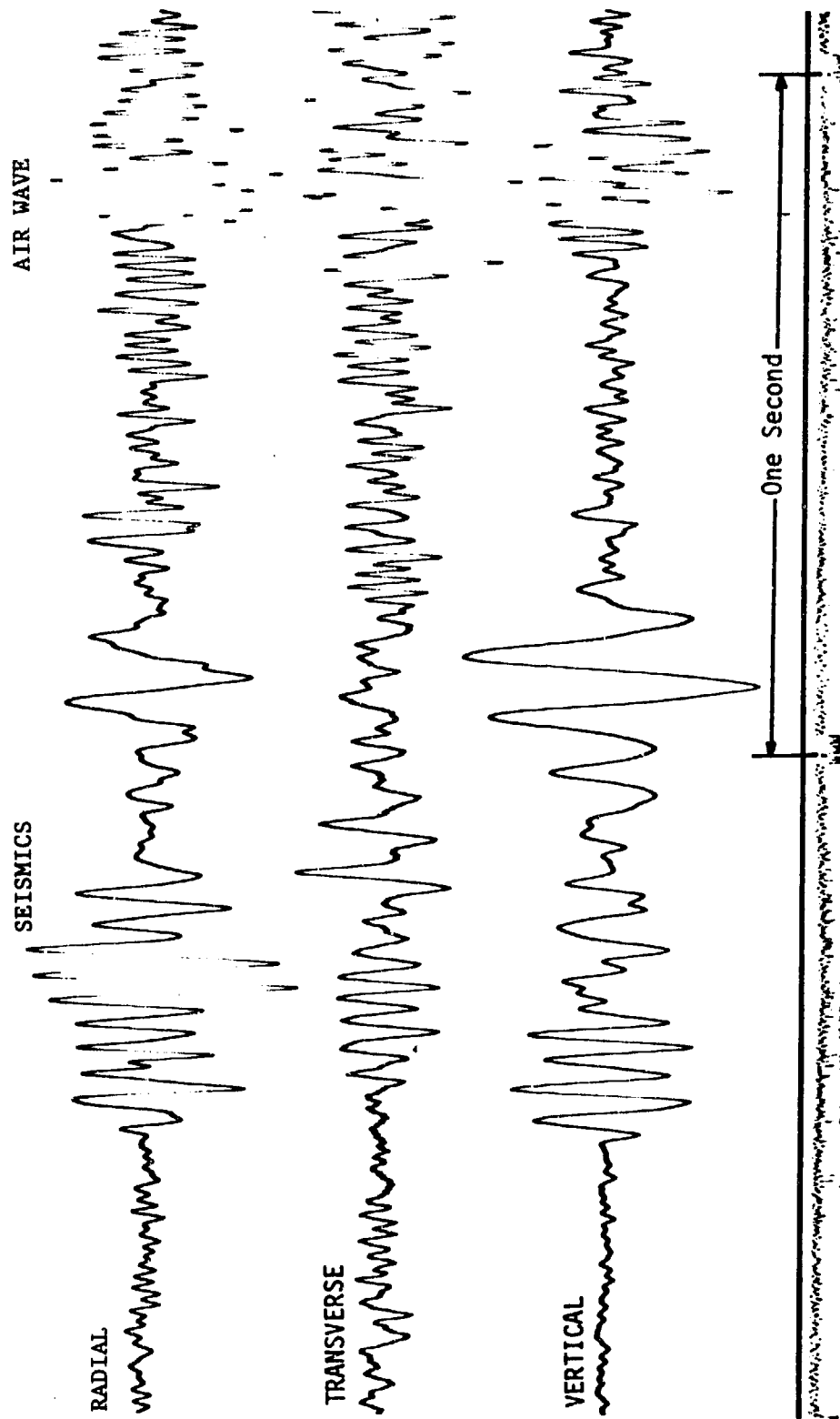


Figure 6. Three Component Seismic Signatures,
105 mm Shell impact, recorded at Ft.
Sill, 11/9/73, Site 4 @ 736.

auto-correlation function. A second signal would then be compared to the first by ratioing the cross-correlation peaks with the stored auto-correlation function. A constant ratio would indicate a recoil from the same source. Conversely, a variable ratio would indicate recoil from another source or shell burst.

2.7 DISPERSION OF SURFACE WAVES

The Rayleigh and Love surface modes generated by mortar recoil and shell impacts will travel at velocities which vary with frequency. If the media is dispersive such velocity differences will be great and the surface wave train will appear spread out. Such phenomena could greatly effect the accuracy of time delay correlations if the path lengths or media characteristics are different. Early in this program model studies using multi-layered dispersion equations were initiated to evaluate the problem of dispersion.

Mortar recoil tends to generate Love surface mode while shell impacts generate predominantly Rayleigh mode. If arrivals from impacts are to be used to correct times for mortar recoil or if they are to be incorporated into a seismic on seismic correction of return fire then such velocities must be similar and in constant ratio over the principal frequency components. Data recorded for the field tests conducted at Ft. Sill, Oklahoma, October 1973 wave has been analyzed for consistency of explosions and recoils. In addition, using a refraction velocity profile obtained from the Ft. Sill, 1971 data theoretical models of surface wave velocity were calculated for various modes.

A series of equations [2], describing the dispersion of surface waves on multi-layered media, were programmed for the digital computer. They relate surface wave phase velocity to frequency. The program input consists of a layered model of shear (β) and compressional (α) wave velocities along with density ratios.

Figures 7 and 8 show the resulting phase velocity curves for both Love and Rayleigh waves. The first four modes have been determined. The curves have roughly the shape of a hyperbola except that the Love modes have as an upper limit to their phase velocities which is the shear velocity in the second layer or half-space. The compressional velocities are based on velocity data obtained at Ft. Sill and shear velocities were obtained from the Handbook [3]. The only difference in Models I and II is that Model II has a layer of twice the thickness of Model I. The effect of thickening the layer is to lower the frequency at which there is a strong upward trend of the phase velocity curve. The upper and lower limits are controlled by the layer and half space shear velocities respectively.

In general, the models indicate that Love modes are close approximations to the Rayleigh modes for high frequencies, i.e., the flat portions of the various curves. The worst approximations occur below frequencies where the mode curves turn upward. This frequency corresponds to a wavelength roughly equal to one-fourth the layer thickness. Thus if the geology has significant layering with thickness three or four times the longest wavelength of interest we can be assured that Love and Rayleigh velocities are nearly the same. For lower frequencies Love and Rayleigh velocities will have an increasing ratio.

The phase velocity curves cannot be applied directly to the available data because shear velocities were unknown. In addition higher frequency waves tend to shift predominant energies to higher modes. Mode identification is not possible with the limited Ft. Sill data.

The use of impact velocities for prediction of recoil surface wave velocities appears to be substantially enhanced if we obtain such velocities from the vertical component. Ft. Sill data shows a very repeatable vertical component from small explosions to recoils

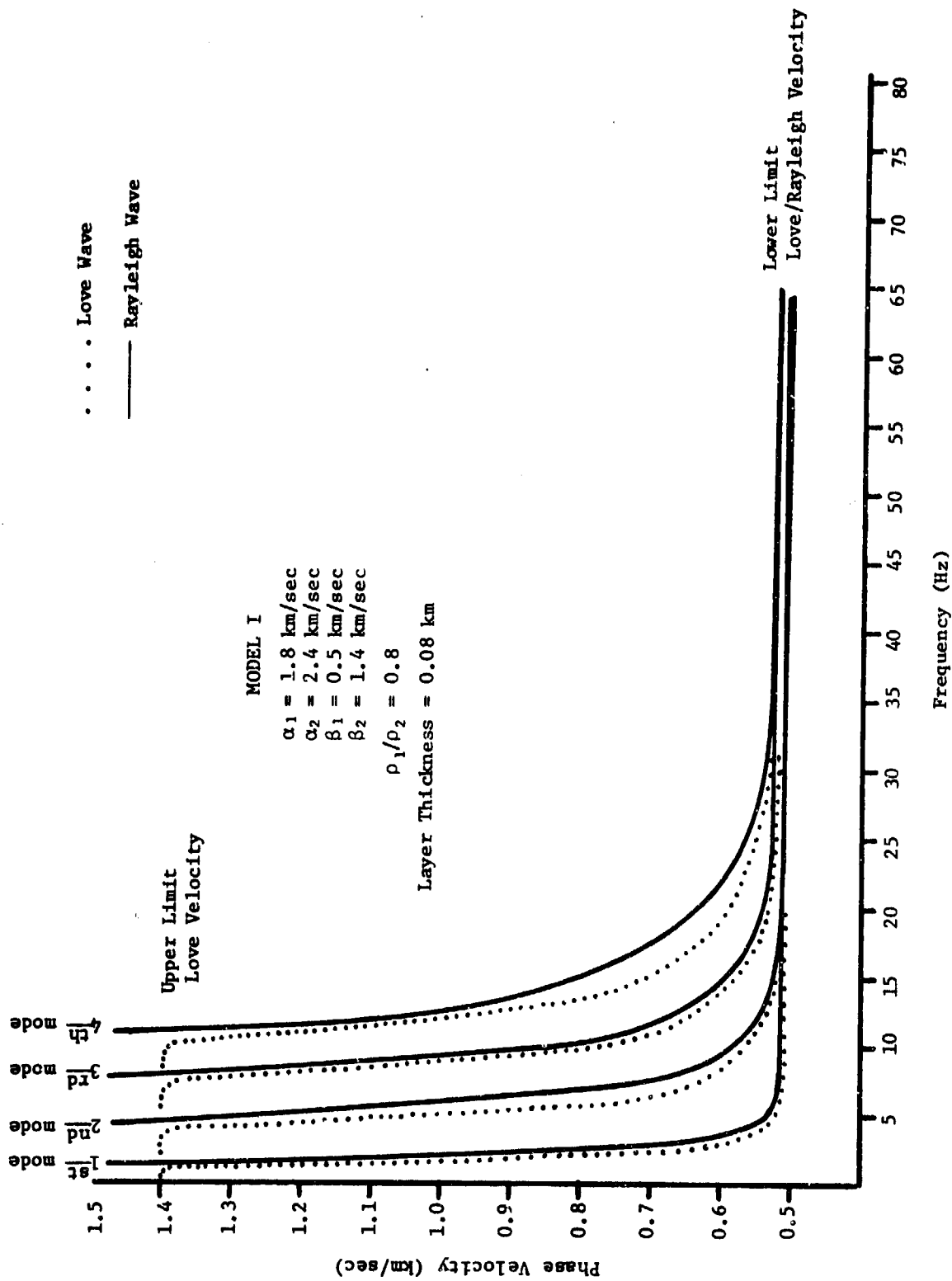


Figure 7. Theoretical Rayleigh and Love Surface Wave Dispersion Curves for Layer/Half-Space Model I.

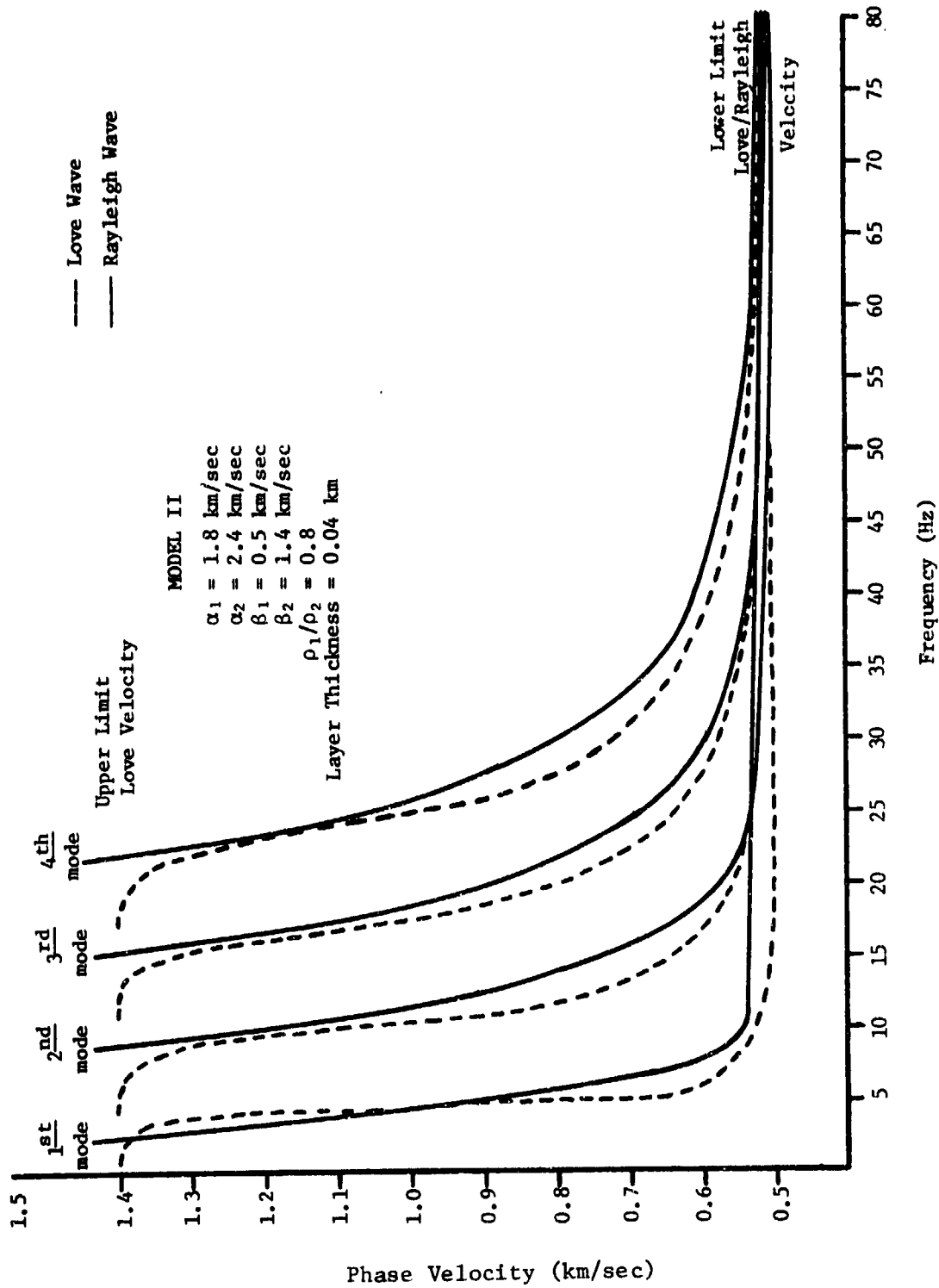


Figure 8. Theoretical Rayleigh and Love Surface Wave Dispersion Curves for Layer/Half-Space Model II.

over the same path (Figure 4). As expected the transverse channels show the greatest dissimilarity between explosions and recoils. The explanation may be that Rayleigh and Love modes are generated in some degree by both sources and that Rayleigh modes show strongest motions on the vertical and longitudinal channels while Love waves exhibit little motion, if any, on the vertical channel.

The model studies which were made indicate that dispersion effects are not significant over the short distance changes to be experienced in impact/recoil analysis. Dispersion effects can, however, be significant when comparing signals which have travelled over great differences in distance. It should be possible to utilize this characteristics for discrimination or cataloging of events which occur over a broad range of distances from the recording sensor package.

DEVELOPMENT OF A LOCATION ALGORITHM

The location algorithm consists of those processing elements and mathematical computing steps needed to obtain a mortar location estimate from sensor time of arrival delays. In this program two computational algorithms for location were developed. Both techniques were based on the observation that mortar recoils and impacts both produce similar seismic signals as measured by a vertical axis seismometer. However, these event types do look appreciably different when observed in the horizontal plane due to the fact that gun recoil generates substantial Love (shear) surface waves and an impact explosion generates only very limited amounts. The vertical axis signals are dominated by Rayleigh surface wave energy. Because these waves have the largest amplitudes they can usually be observed at greater distances from equal noise levels than first arrival compressional waves. The exception to this case would occur if the media were sufficiently dispersive so as to spread out the surface wave train causing a rapid decrease in amplitude.

The first technique described below does not rely specifically on either the surface or the compressional wave portion but rather on any large feature of the seismic wave train found suitable for computing difference in time of arrival to field emplaced sensors. The second technique relies on the similarity of the signals from recoil and explosion and, therefore, more on the surface wave portions of the seismic signature. Both techniques for location require registration or pre-calibration of the area containing the energy mortar. No approach was found which could utilize seismic mortar signature data singly to locate position of enemy fire, i.e., additional signal arrival time information is needed from known source locations near the enemy position in order to provide a means

location. It remains possible that these sources of information could be something other than impacts if locations are known. To obtain location we must either know the individual sensor path velocities to the enemy gun position or we must have observed impulsive signals from a known location in its vicinity.

3.1 HYPERBOLIC LOCATION

The arrival time differences of seismic surface waves to possible pairs of seismometers are measured and locations computed by the conventional method intersecting hyperbolic curves. Assuming a rectangular coordinate system is used the basic equation is given as

$$F_{ij}(x,y) = [(x-x_i)^2 + (y-y_i)^2]^{1/2} - v_i/v_j [(x-x_j)^2 + (y-y_j)^2]^{1/2} - \Delta T_{ij} v_i$$

$$F_{ij}(x,y) = 0$$

where (x,y) are the coordinates of the seismic source (x_i,y_i) , (x_j,y_j) are the coordinates of the two sensors, ΔT_{ij} is the arrival time difference between the two sensors; v_i, v_j are the two source/sensor path velocities. The only difference between this formulation and the conventional one used for sound ranging is the introduction of individual path velocities. Because of spatial variations in surface geology path velocities to individual spaced sensors cannot be expected to be the same. Having estimates of the velocities these equations may be solved simultaneously for a sensor triple.

Path velocity estimates are obtained by timing the waves generated by return fire impacts. These path velocity estimates are then used together with current or previously measured ΔT 's from enemy recoil to

re-estimate the point of enemy fire. Return fire is directed to this new estimate. Improved estimates of path velocities are obtained by using a Kalman filter [4] to provide increasing accuracy to the estimate of enemy fire. In this sense the location algorithm adaptively processes the sequential data. The success of such a processor applied to acoustic arrivals would, of course, be dependent on stability of atmospheric conditions which effect velocity.

To solve these equations $F(x,y)$ we can linearize them by expanding in a Taylor series about a trial point (x_p, y_p) so that

$$F(x,y) = F(x_p, y_p) + \left. \frac{\partial F}{\partial x} \right|_{x_p, y_p} (x-x_p) + \left. \frac{\partial F}{\partial y} \right|_{x_p, y_p} (y-y_p)$$

which is a linear form of $F(x,y)$. Having estimates of the path velocities these equations may be solved simultaneously for a sensor triple.

An alternative method of solution of $F_{ij}(x,y) = 0$ and $F_{jk}(x,y) = 0$ which was found to be superior is obtained by formulating

$$G_{ijk}(x,y) = F_{ij}^2(x,y) + F_{jk}^2(x,y)$$

where $F_{ij}(x,y) = F_{jk}(x,y) = 0$ implies the surface $G(x,y)$ is at a minimum. Finding such a minimum is accomplished by the method of steepest descent. The gradient $\nabla G(x,y)$ is in the direction of maximum change so the process moves by trial from a starting point (x_p, y_p) in the direction given by $-\nabla G(x,y)$. After a few iterations a good approximation of x,y can be found such that

$$F_{ij}(x,y) = F_{jk}(x,y) = 0$$

In formulating the Kalman filter the basic state equation consisted of the path velocities.

$$V_k = V_{k-1} + W_{k-1}$$

where V_k is the state vector of the reciprocal path velocities and W_{k-1} is the state Gaussian noise. Since the path velocities were assumed to be constant from the individual sensors to the locations of enemy fire and impacts from return fire W_{k-1} is taken as zero for all iterations k . In addition to the state equation we have the measurement equation:

$$Z_k = H_k V_k + M_k$$

where Z_k is the measurement vector of observed time difference of arrivals (ΔT 's). H_k is the observation matrix containing sensor impact distances d_{ik} and M_k is the Gaussian measurement noise vector associated with Z_k . Using the basic time difference equation for sensors i and j .

$$\Delta T_{ij} = \frac{d_i}{v_i} - \frac{d_j}{v_j}$$

The matrix H_k is $2p-2$ by p with form:

$$H_k = \begin{pmatrix} d_{1k}, & -d_{2k}, & 0, & 0, & \dots, & 0, & 0 \\ 0, & d_{2k}, & -d_{3k}, & 0, & \dots, & 0, & 0 \\ & & \vdots & & & & \\ 0, & \dots, & 0, & \dots, & 0, & d_{(p-1)k}, & -d_{pk} \\ d'_{1k}, & -d'_2, & 0, & 0, & \dots, & 0, & 0 \\ 0, & d'_{2k}, & -d'_{3k}, & 0, & \dots, & 0, & 0 \\ & & \vdots & & & & \\ 0, & \dots, & 0, & \dots, & 0, & d'_{(p-1)k}, & -d'_{pk} \end{pmatrix}$$

where the d and d' are distances from two separate shots. In

applying a Kalman filter data sets may be treated sequentially or simultaneously with the same resulting estimate of V_k . Our approach took data in pairs of sets to avoid the difficulty arising from the fact that there are $p-1$ ΔT 's and p path velocities.

The recursive estimate \hat{V}_k of the state vector V_k is given as:

$$\hat{V}_k = \hat{V}_{k-1} + K_k (Z_k - H_k \hat{V}_{k-1})$$

where K_k is the Kalman filter matrix and minimizes $E[(\hat{V}_k - V_k)^T (\hat{V}_k - V_k)]$. The filter K_k is obtained from

$$K_k = P_{k-1} H_k^T (H_k P_{k-1} H_k^T + R_k)^{-1}$$

where $P_k = P_{k-1} - K_k H_k P_{k-1}$ and $R_k = \text{covariance of } M_k$.

When a new measurement Z_k is received the algorithm has already calculated P_k and \hat{V}_{k-1} from the previous iteration. We also have H_k by calculation of the sensor/impact distances using the current target location estimate. P_0 can be taken as the identity matrix and V_0 as the initial estimate of the path velocities in order to start the recursive process. We now have all the information needed to obtain a new estimate of the state vector V_k which can then be used with the ΔT 's from enemy recoil to estimate the location coordinates (x_{k+1}, y_{k+1}) .

Thus this algorithm allows one to obtain an updated estimate of the location of enemy fire by obtaining successively improved estimates of the individual seismic path velocities to that point of fire. Since the mortar recoil signatures are highly repeatable observation of successive firing can only help improve the estimates of ΔT but not the path velocities. Improvement in path velocity estimates are obtained by timing the signals from known impact locations.

3.2 METHOD OF RELATIVE TIME DIFFERENCE

A second algorithm was developed based upon relative comparison of impact and recoil signals. The time of arrival of seismics from an impact are the same as a recoil if that impact occurs at the same position as the recoil. Thus the observation of the relative difference in arrival times between an impact and a recoil can be used to locate one event with respect to the other. Furthermore, if we assume that the paths to an impact in the vicinity of a recoil are unchanged outside of path length and the velocity of the seismic waves are constant in the region of impacts and recoil then location of the enemy recoil is possible if the approximate position of the impacts are known. Observation of the difference in arrival times between an impact and a recoil is accomplished by aligning the signals at one sensor and measuring the time difference between the others. A minimum of four sensors are required to obtain an estimated location plus the wave velocity in the vicinity of the known impact and estimated recoil.

The solution is obtained from intersection of perpendiculars constructed with respect to lines passing through each sensor and the point of impact. Figure 9 provides a geometric construction of the solution for four sensors. The relative ΔT 's as calculated above are equal to the actual delays (as if the two events occurred simultaneously) plus a constant. Positions on respective lines are now found by adding in an arbitrary constant k and moving a distance $(\Delta T + k) \cdot V$ from the point of impact. At each position a perpendicular P (or circular arc) is constructed.

The equation of the family of lines (perpendiculars P) parallel to a line which passes through the desired location and which is perpendicular to the sensor impact line is given by

$$Y = M_j x + b_j(k)$$

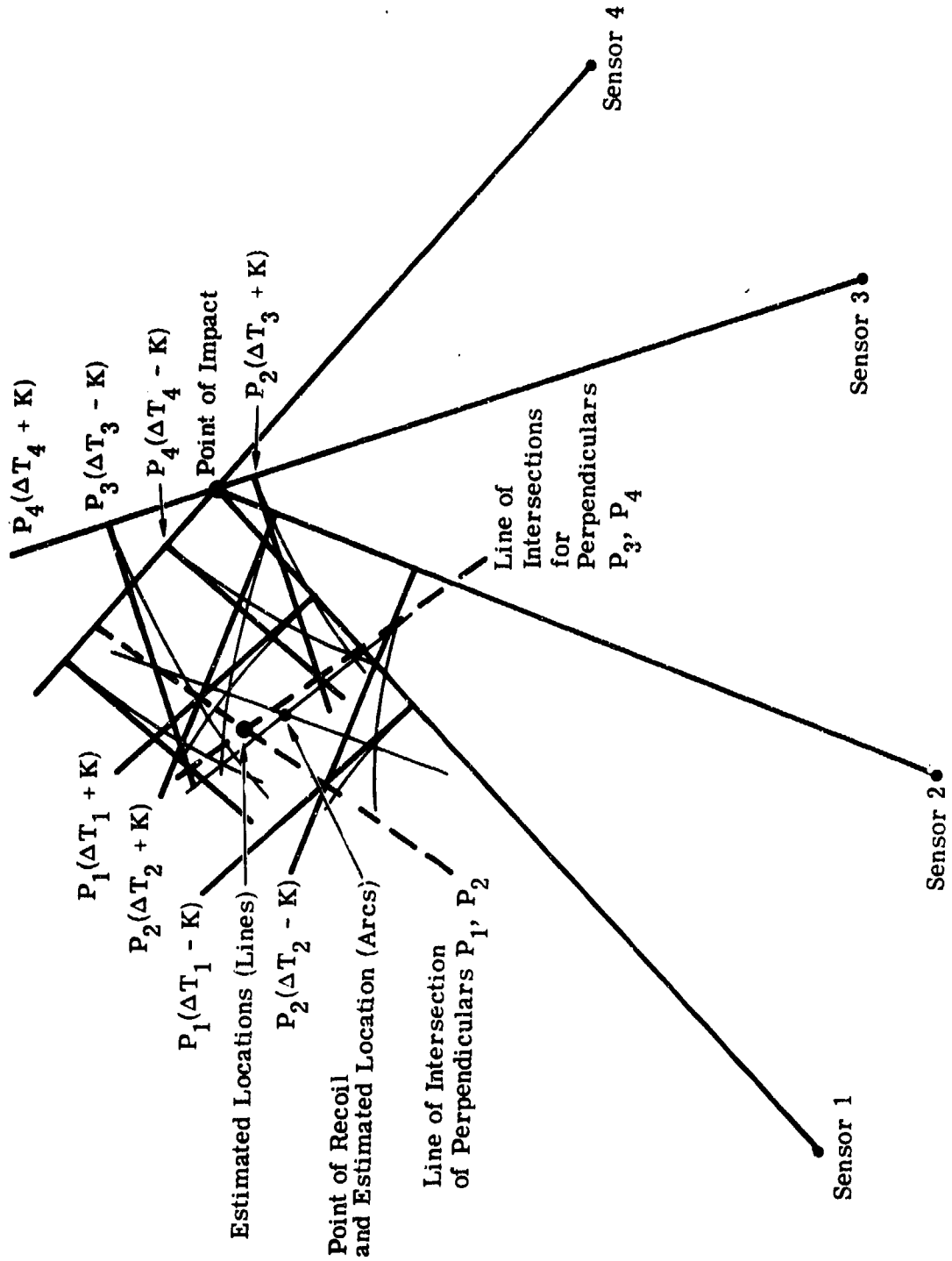


FIGURE 9. GEOMETRIC CONSTRUCTION OF SEISMIC RANGING ALGORITHM

where M_j is the inverse slope of a line between sensor j and the known impact (X_I, Y_I) . The intercept $b_j(k)$ is found as

$$b_j(k) = (Y_I - [\Delta T_j + k] V \sin \theta_j) - M_j(X_I - [\Delta T_j + k] V \cos \theta_j)$$

where $\theta_j = \pi/2 - \text{TAN}^{-1}(M_j)$. The intersection of such perpendiculars as determined from two separate sensors form a line which contains the estimate. The intersection for sensors i and j has coordinates:

$$X^*(k) = (\Delta T_j V \sin \theta_j - \Delta T_i V \sin \theta_i + k V \sin \theta_j$$

$$- k V \sin \theta_j - (M_i - M_j) X_I - M_j \Delta T_j V \cos \theta_j$$

$$+ M_i \Delta T_i V \cos \theta_i - k M_j V \cos \theta_j + k M_i V \cos \theta_i) / (M_j - M_i)$$

$$Y^*(k) = M_j X^*(k) + b_j(k)$$

The line of intersections is given parametrically as $X^*(k)$, $Y^*(k)$. A second line of intersections generated by a second set of two sensors can be solved simultaneously with the first to produce an estimate of location.

If arcs are generated from respective sensor positions instead of perpendiculars a more accurate estimate can be obtained. This estimate assumes, however, a uniform known velocity throughout, as was the example case of Figure 9. In later simulations of the method of arcs certain instabilities resulted which did not occur when using perpendiculars. For this reason the method of arcs was discarded in favor of the method of perpendiculars in conducting the simulations.

While there are similarities between this approach and registration as used for acoustic sound ranging there are important differences. First, the path velocities effects are limited to a region near the impacts and recoils. Secondly, the velocities are constant in time and do not affect the solution by an great degree.

3.3 SIMULATION OF LOCATION ALGORITHMS

The computational algorithms could not be evaluated in forms of seismic field data recording which existing prior to this study program. Simulation was chosen as a means of investigating the location capabilities of these algorithms.

Several sources of error are present in computation of location estimates.

1. Sensor location error
2. Measurement error for ΔT
3. Dispersion and aiming error for return fire
4. Errors in the estimates of surface wave velocities.

By using simulation techniques the effect of each of the errors can be examined and the overall performance of the procedures evaluated.

Flow diagrams for each simulation program are provided in Figures 10 and 11. Input data requirements in each case include a rough first location estimate based on the first observed enemy recoil. In actual practice a first estimate could be provided by prior calibration of the area or use of air wave directionality.

Error sigmas needed for simulation were essentially unknown and should be considered carefully when examining the results. Within each simulation program the error sigma were used to generate random values for each parameter. Representative input values for the simulation programs are shown in Table 1. Values of the measurement errors were specified at 100 m path separation distance. For paths

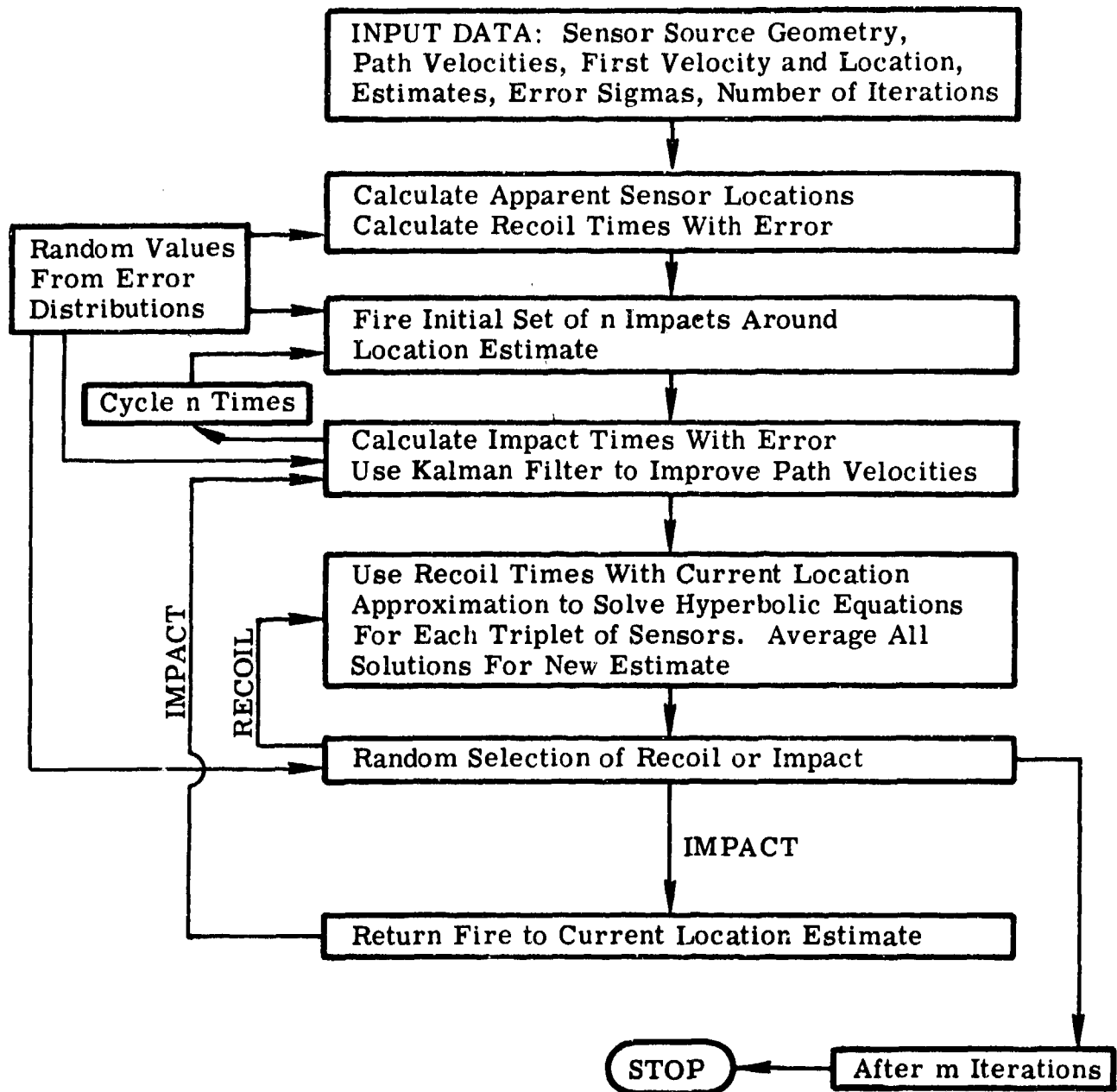


FIGURE 10. SIMULATION PROGRAM FOR A HYPERBOLIC FIXING LOCATION ALGORITHM

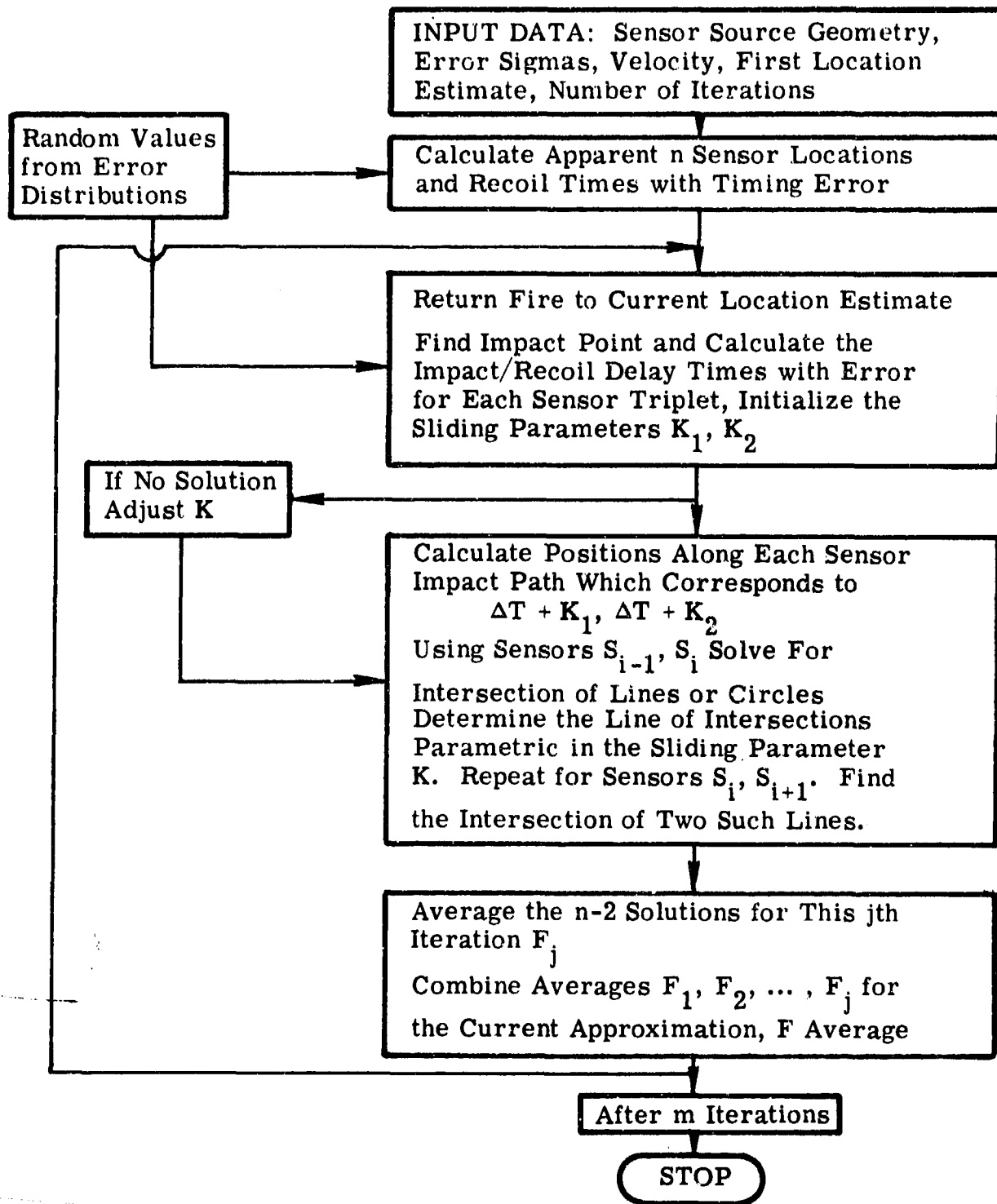


FIGURE 11. SIMULATION PROGRAM FOR A SEISMIC RANGING LOCATION ALGORITHM

TABLE 1
SIMULATION INPUT PARAMETERS

<u>Parameter</u>	<u>Values</u>	<u>Comments</u>
Range error σ_R	22.7m	81 mm mortar return fire. Round dispersion errors.
Deflection error σ_D	7.2 m	Approximates short range artillery.
Measurement error σ_T	5-40 ms	Delay timing errors at 100 m.
Sensor Position error σ_S	5-20 m	Same error in both x and y directions.
Initial Source Location error	100-1000 m	Separation distance between the true location and first estimate.
Path Velocities	400-1200 m/sec	For seismic surface waves.

of greater separation the σ_T was taken to be proportionately larger, i.e., $\sigma_T(200 \text{ m}) = 2\sigma_T(100 \text{ m})$. The actual relationship between σ_T and separation is unknown. Fortran computer programs for each simulation algorithm are listed in Appendix A. These programs were built up on an IBM 370 system.

The effect of using a Kalman filter is demonstrated in Figure 12. Here convergence of mean path velocity errors are shown as a function of the number of impacts. The bars indicate the range of path velocity errors. Beginning with a large mean path velocity error 100 m/sec (mean path velocity = 600 m/sec) and a rather large measurement error sigma of 20 ms. Eight to 10 rounds appear sufficient for adequate convergence. The overshoot which appeared at 4 rounds is a characteristic of the Kalman filter.

Typical results from simulation of the hyperbolic algorithm for various values of σ_S and σ_T are given in Table 2. The relationship between the location estimate error and the average velocity error was investigated for eight successive impacts and various values of σ_T . With increasing scatter the points plotted in Figure 13 show that the location error increases directly with the average velocity sensor after eight impacts. The initial average path velocity error was for each trial in excess of 100 m/sec.

The input sensor geometry consisted of five to seven sensors on a line spaced from 100 to 1000 meters. The spacing used in a majority of cases was 500 meters. The position of enemy recoil was located 1500 to 2500 m from the center of the baseline.

Results from simulating the seismic ranging algorithm have been plotted as histograms in Figures 14 through 17. Each histogram describes the number of impacts which resulted in a location estimate with less than 50 m error. The abscissa shows the sequential round number with percent convergence after three shots. Each histogram represents 200 independent trials. Individual histograms are shown

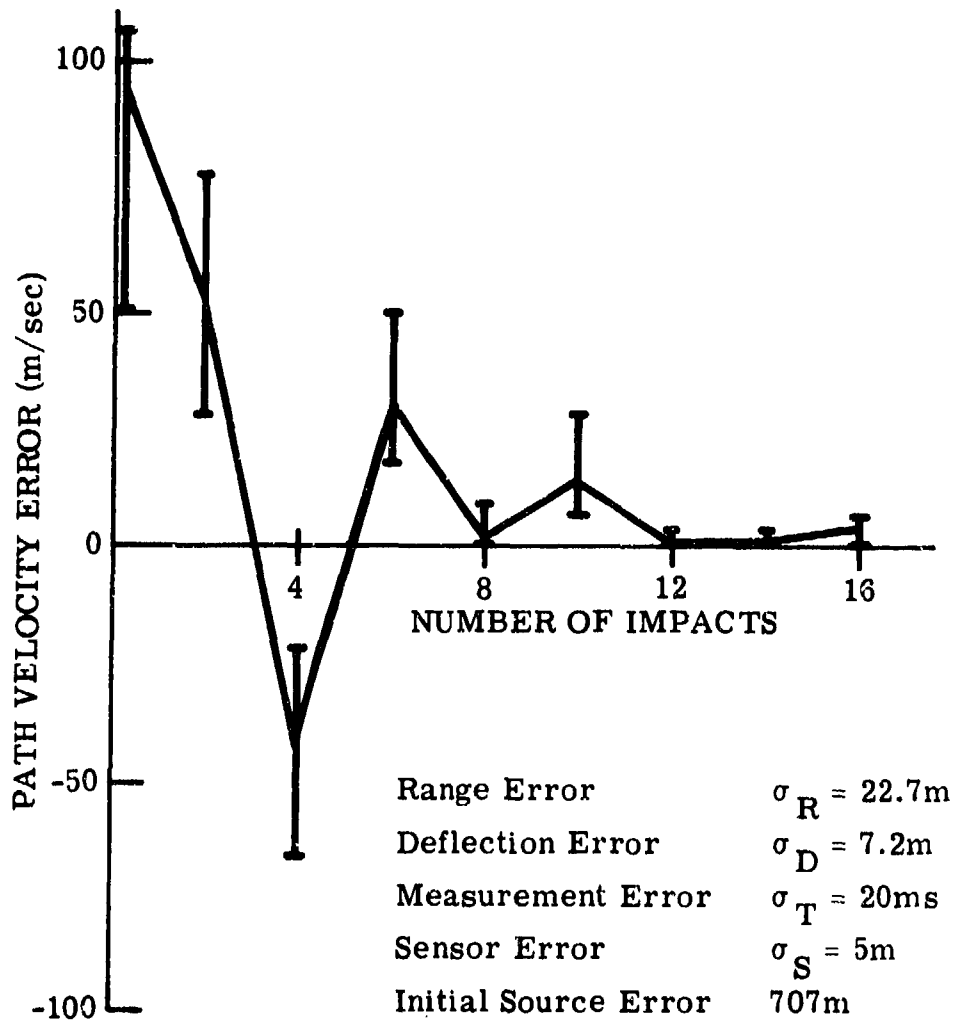


FIGURE 12. CONVERGENCE OF MEAN PATH VELOCITY ERRORS
 USING KALMAN FILTER SIMULATION PROGRAM

TABLE 2
 SOURCE ESTIMATE ERRORS (m) ASSOCIATED WITH ORDERED SEQUENCES FOR VARIOUS σ_S AND σ_T IMPACTS FOLLOWED BY RECOILS. Mean initial path velocity error of 10m

Number of Impacts	2				4				6			
	1	2	3	4	1	2	3	4	1	2	3	4
Sequential Recoils	1	2	3	4	1	2	3	4	1	2	3	4
$\sigma_T = 10\text{ms}$ $\sigma_S = 10\text{m}$	85	84	71	64	71	57	46	38	77	36	12	12
$\sigma_T = 10\text{ms}$ $\sigma_S = 20\text{m}$	148	145	145	145	103	102	89	99	18	50	53	52
$\sigma_T = 10\text{ms}$ $\sigma_S = 5\text{m}$	47	39	32	31	13	10	20	25	44	40	39	39
$\sigma_T = 20\text{ms}$ $\sigma_S = 5\text{m}$	24	39	38	38	14	18	15	6	117	15	37	13
$\sigma_T = 30\text{ms}$ $\sigma_S = 5\text{m}$	192	282	88	205	113	110	119	125	172	171	143	154
	146	134	131	126								

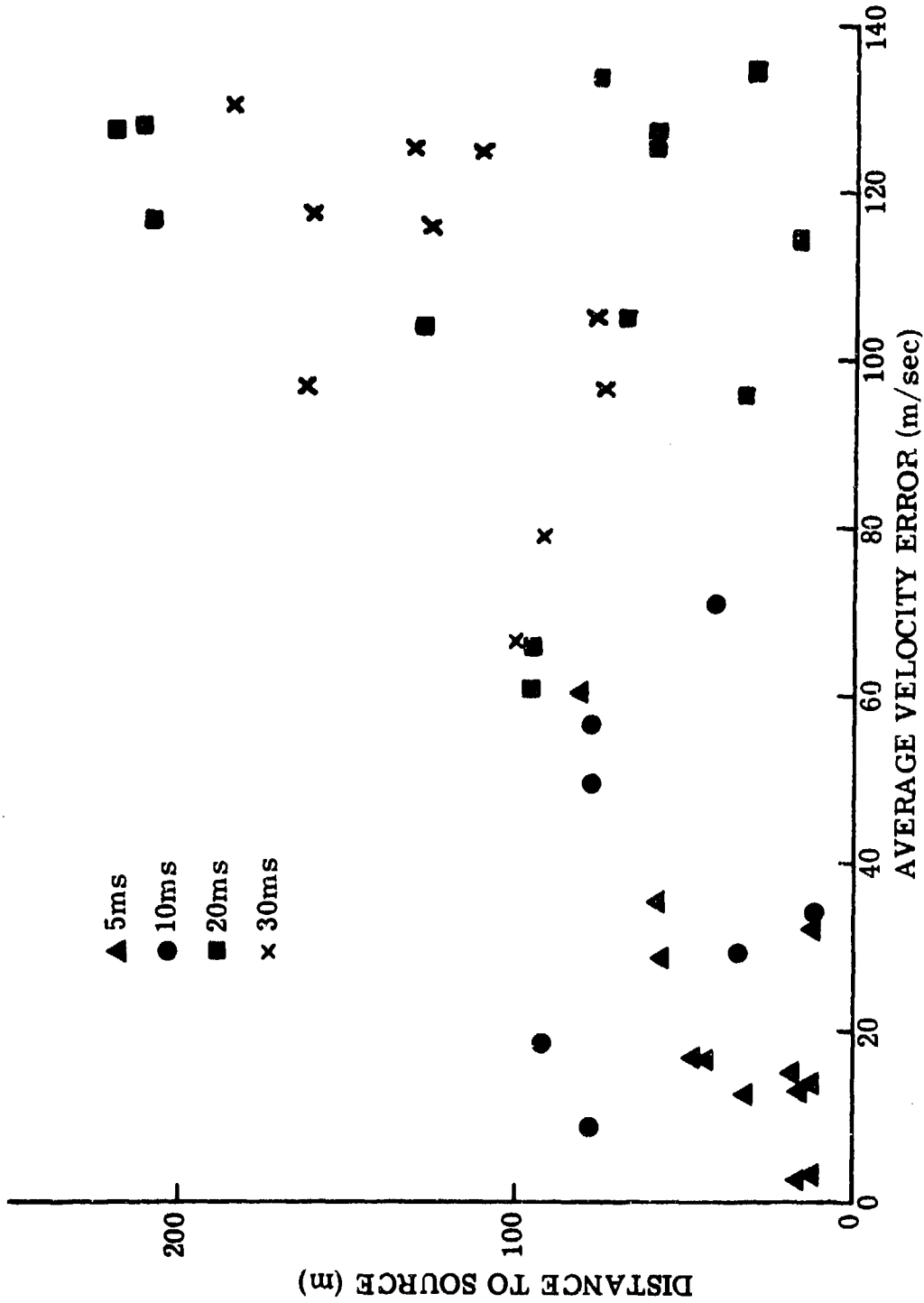


FIGURE 13. ERROR IN SOURCE LOCATION ESTIMATE AFTER EIGHT IMPACT VS. AVERAGE VELOCITY ERROR FOR VARIOUS σ_T VALUES

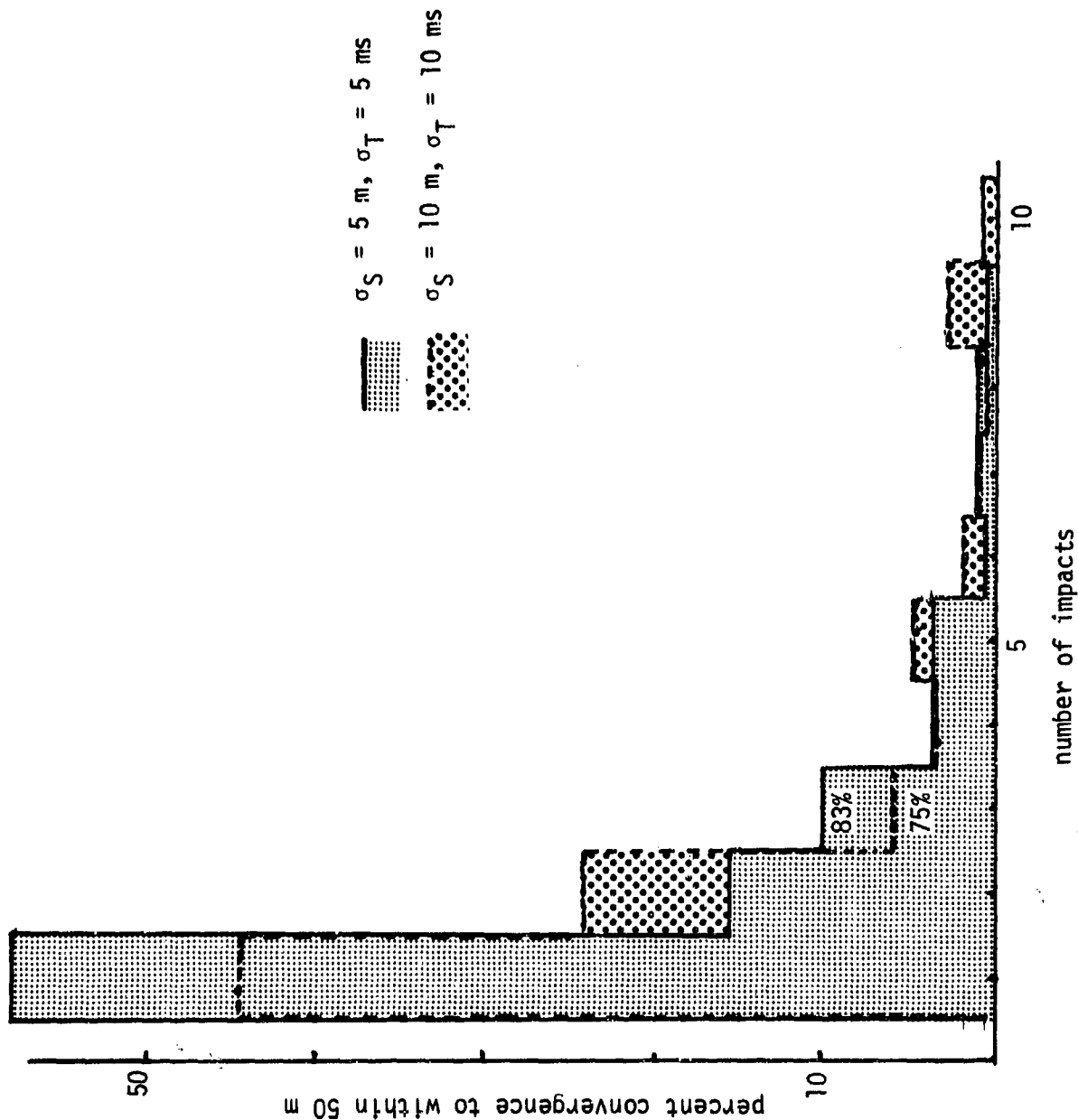


FIGURE 14. HISTOGRAMS FROM RANGING LOCATION SIMULATION. INITIAL LOCATION ERROR EQUALS 200 m. A BASELINE OF FIVE SENSORS WAS USED.

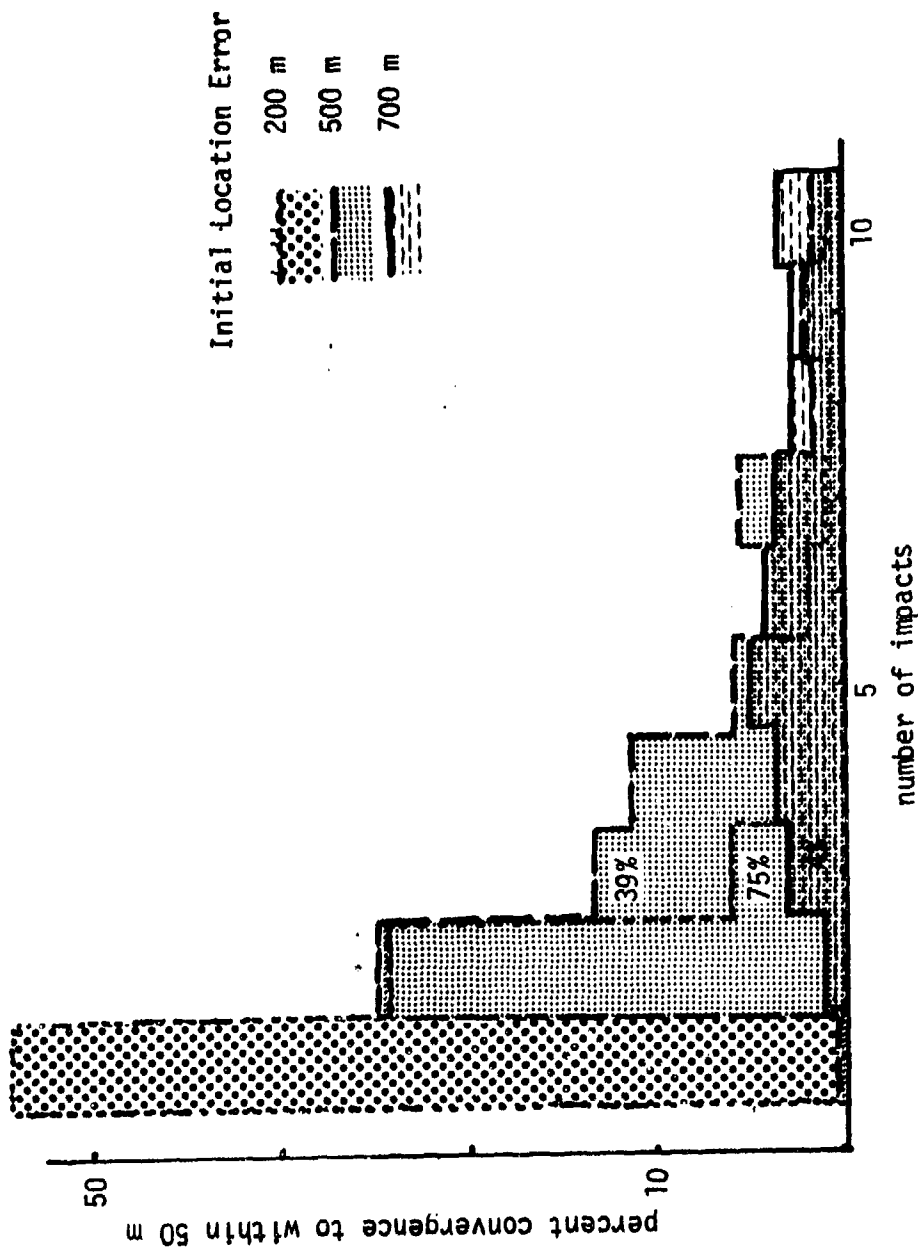


FIGURE 15. HISTOGRAMS FROM RANGING LOCATION SIMULATION. $\sigma_T = 10$ ms, $\sigma_S = 10$ m. FIVE SENSORS.

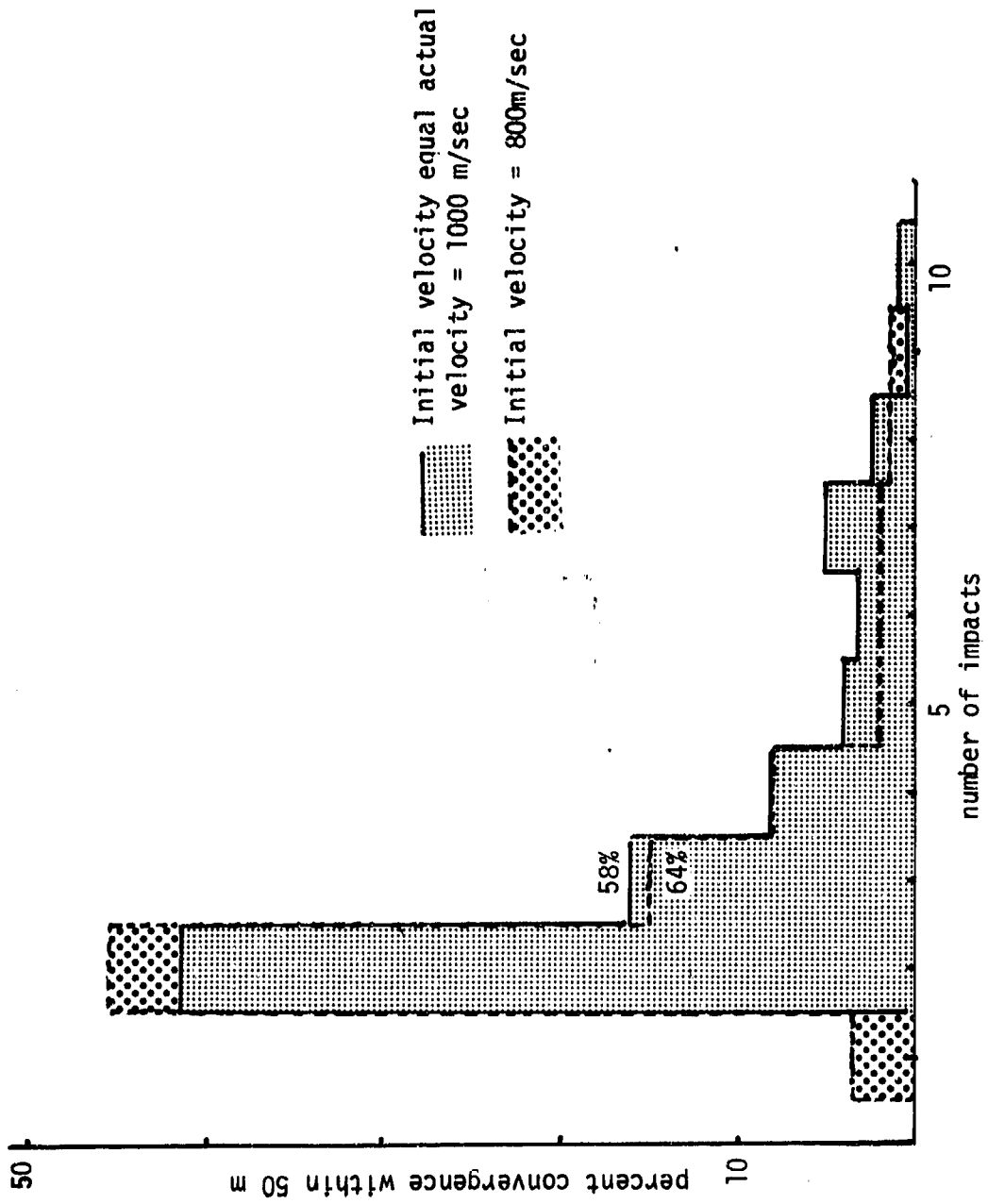


FIGURE 16. HISTOGRAMS FROM RANGING LOCATION SIMULATION. $\sigma_T = 5$ ms, $\sigma_S = 5$ m. INITIAL LOCATION ESTIMATE ERROR EQUALS 500 m.

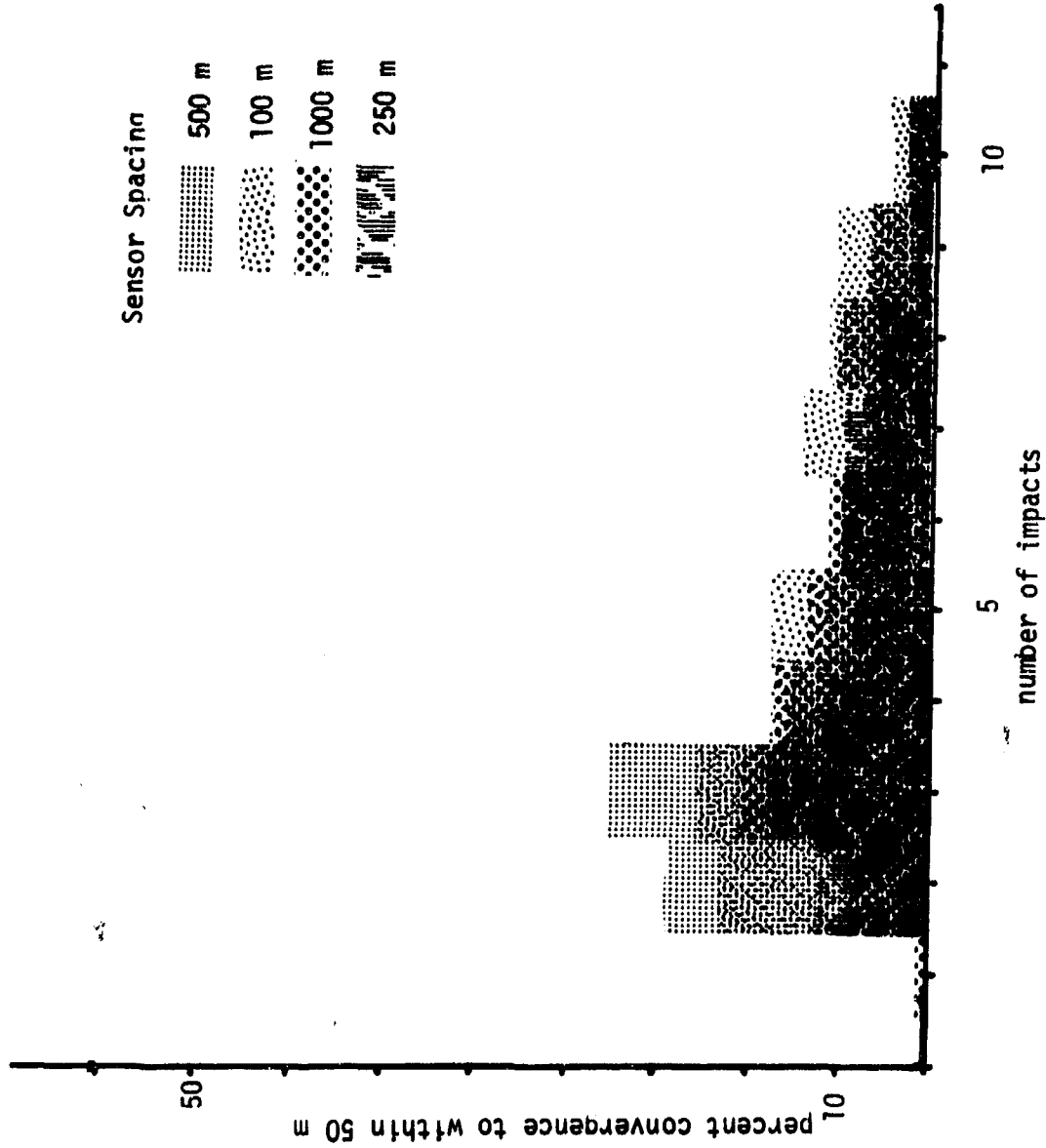


FIGURE 17. HISTOGRAMS FROM RANGING LOCATION SIMULATION. $\sigma_T = 10$ ms, $\sigma_S = 10$ m.

with respective error assumptions. In Figure 14 histograms resulting from the simulations show effect of increasing error sigmas for sensor location and time measurement. The effect of increasing initial location error can be seen by comparison of the three histograms in Figure 15. Figure 16 indicates that the initial velocity error has little effect on the algorithms location capability. Finally, the effect of sensor spacing is indicated in Figure 17.

It appears from these simulation results that the error in initial location is most sensitive to the ultimate ability to compute good locations. Sensor spacing and initial velocity estimates do not greatly influence the final result. The effects of measurement and sensor location errors are on the same order and increasing errors progressively degrade the result. In order to achieve acceptable results from the location programs it appears that measurement sigmas should not exceed 10 ms and sensor location sigmas should not exceed 10 or 20 meters.

These results are from simulation and as such cannot provide good evaluation without sufficient field data. For this reason the study embarked on a field-measurements program in order to provide a more complete basis for evaluation.

3.4 DIRECTION ANALYSIS METHOD FOR ACOUSTIC ARRIVALS

Both of the techniques developed require a first estimate of location to start the process. This first estimate does not have to be highly accurate but should be within a few hundred meters of the target. One possible method which could be used to obtain this type of information is to examine the directionality of the seismic and acoustic signals from enemy mortar recoil and muzzle blast. Utilizing direction (azimuth) information from multiple three component seismometer packages a rough location can be calculated. The acoustic signals potentially have greater possibilities for source direction

determinations because their signals are much larger. The following approach based on signal energy was developed for signal direction determinations.

The direction of a wavefront normal is the direction of maximum energy flow in the horizontal plane. This direction can be found for a bundle of energy in the following way. Let $L_i = L(t_i)$ and $T_i = T(t_i)$ to be digitized signals received on the longitudinal and transverse seismometers, respectively, at time t_i . The bundle of energy passing during the time from t_i to t_j will be proportional to

$$E_L = \sum_{k=i}^j L_k^2 \quad \text{on the longitudinal component,}$$

$$E_T = \sum_{k=i}^j T_k^2 \quad \text{on the transverse component, and}$$

$$E = E_L + E_T \quad \text{total.}$$

If the seismometers were planted at an angle θ counter-clockwise to the way they were planted above, the signals would be

$$\begin{pmatrix} T_i(\theta) \\ L_i(\theta) \end{pmatrix} = \begin{pmatrix} \cos \theta & \sin \theta \\ -\sin \theta & \cos \theta \end{pmatrix} \begin{pmatrix} T_i \\ L_i \end{pmatrix}$$

and the energy equations would be

$$E_L(\theta) = \sum_{k=1}^j [L_k(\theta)]^2 ,$$

$$E_T(\theta) = \sum_{k=1}^j [T_k(\theta)]^2 \text{ and}$$

$$E(\theta) = E_L(\theta) + E_T(\theta) .$$

The direction of maximum energy flow will be the angle θ from the longitudinal component for which $E_T(\theta)/E_L(\theta)$ is a minimum. In other words, we rotate the seismometers until the ratio of transverse to longitudinal energies is a minimum. Then the rotated longitudinal component will be parallel to the Rayleigh wavefront normal.

A closed form of the angle θ for which $E_T(\theta)/E_L(\theta)$ is minimal can be derived as follows. We first note that $E(\theta) = E$, i.e., the total energy in the horizontal plane is not dependent on the way the seismometer is planted:

$$\begin{aligned} E(\theta) &= E_T(\theta) + E_L(\theta) \\ &= \sum_{k=1}^j [T_k(\theta)]^2 + \sum_{k=1}^j [L_k(\theta)]^2 \\ &= \sum_{k=1}^j \{ [T_k(\theta)]^2 + [L_k(\theta)]^2 \} \\ &= \sum_{k=1}^j \begin{pmatrix} T_k(\theta) \\ L_k(\theta) \end{pmatrix}^t \begin{pmatrix} T_k(\theta) \\ L_k(\theta) \end{pmatrix} , \text{ t for transpose} \\ &= \sum_{k=1}^j \left[\begin{pmatrix} \sin \theta & \cos \theta \\ -\cos \theta & \sin \theta \end{pmatrix} \begin{pmatrix} T_k \\ L_k \end{pmatrix} \right]^t \left[\begin{pmatrix} \sin \theta & \cos \theta \\ -\cos \theta & \sin \theta \end{pmatrix} \begin{pmatrix} T_k \\ L_k \end{pmatrix} \right] \end{aligned}$$

$$\begin{aligned}
 &= \sum_{k=1}^j \begin{pmatrix} T_k \\ L_k \end{pmatrix}^t \begin{pmatrix} \sin \theta & \cos \theta \\ -\cos \theta & \sin \theta \end{pmatrix}^t \begin{pmatrix} \sin \theta & \cos \theta \\ -\cos \theta & \sin \theta \end{pmatrix} \begin{pmatrix} T_k \\ L_k \end{pmatrix} \\
 &= \sum_{k=1}^j \begin{pmatrix} T_k \\ L_k \end{pmatrix}^t \begin{pmatrix} 1 & 0 \\ 0 & 1 \end{pmatrix} \begin{pmatrix} T_k \\ L_k \end{pmatrix} \\
 &= \sum_{k=1}^j \begin{pmatrix} T_k \\ L_k \end{pmatrix}^t \begin{pmatrix} T_k \\ L_k \end{pmatrix} \\
 &= \sum_{k=1}^j (T_k^2 + L_k^2) \\
 &= \sum_{k=1}^j T_k^2 + \sum_{k=1}^j L_k^2 \\
 &= E_T + E_L \\
 &= E
 \end{aligned}$$

We now can see that $E_T(\theta)/E_L(\theta)$ is minimal when $E_L(\theta)$ is a maximum:

$$E_T(\theta) + E_L(\theta) = E = \text{const},$$

or

$$E_T(\theta)/E_L(\theta) = \text{const}/E_L(\theta) - 1.$$

The right-hand side is clearly minimal when $E_L(\theta)$ is maximal. To find the desired angle we find θ for which $E_L(\theta)$ is a maximum.

$$\begin{aligned} \frac{d}{d\theta} [E_L(\theta)] &= \frac{d}{d\theta} \sum_{k=1}^j [L_k(\theta)]^2 \\ &= 2 \sum_{k=1}^j L_k(\theta) \frac{d}{d\theta} [L_k(\theta)] \end{aligned}$$

Setting this equal to zero,

$$\begin{aligned} 0 &= \sum_{k=1}^j L_k(\theta) \frac{d}{d\theta} [L_k(\theta)] \\ &= \sum_{k=1}^j (-\sin\theta T_k + \cos\theta L_k) \frac{d}{d\theta} (-\sin\theta T_k + \cos\theta L_k) \\ &= \sum_{k=1}^j (-\sin\theta T_k + \cos\theta L_k) (-\cos\theta T_k - \sin\theta L_k) \\ &= \sin\theta \cos\theta \sum_{k=1}^j T_k^2 + (\sin^2\theta - \cos^2\theta) \sum_{k=1}^j T_k L_k - \sin\theta \cos\theta \sum_{k=1}^j L_k^2 \end{aligned}$$

Let $A = \sum_{k=1}^j T_k^2$, $B = \sum_{k=1}^j T_k L_k$, $C = \sum_{k=1}^j L_k^2$ and

divide by $-\sin\theta \cos\theta$:

$$-A - \frac{\sin^2\theta - \cos^2\theta}{\sin\theta \cos\theta} B + C = 0$$

This can be written as

$$\tan\theta - \frac{1}{\tan\theta} = \frac{C - A}{B},$$

or as

$$\tan^2\theta + \frac{A - C}{B} \tan\theta - 1 = 0 ,$$

$$\tan\theta = \frac{1}{2} \left(\frac{C - A}{B} \pm \sqrt{\left(\frac{C - A}{B} \right)^2 + 4} \right) .$$

Of the two solutions, the θ which makes $E_L(\theta)$ larger is the angle between the longitudinal component and the Rayleigh wavefront normal.

SYSTEM DESIGN CONSIDERATIONS

The system will be based upon a distributed field of seismometers which partially surround the enemy weapons. Given the arrival times of several mortar recoil signals the problem reduces to computation of locations from sets of three or four sensors by the method of intersection of hyperbolic curves. Discrimination of the seismic recoil signals from shell impact signal is necessary when multiple events can occur with rapid succession. In this case, arrival must be sorted out according to source. The shell impacts from friendly return fire can be used to provide calibrating path velocities and can be incorporated into a "seismic on seismic" location estimate. At present, the seismic mortar system is envisioned to consist of: (1) several, three orthogonal component sensor units equipped with signal processing electronics and data transmission capabilities, and (2) a central (base operated) receiver, processor, location computer, and display unit. A block diagram is shown in Figure 18.

The first three blocks constitute the remote battery-powered sensor package. The necessary data from this sensor could be digitized and transmitted by radio frequency (RF) link to a small processing computer controlled by the system operator.

In the present concept the sensor package should be small, light weight, low cost, and perhaps expendable. The unit's principal functions will detect, identify, and report impacts and recoils. The unit will likely not be able to discriminate weapon type or source. The sensor will become activated by a basic amplitude/time threshold. With threshold activation incoming analog signals will be digitized and stored for data transmission and identification. Perhaps the best available means for identification can be made by observing the air wave arrival. The logic would say an event has occurred within a

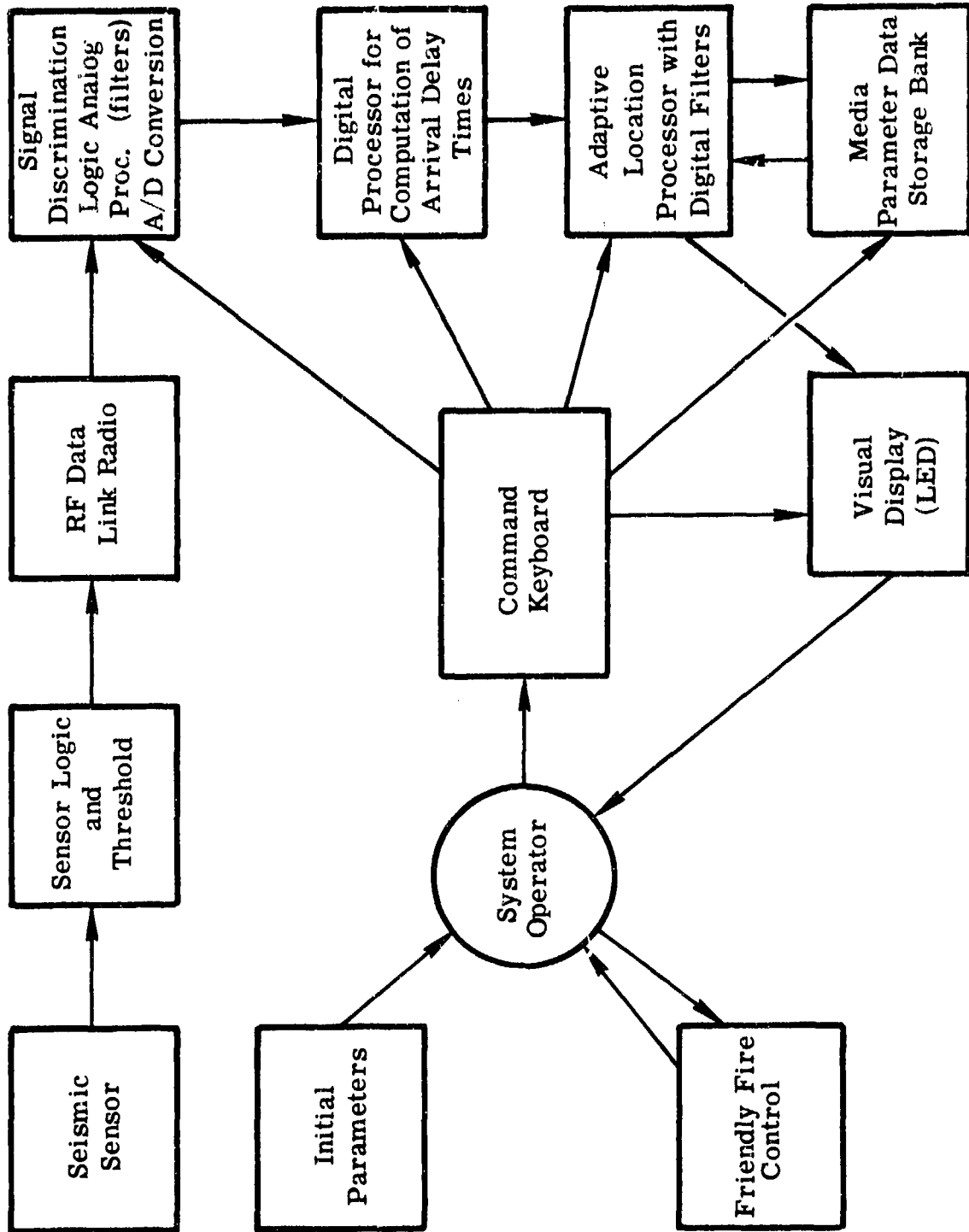


FIGURE 18. SEISMIC MORTAR LOCATION SYSTEM

proper time lag of the threshold seismic and which has suitable amplitude/frequency/duration characteristics. Thus the seismic activation is confirmed as that from an impact or recoil by presence of an air wave.

Data burst transmission should begin as soon as possible after the air wave arrival. Depending on RF data transmission capabilities signals may have to be staggered to prevent overlapping transmissions from several activated sensors.

Without special provisions the minimum time spacing between events may be as much as five seconds. If a push down stack or some similar technique is employed this time could be reduced to as little as two or three seconds. The lower limit would be predicated by desired seismic trace length.

When rapid fire occurs seismic signatures will overlap in time which may destroy their usefulness for timing information.

The remote battery-powered sensor must be able to generate an electric signal corresponding to ground velocity of adequate signal-to-noise ratio (S/N) in the range of seismic frequencies (10-40 Hz) that contain mortar location information. A small, light-weight, compact seismometer such as the Sparton device, with characteristics shown in Figure 19 would provide sufficient sensitivity. A preamplifier with a gain of about 4000, not a difficult requirement, would then be necessary to increase this maximum seismometer output to 1 volt, an amount appropriate for the succeeding circuitry. A seismometer with greater sensitivity could be used but it would probably be larger, heavier, and more fragile; so it seems more reasonable to use electronic amplification instead. At the above stated signal levels the S/N ratio would not be degraded by electronic noise. The amplifier could be a metal oxide semiconductor (MOS) integrated circuit (IC) that could operate from small batteries for 90 days without difficulty. Total system power requirements will be discussed later in this section.

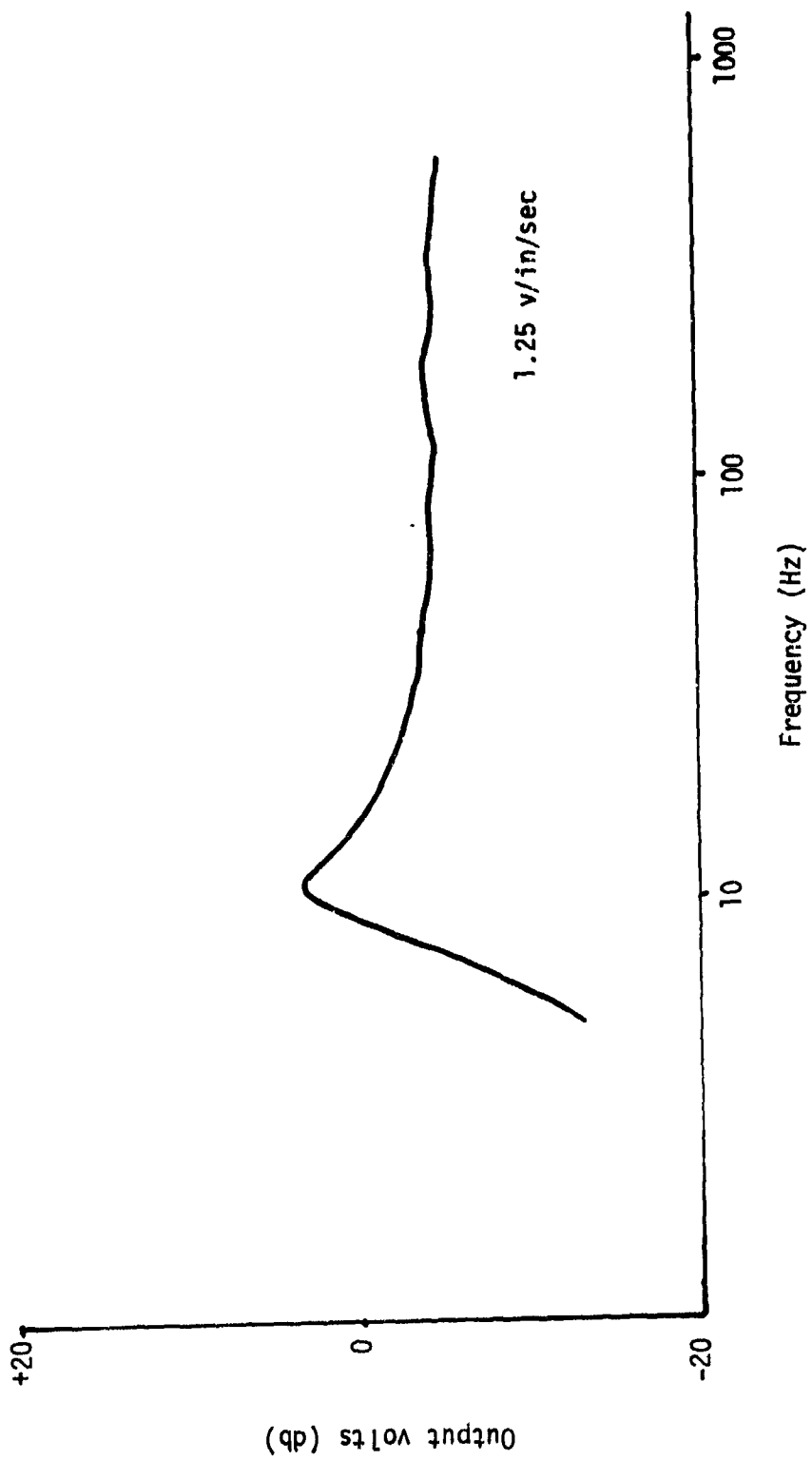


FIGURE 19. RESPONSE CURVE FOR SPARTON SEISMO METER

Because there are many frequency components generated in a battlefield situation, the low pass (LP) and high pass (HP) filters, are necessary to remove unnecessary and detrimental frequencies. In this manner, the S/N ratio of the electrical signal may be enhanced. Adjustment of amplifier gain and the placement of LP and HP cutoff frequencies will be possible to adapt the sensor package to that geology.

The remaining functions in the sensor are the threshold circuit, A/D conversion, and an RF data link. It is not an effective use of battery power to transmit data continually since useful data only occurs during and immediately after each shot. Therefore, a circuit is necessary to determine when the seismic signal has exceeded a pre-set threshold and then the transmitter is turned on for a short time to relay the information. This approach is also desirable from the security standpoint because short bursts of RF are more difficult to monitor and detect by the enemy. Additionally, RF bursts will occur during mortar acoustic reports which means that acoustic indications from the enemy's monitor receiver will be masked by the external muzzle and impact sounds.

The central processing unit contains the equipment to receive and detect the RF signals. The source of the digital data transmission can be identified by a sensor code. Digital samples will be stored in memory locations known to the computer program. Storing of all sensor outputs will begin when the first RF transmission occurs. To store only useful data, the digitizing will continue for that shot or series of shots only sufficiently long enough to collect the seismic wave data.

Only a small fraction of program time will be used to acquire new data. The remaining block of Figure 18 represents functions performed by the processor during most of the program time. Actually, the main program will be interrupted relatively infrequently to gather

new data. The keyboard and display may also be serviced on an interrupted basis such as, when a command changes or when the visual display needs updating.

4.1 POWER CONSUMPTION

Concerning the sensor package only, the power requirements of the RF transmitter are the most difficult to establish and may be the most severe if high transmitter power is needed. For this range and frequency over water, one-half watt of RF power input to the transmitter should be sufficient, assuming the usual military band of buoy frequencies of about 170 megahertz is used. To be ultra-conservative and for land-based use if one assumes that a transmitter of 5 watts input power is required and that a single-event transmission takes 2 seconds; then 5 time 2 or 10-watt seconds are needed for each event. The energy density of an advanced nickel-zinc battery is about 40 watt-hours per pound or 144,000 watt-seconds per pound. This means that a one-pound battery should transmit for 14,400 events. If a 90-day life is necessary, then a firing rate of $90 \times 24 \times 60$ or 33,600 minutes per month divided by 14,400 possible transmissions or about 2 shots per minute can be tolerated. This is the rate for a group of weapons.

The remaining electronics in the sensor package have minimal power requirements. assuming 10 operational amplifiers are needed, with each using 1000 μ watts, a conservative estimate for low-power devices, 10,000 μ watts times 2500 hours in 90 days is 25 watt hours, less than a one-pound battery. This amount of power must be adequate with the sensor either operating as an RF device since these circuits are operating continuously. It should be understood that this estimate of required battery power is very conservative. A 0.5 lb battery will buy 10 days of operation and 3 km transmission range which is a more practical estimate.

All sensors will send their data, via RF to a central location. If this digital processor is of MOS design, power requirements will be low especially if an electro-mechanical disc/drum memory is not necessary. The addition of the LED/liquid crystal display and control functions completes the processor with the total power requirements estimated at 10 watts without any mechanical components. This 10 watts could be provided by a small 5-lb rechargeable battery unit good for one or two days of operation. If the batteries are of the quick recharge type such as lead-cobalt they could be used until recharging was necessary when a vehicle engine-mounted generator could quickly recharge them for further operation. The volume and weight of the sensor units and central computer are such that two or three men could carry the system. The total weight of the system, including 10 sensor packages, would be on the order of 75 lbs. This estimate assumes a 10-day sensor battery life. A total system cost (on a production basis) is estimated to be \$5K to \$6K. An estimate of component sizes, weights, and costs, based on prior experience with electronics, are given in Table 4.

In summary, the system just described should not be difficult to design and deploy. There are no components approaching state-of-the-art limitations. There have been many types of buoys built previously and quite some time ago. In the digital processing, some custom LSI design may be necessary but that too has been done before, though more recently. The buoys should not contain many components so that failure rate during battery life could be made low by selection of components and adequate specification and testing. Plug-in spare units or circuit cards could be used to increase the MTBF (mean time between failures) of the central processing gear since there are many more components involved than in the buoys. The most fragile element of the entire system would probably be the magnetic drum or disc to head interface if that type of storage were used.

TABLE 3

Estimated Component Volume, Weight, and Cost of the
Seismic Mortar Location System

<u>Component</u>	<u>Size</u> (cu. in.)	<u>Weight</u> (lb)	<u>Est. Cost*</u> (\$)
Seismometer	1	0.5	5
Amplifier and Filters	8	0.5	20
Threshold, Switch and Line Driver	1	0.5	5
A/D Conversion	30	0.5	50
RF Transmitter	4	0.5	20
Battery	6	0.5 (10 day)	10
Enclosure	64	1.0	10
Total	4 x 4 x 4	4.0 lbs/ unit	70/unit *
<u>Data Processing</u>			
Receivers	0.12	3.0	1000
Central Processing Unit	0.25	10.0	2000
Digital Storage	0.50	2.0	500
Display, Control, Batteries, and Enclosure	0.50	20.0	1000
Total	1.37 13 x 13 x 13	35 lbs/ unit	4500/unit

*Based on 100 units

FIELD MEASUREMENTS PROGRAMS

In order to evaluate the use of seismic data for mortar location a series of field measurements was initiated during the second phase of the project. Seismic mortar and explosion data were collected at two sites, Twenty Nine Palms and Camp Pendleton, California during February and March of 1975.

The object in this field exercise was to simulate as near as practical those battlefield conditions of mortar ranging. To do this we needed to make recordings of enemy recoil and friendly shell bursts. Enemy mortar fire can be represented by firing conventional 81 mm mortars. It was not practical to observe the effect of friendly fire directly. To impact the vicinity of a mortar firing position would have required setting up in an impact zone which is generally not permitted. Live impacts have the additional problem that each must be surveyed to an accurate position.

During a previous program which included field work at Ft. Sill, Oklahoma it was determined that 105 mm shell impacts could be simulated seismically with a TNT detonation. This technique was used exclusively throughout the field work in order to record the effect of friendly fire.

Reflecting the requirements of the derived algorithms specific objectives of the field program included collection of data which could evaluate the similarity of impacts and recoils as a function of separation distance. In addition we had hoped to evaluate the concept of firing into an area (simulated by explosions) for purposes of calibration of path velocity.

5.1 FIELD MEASUREMENT PROGRAM - TWENTY NINE PALMS MARINE BASE

The field measurements at Twenty Nine Palms were made at locations near Deadman's Lake and Camp Wilson (see map in Figure 20). The topography was flat in this area. Surface material in this area consisted of unconsolidated rock and sand with an underlying bedrock which consisted mostly of granite. Depths to the bedrock material was guessed to be a few hundred feet. After preliminary examination of seismic recording was made in this area, it was felt that most of the seismic energy travelled along paths in the upper unconsolidated material.

A series of nine three-component seismometer packages were instrumented along a line parallel to and located 300 meters inside the southern boundary of the BRAVO-1 impact area. Mortar firing positions were located along a 2.5 kilometer line of 0.5 kilometer intervals and perpendicular to the sensor base line. The main firing line ran from the center of the sensor line (5th sensor position) to a position near Camp Wilson. Two pound TNT shots were to be fired in a cluster pattern around each mortar firing position simulating friendly impacts. A plan of this field geometry is shown in Figure 21. A standard 81 mm mortar was used to fire rounds over the sensor line into the BRAVO-1 impact area. All explosion, seismometer, and firing positions were surveyed by the base surveying team.

5.1.2 INSTRUMENTATION

Figure 22 depicts the instrumentation which was used in digitally recording the seismic data in the field. This system, housed in a van, is capable of recording up to 15,000 samples per second with a dynamic range of 84dB, 14 bits per sample, full frequency resolution being limited to 75 Hz by the antialiasing filters. The controlling computer was an Interdata Model 7/16 processor with 16,384 eight bit bytes of 1,000 ns core memory.

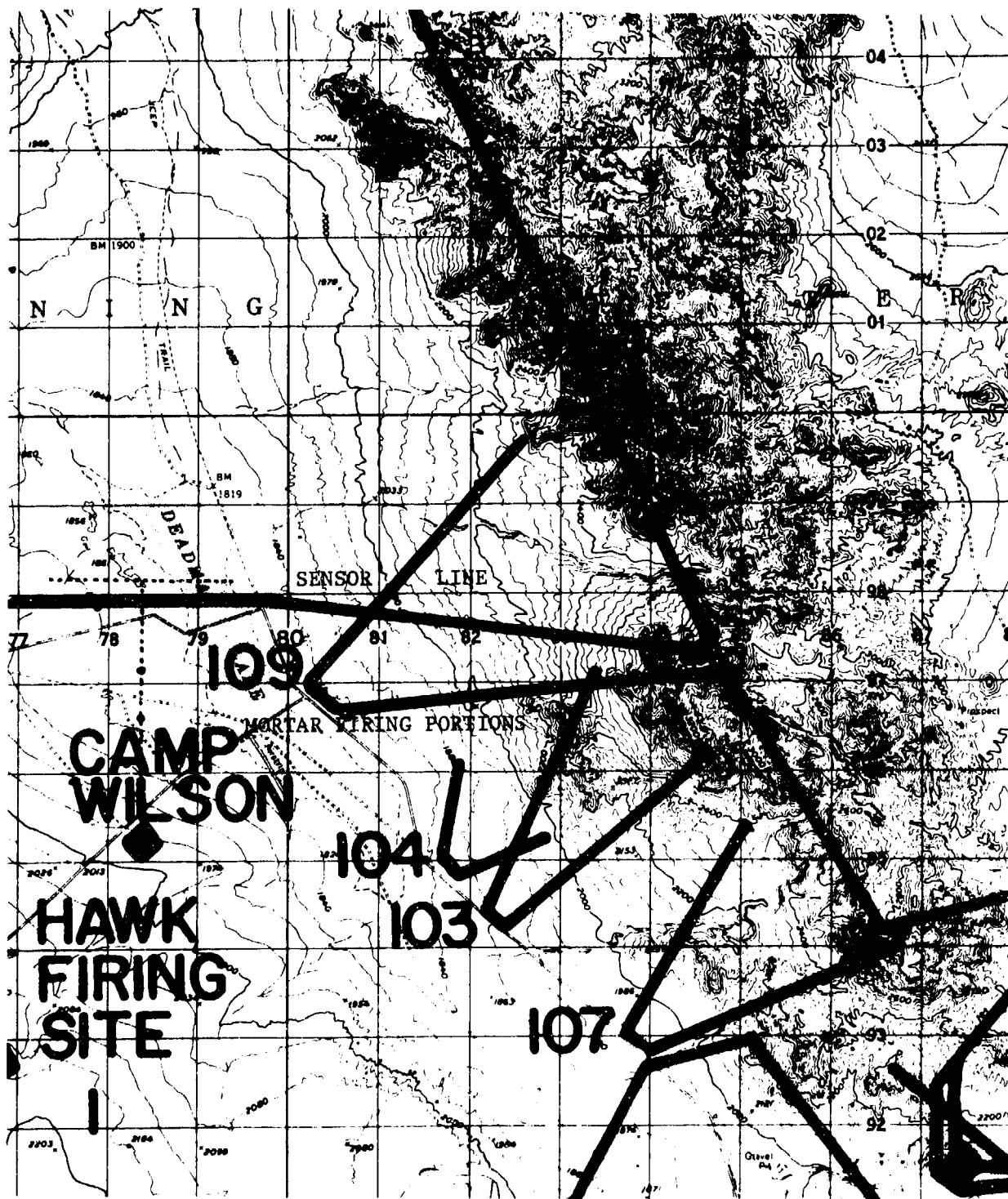


FIGURE 20. FIELD MEASUREMENT SITE, TWENTY NINE PALMS, CALIFORNIA

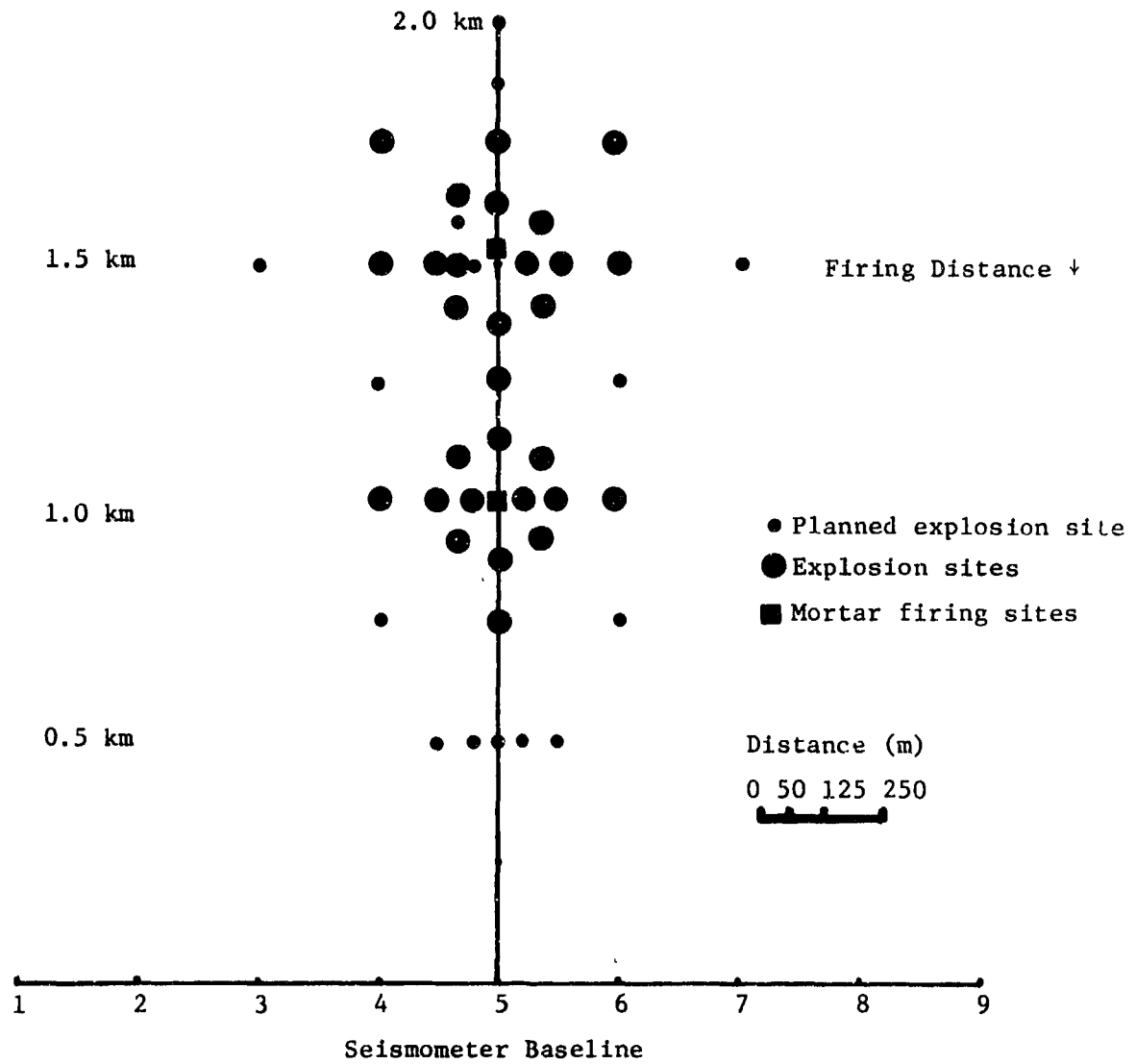


FIGURE 21. FIELD GEOMETRY AND SENSOR PLACEMENT AT TWENTY NINE PALMS MARINE BASE

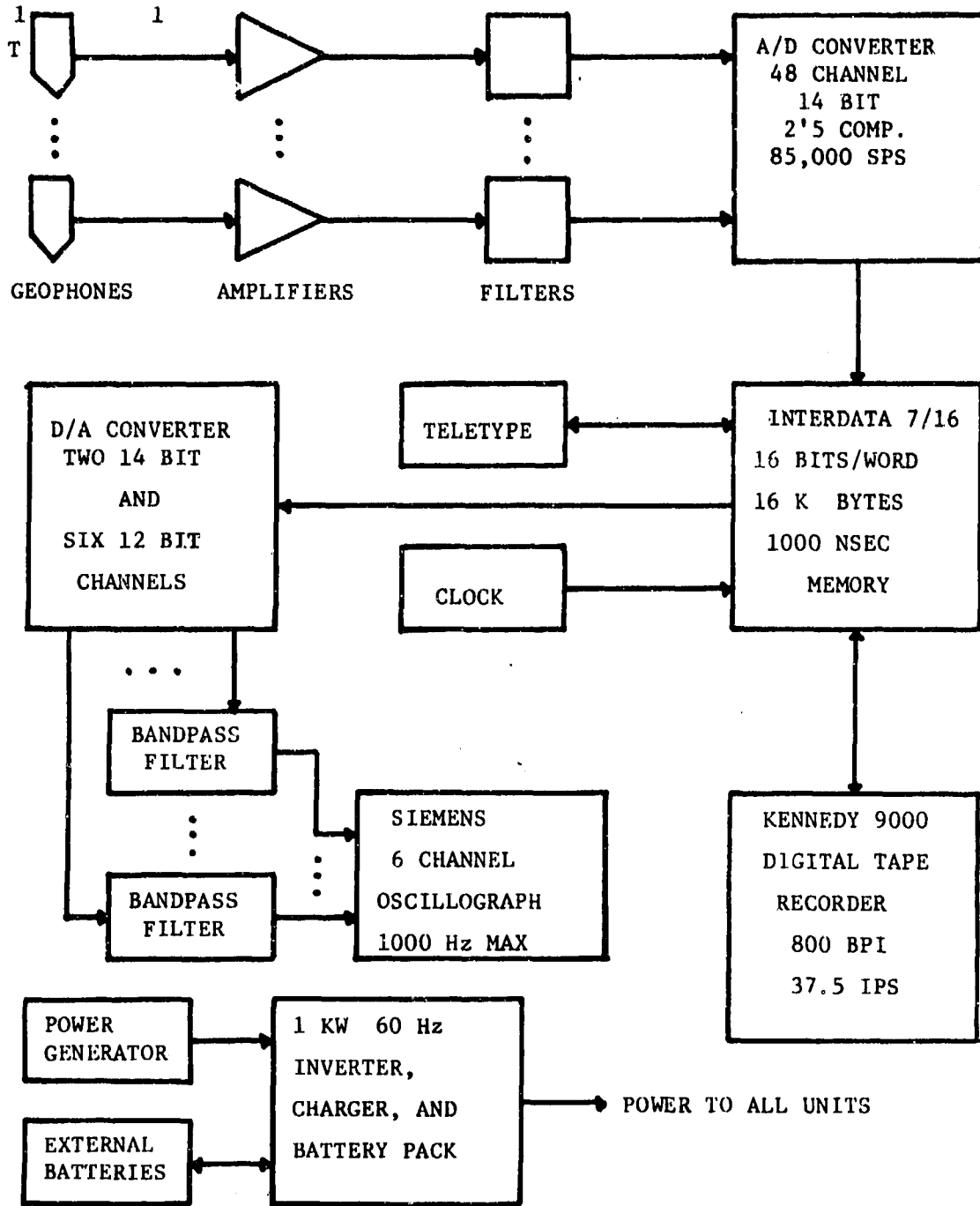


FIGURE 22. DIGITAL RECORDING INSTRUMENTATION

Existing peripheral equipment included an ERIM built 1.2 megacycle clock, an Analogic series AN5800 A/D and D/A converter, an ASR model 33 teletypewriter, an Interdata Hexadecimal I/O panel and a Kennedy 9000 digital tape recorder.

Nine three-component-orthogonally mounted Hall Sears model HS-10 seismometers were used. These velocity transducers have a resonant frequency of 2 Hz and a damping factor of approximately 0.64. They have been calibrated on ERIM's shaketable. Each instrument has a response to motion perpendicular to its axis which is 30 dB down from its response to on-axis motion. Figure 23 is a typical amplitude response curve for these instruments. Each seismometer was connected to the field recording van using standard WD-1 communication wire.

Each signal was amplified at the seismometer to reduce the percentage of induced noise in the line carrying the signal to the recording van. Ithaco model 9121-73 seismic amplifiers, powered by automotive type 12 v. lead-acid batteries, were used here. They can be adjusted from -12 to 96 dB in 6 dB intervals and are capable of providing an output signal of 5 v. rms. Their low and high cutoff frequencies are 0.3 Hz and 1,000 Hz, respectively, and they generate 2 μ v equivalent input noise. Zero times were generated for each event by radio transmission of the immediate seismic impulse.

Research at this laboratory has shown that the signals of interest for long range detection of recoil have a spectral peak near 15 Hz with energy possibly as high as 20 Hz. Therefore, filters with a response as shown in Figure 24 were placed in the system before the data was digitized to prevent the aliasing of higher frequency energy into the wanted data band. Since the sampling frequency was 300 Hz, input data to the system had to be attenuated an amount equal to the dynamic range of the system at the Nyquist frequency or 150 Hz. This condition was insured by the combination of the use of the filters and the character of the mortar recoil seismic signals.

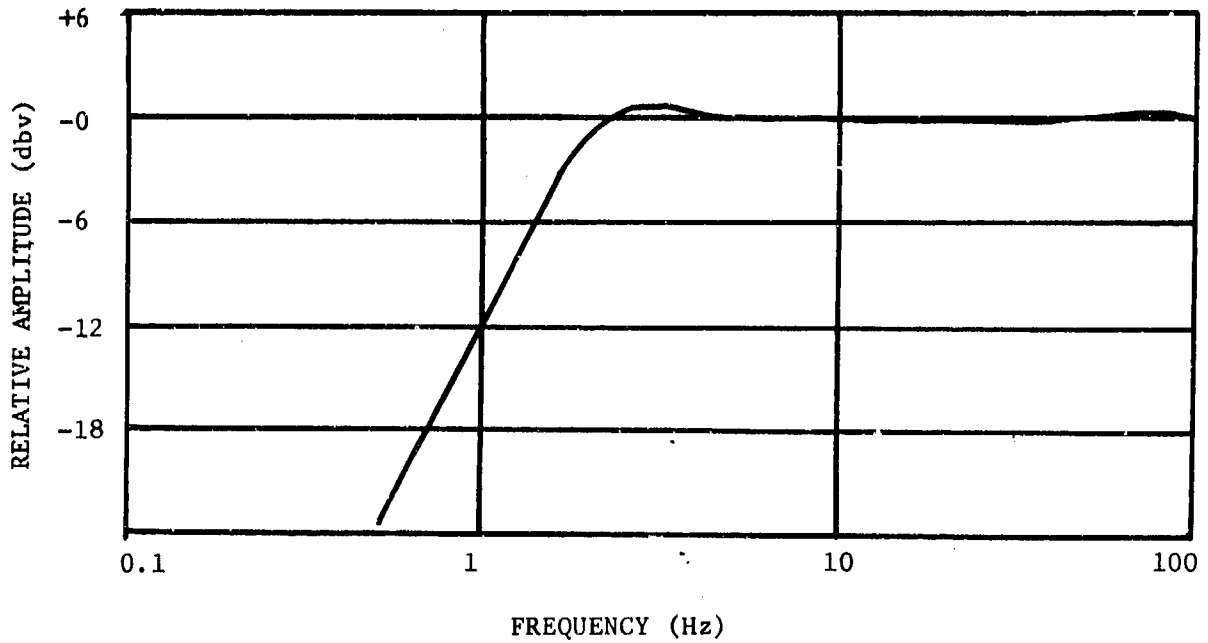


FIGURE 23. TYPICAL RESPONSE OF GEOSPACE MODEL HS-10 AS CALIBRATED ON ERIM'S SHAKETABLE: DAMPING FACTOR OF APPROXIMATELY 0.64

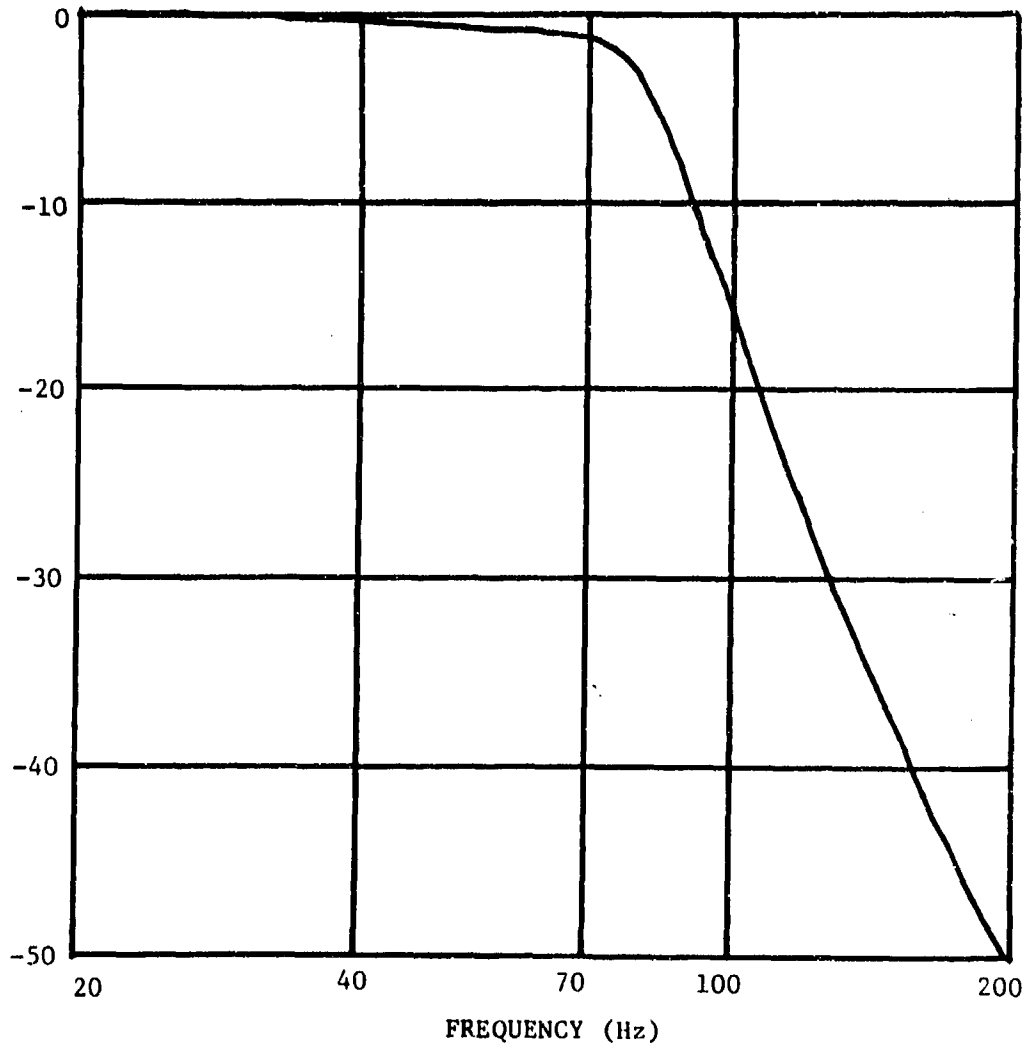


FIGURE 24. ANTI-ALIAS FILTER RESPONSE. Output voltage is dB relative to 0dB input

The filter outputs were sequentially sampled and digitized with a skew of 1/85,000 second between adjacent channels. The digitizing rate was 300 samples per second. Full scale A/D conversion is -5v to +5v. Amplifier gains were set so that the input seismic signal plus noise were within 6 dB of full scale without over-recording. The samples were stored in a buffer, under software control, and then written on digital tape.

The quality of the data was monitored continually. Oscilloscopes were used at the input panel during an event and hard copy traces were produced after each event on a Seimens 6 channel oscillograph.

5.1.3 DATA COLLECTION

The seismic data collected at the Twenty-Nine Palms site was generally quite good but not totally free of problems. Bad weather and uncontrollable delays prevented the field team from collecting all data as originally planned. Mortar firings were completed at the 0.5, 1.0, 1.5, and 2.0 km sites using standard HE rounds. Firings were made at charge 7 or 8 and at elevations to yield a 3.0 or 3.5 km range. All mortar firings were made by Camp Pendleton infantry mortar crews. Because of delays and high wind conditions no data was collected at the 2.5 km site and mortar signatures from the 2.0 and 0.5 site were noisy and not suitable for further analysis. Time limitations prevented the crew from making all the explosion shots as planned. However, complete sets were obtained for the 1.0 and 1.5 km sites. A total of 40 explosions and 38 mortar firings were recorded at the Twenty Nine Palms site. The stars next to the surveyed locations of the field geometry map of Figure 22 show positions for which explosions were detonated. All explosions were fired by base EOD personnel.

5.1.4 DATA QUALITY

Data quality was very good for a major portion of the events recorded except during windy conditions. Signal-to-noise levels were generally high due to the quiet nature of this area. Some instrumentation problems did occur for a couple of channels at sensor one and sensor nine later in the field session. The problem was not detected since other sensor packages were being monitored.

5.2 FIELD MEASUREMENT PROGRAM - CAMP PENDLETON, CALIFORNIA

A second group of seismic recordings were made at Camp Pendleton firing ranges. This area has a more rugged terrain and high seismic noise levels generated by base activities which presented a sharp contrast to conditions found at Twenty Nine Palms.

It was more difficult to set up in this area because of the hilly terrain and the constraints imposed by the firing range layout. A map of the Camp Pendleton site area is shown in Figure 25 with the placement locations of the nine seismometer packages in the X-ray impact area. Mortar firings were made from ranges 108, 108A, and 111. Range 108A was located approximately halfway between range 108 and range 115. Figure 26 shows the approximate location of the explosion shots, which simulate impacts in the area of each mortar firing position. Because of the terrain we were unable to lay them out in a uniform pattern.

The area surface material was felt to consist largely of hard-rock with a shallow layer of surface soil material. On steep slopes rock outcropping was frequent. The recording area exhibited several hundred feet of relief. Basically there was a single ridge system separating the seismometer positions located in an outwash from the firing positions on range 108. From range 111 this separation amounted to a two ridge system.

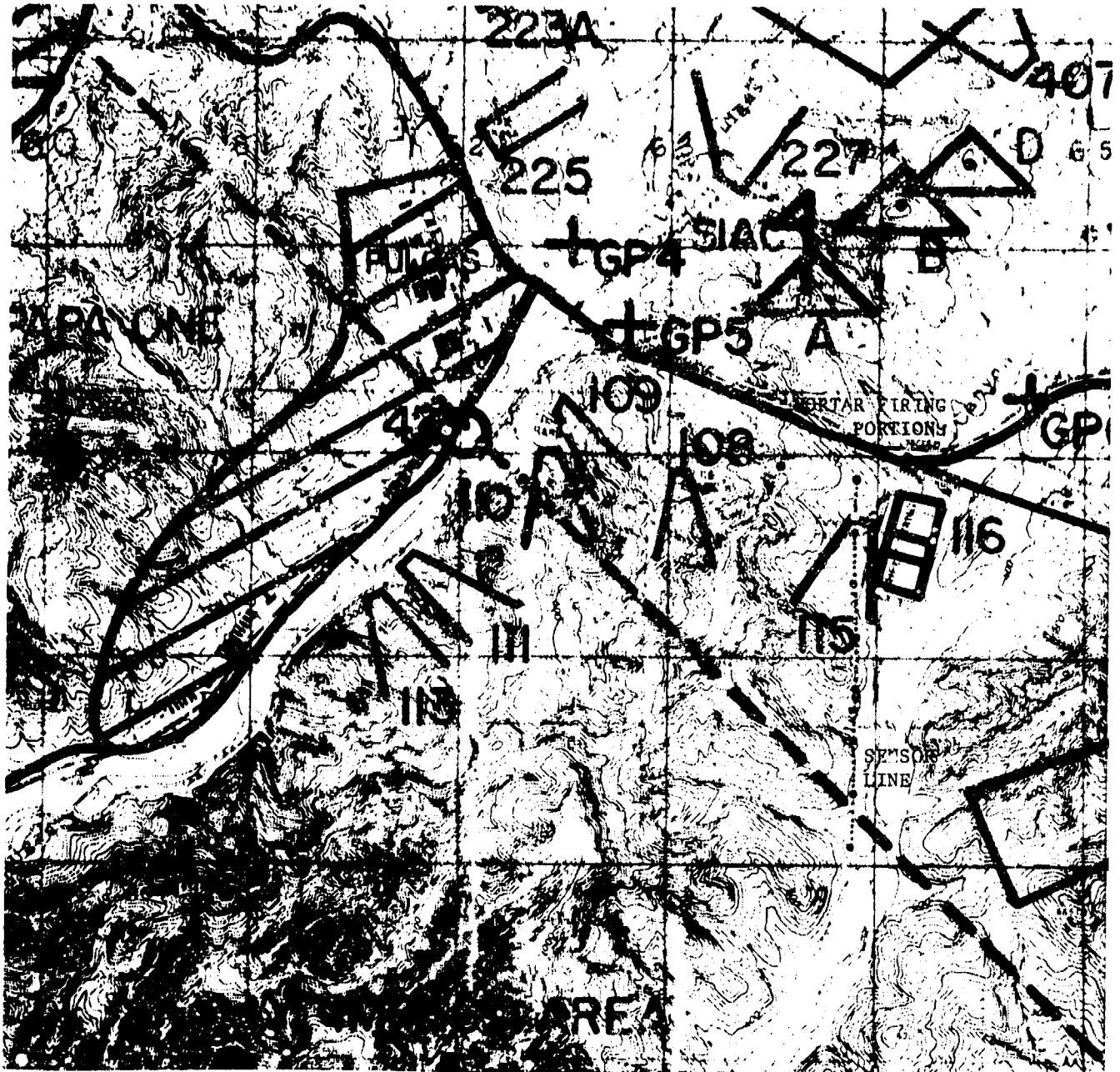


FIGURE 25. FIELD MEASUREMENT SITE, CAMP PENDLETON, CALIFORNIA

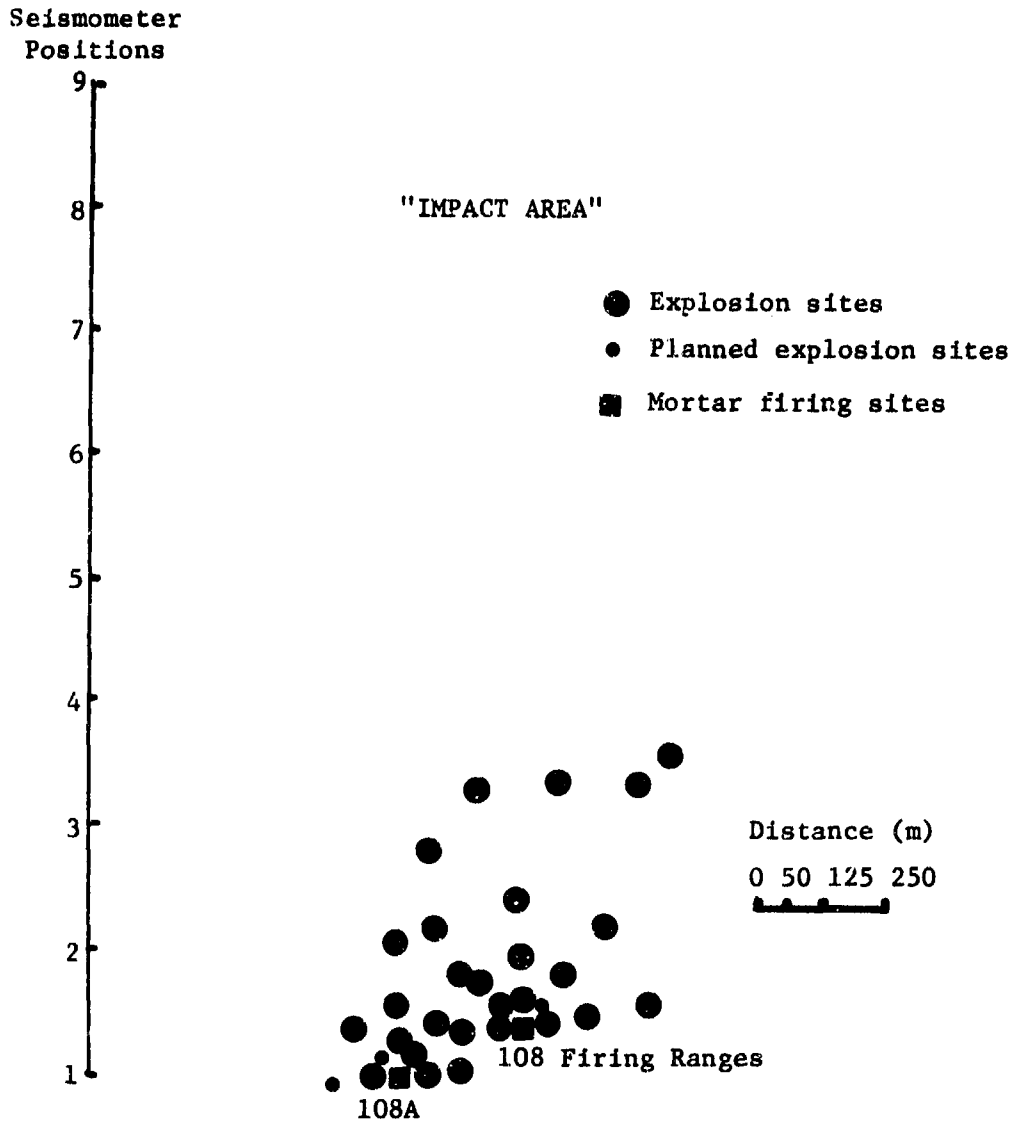


FIGURE 26. FIELD GEOMETRY AND SENSOR PLACEMENT AT CAMP PENDLETON

All instrumentation was the same as that described earlier.

5.2.1 DATA COLLECTION

A total of 53 two pound shots and 27 mortar rounds were fired at the Camp Pendleton site. Many of these events were duplicate measurements which were found necessary because of the high general noise conditions and frequent interference by tanks, trucks, artillery, and helicopters. Noise levels at Camp Pendleton were approximately 20 dB higher than those which were common at the Twenty Nine Palms site. Mortar firings were made at the standard positions at each range. Rounds were fired at charge 7 and at high elevations. Explosions were detonated in the vicinity of each mortar firing position. Locations surveyed by a Marine Corps support team are shown in Figure 26 with starred position indicating those which were utilized during the recording program.

5.2.2 DATA QUALITY

Except in one or possibly two instances seismic signals from 81 mm mortar recoil could not be observed at any sensor. The exceptions are of poor quality and uncertain because of the large number of interfering sources. The two pound explosions were generally observed seismically out to the fifth or sixth sensor position but lost in the noise at greater ranges. Many of the recordings were rendered useless because of interfering events.

DATA ANALYSIS AND RESULTS

Our approach in analyzing the field data was to first examine the data visually and eliminate those events which were not considered useful because of their high noise levels on instrumentation problems. Basic processing including identification events zero times, and correlation parameters was completed on a PDP-8 special purpose computer system. Seismic and acoustic travel times were calculated using first arrival and peak correlation sample locations. Actual travel times or unnormalized relative times for each event along with shot and sensor position information served as input to the location computer code. These data were not computer analyzed for purposes of discrimination of recoil from explosion events.

6.1 RESULTS OF VISUAL EXAMINATION

The field measurement program produced a total of 4,266 records each with a seismic and acoustic signature. It was considered impractical to process every possible record. Visual selection of a subset of data based upon the following criteria.

1. Where events were repeated the event with best signal-to-noise was selected.
2. The largest seismic and acoustic signals were observed on the vertical channel. Also greatest correlation between shots was observed on the vertical oriented seismometer. For these reasons only the vertical channel was processed with the exception of directional analysis.
3. Since the signatures from mortar recoil were repeatable only two or three events from each firing site were selected for processing.

The events analyzed include most of those which have circles in Figures 21 and 26. A list of the survey coordinates of all these events is given in Appendix B .

The frequency content of the seismic signatures was examined using variable Kronkite analog filters in conjunction with the digital recording system. Figure 27 shows example passbands of an explosion. Note that only slight noise reduction is obtained after using the filter passband. The principal frequency components of the seismics occur near twenty hertz with most of the energy at frequencies less than forty hertz. Unfortunately, some of the principal spectral components of wind, vehicles, and aircraft, i.e., in this frequency band (10-40 Hz). It was concluded that signal-to-noise improvement could not be greatly enhanced by simple passband techniques. Visual examination of the three component data indicated two features:

1. the surface waves on the vertical channel were usually the largest seismic signal; and
2. the surface waves showed a great deal of similarity from shot to shot. Figure 28 shows examples of the three component analog records from two explosions which were fired at different positions. Figure 29 shows the vertical axis seismics from two explosions separated by 125 meters as received at each of the seismometer array stations. The events overlay one another to demonstrate the similarity of signals. Also note that these signals appear more similar between events than as between stations.

6.2 TRAVEL TIME CALCULATIONS

Acoustic and seismic travel times for the first arriving signals were calculated by first locating the zero time and picking the first arrival to the nearest digital sample. For acoustic signal the resulting travel time is similar to that which would be obtained by thresholding. Due to the variances in seismic record and noise levels simple thresholding would prove very inaccurate. Timing was made on the basis of common feature recognition along the linear

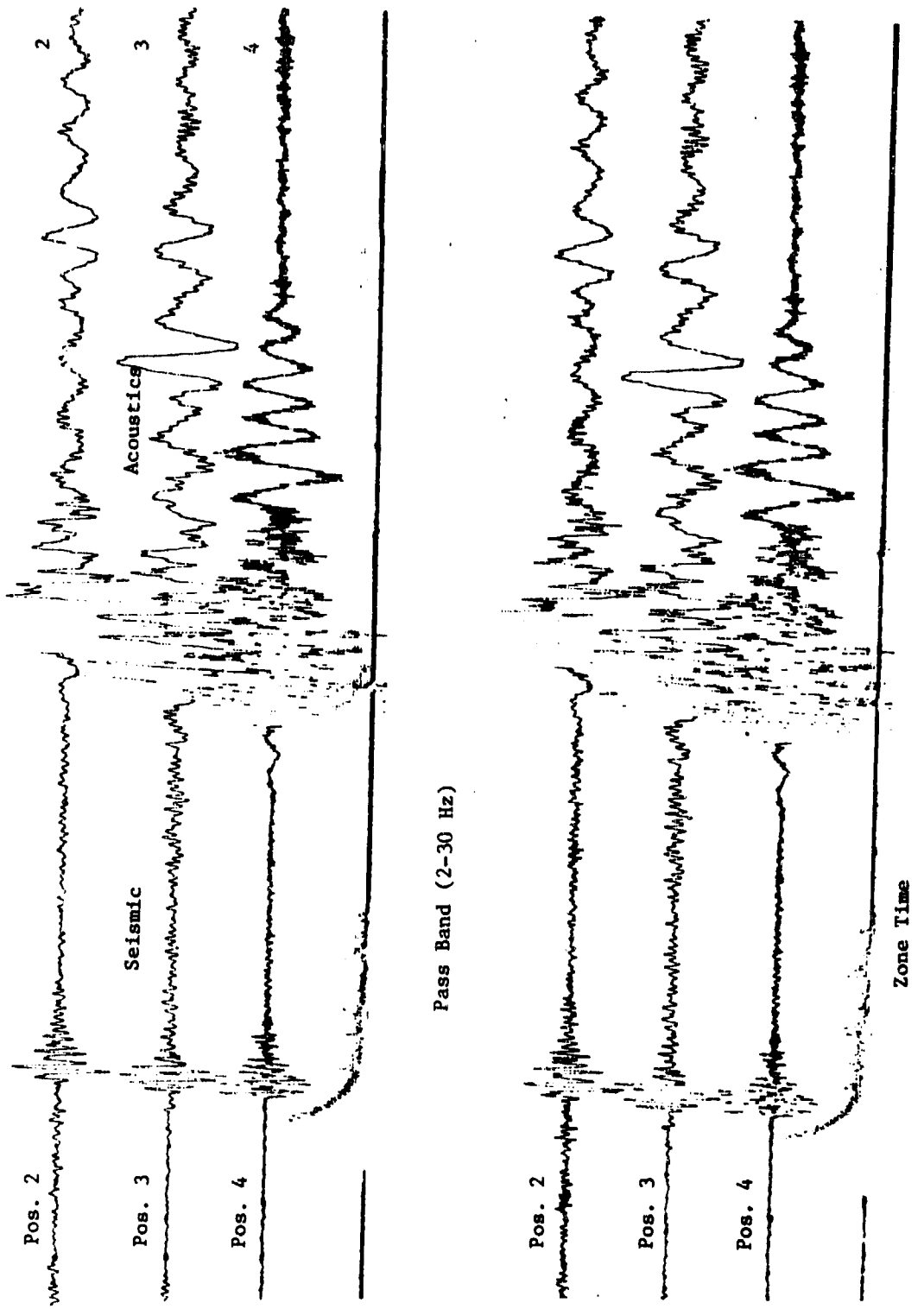


FIGURE 27. SELECTED VERTICAL COMPONENT PASSBANDS FOR EXPLOSION EVENT 07, TWENTY NINE PALMS SITE

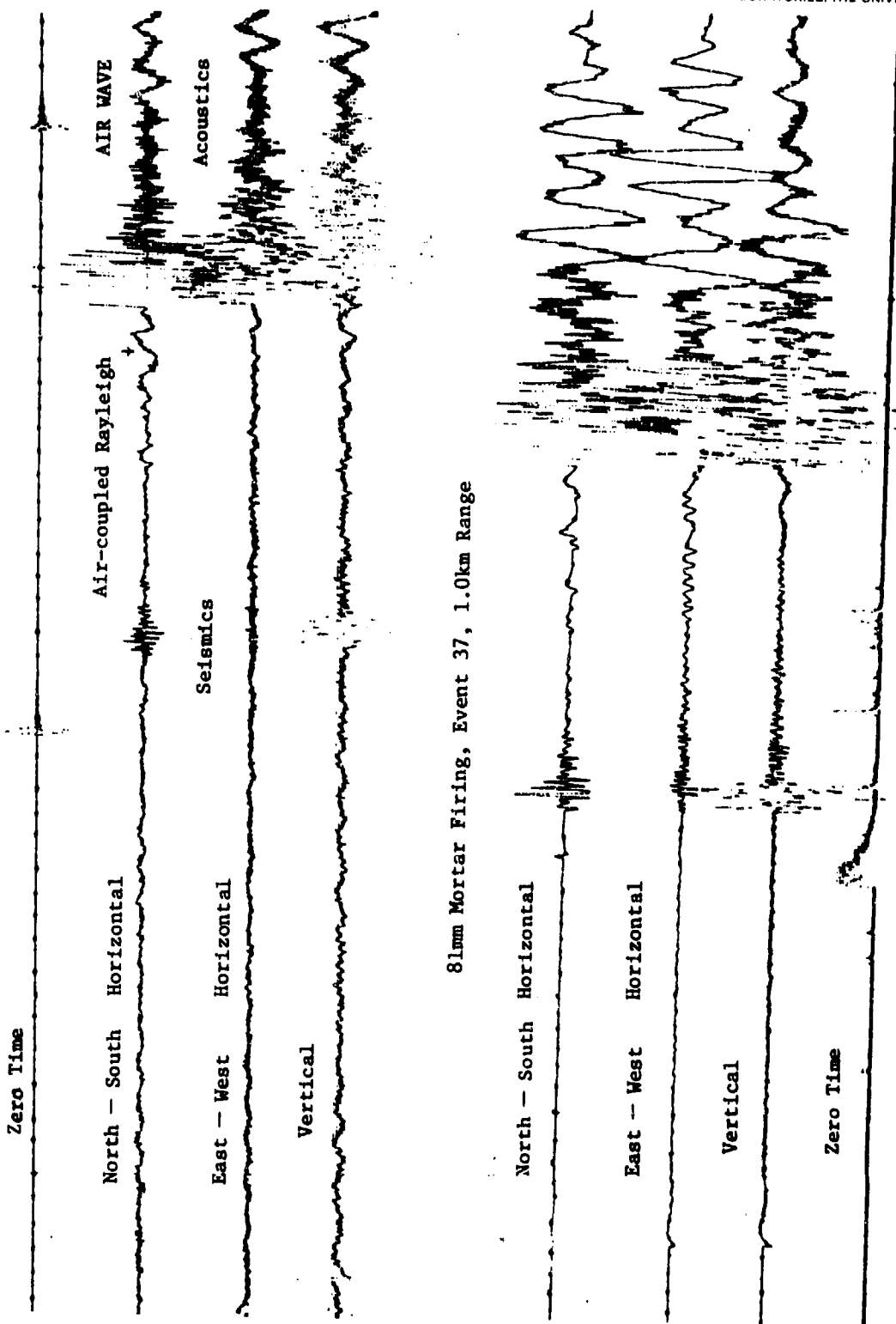


FIGURE 28. THREE COMPONENT SEISMOGRAMS FROM TWENTY NINE PALMS SITE

Note: The East-West horizontal seismometer was oriented to the sensor baseline.

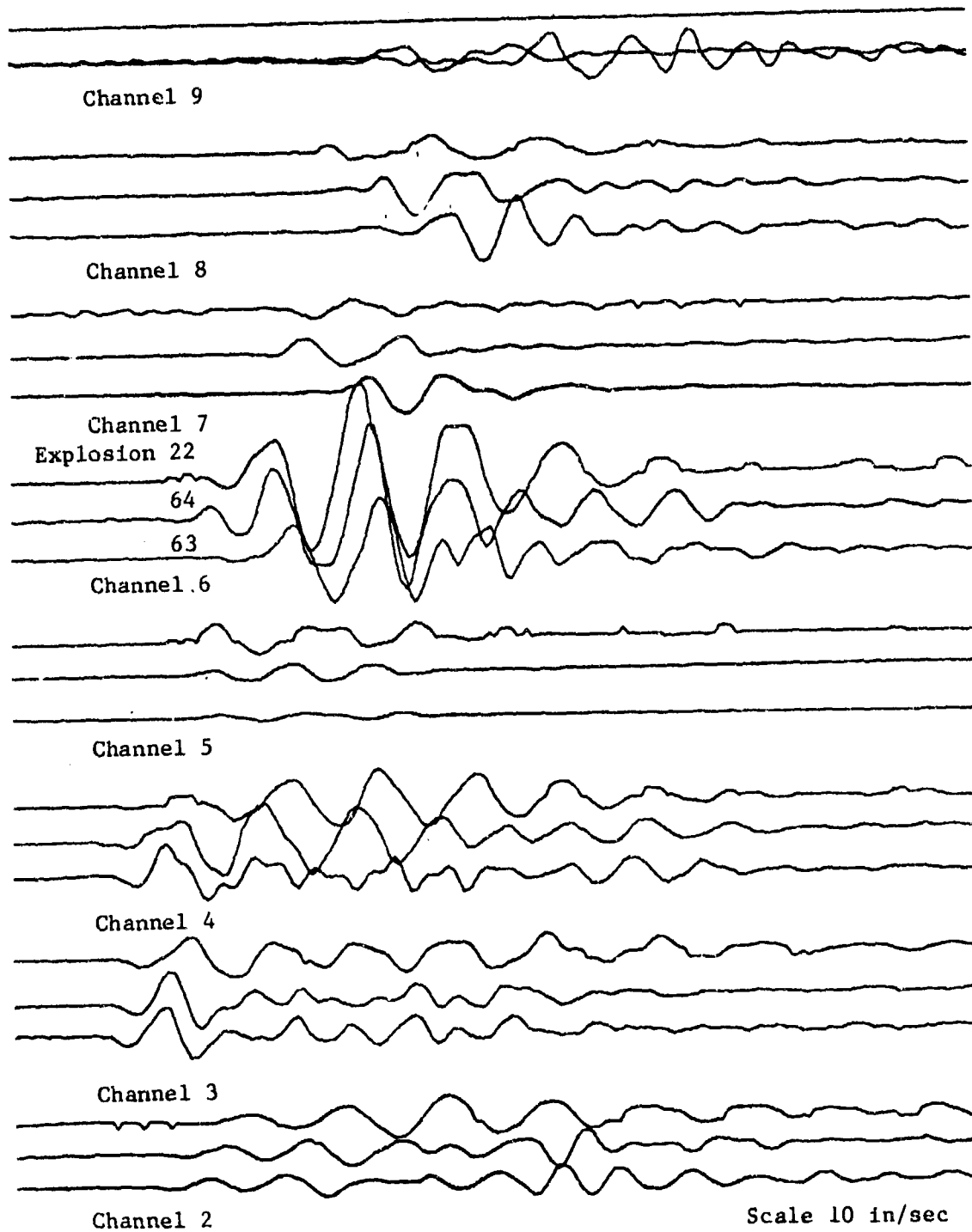


FIGURE 29. VERTICAL AXIS SEISMICS FROM THREE EXPLOSIONS SEPARATED BY 125 METERS BETWEEN EACH SHOT. Event 22 is located at the 1.5 km mortar firing position, Twenty Nine Palms

array. Using seismic first arrivals presented some difficulty because this signal is usually not the largest and is often obscured by background noise. Some travel time information is contained in Appendix B. Cross correlation analysis was also used to gain time of arrival and is discussed in a later section. Air coupled Rayleigh waves were observed as distinctive pre-acoustic wave arrivals. They were, however, not consistently observed and therefore not considered for analysis.

6.3 SOURCE DIRECTION DETERMINATIONS

As previously discussed each location algorithm requires an initial rough location estimate based on the first observations of enemy fire. One possibility is to obtain signal directivity from each three component sensor by measuring the relative signal (mostly acoustic) energy on each horizontal channel. A computer program was written based upon the computational method discussed in section . A total of 15 events from the Twenty Nine Palms data were used to test this approach which had appeared encouraging from a few simple in-house laboratory experiments. Approximate angular deflections were estimated to the nearest five degrees. Figure 30 shows the typical output of the processor with the top trace representing the estimated angular deflection with time and the bottom trace showing the energy rate. In order to obtain an estimate the top trace is weighted by the bottom trace. The results are summarized in Table 5 They were not very encouraging. Overall the method could pick 90 degrees window which contained the correct azimuth 78 percent of the time. One possible source for the error could be corregations in the acoustic wavefront. While this method did not prove successful further work is needed to fully investigate this possibility. Other possibilities of obtaining initial location estimates include, of course, using acoustic and/or seismic data with velocity guesses and the hyperbolic method.

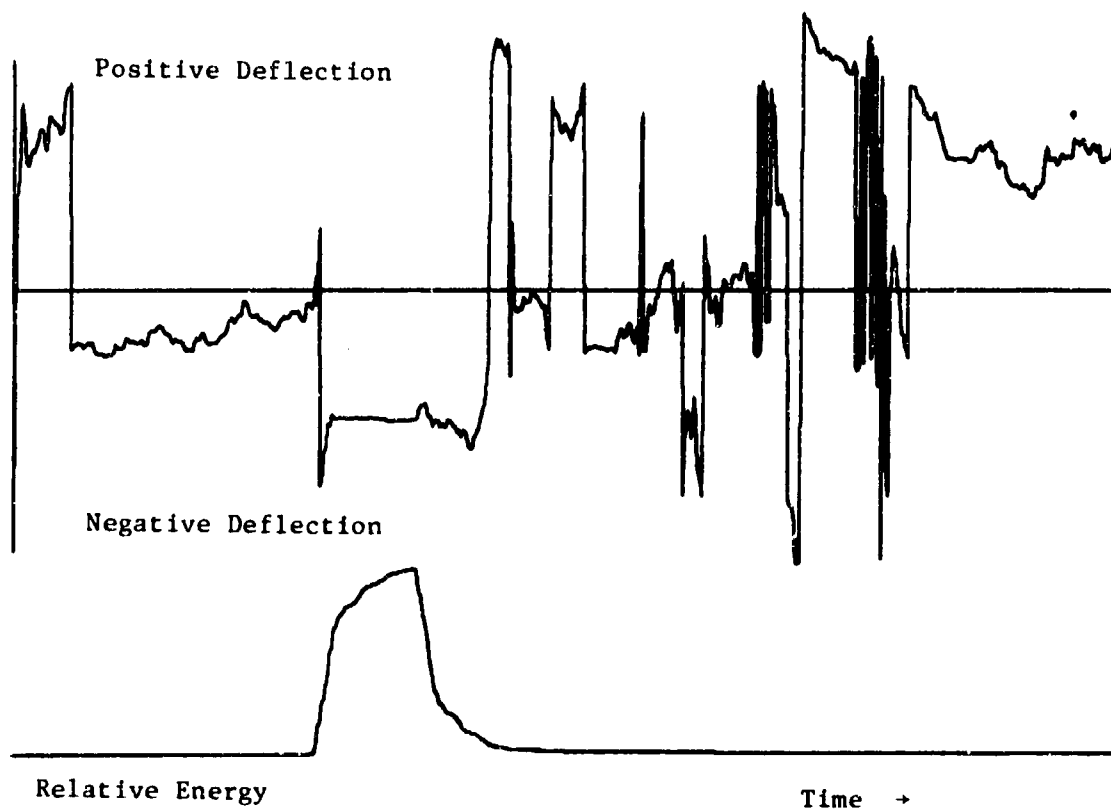


FIGURE 30. PLOT OF THE TIME VARYING ANGULAR DEFLECTIONS AS DETERMINED BY THE COMPUTER ALGORITHM FROM THE ACOUSTIC SIGNATURE. SHOT 307. TWENTY NINE PALMS.

TABLE 4

 APPROXIMATE ANGULAR DEFLECTIONS (Degrees) AS ESTIMATED.
 From the Muzzle Blast

<u>Event</u>	<u>1</u>	<u>2</u>	<u>3</u>	<u>4</u>	<u>5</u>	<u>6</u>	<u>7</u>	<u>8</u>	<u>9</u>
3	-50	-	-50	-35	-50	-30	0	-40	-50
5	-40	-40	-50	-60	-10	-30	-50	+60	+60
7	+40	-40	-40	+15	+50	0	-30	+60	+40
8	+60	-35	-60	-10	+50	0	-15	+50	+40
9	0	-35	-55	+5	+50	+60	-15	+45	+35
10	+60	-40	-50	-10	+50	+0	-15	+45	+40
11	-50	-40	-60	-15	+60	+60	-20	+45	+35
13	-15	+80	-55	+10	+10	-10	+60	+60	+45
15	-10	+80	-60	+50	+15	-15	+60	+50	+40
16	-10	+80	-60	+60	+10	+60	+60	+45	-
19	-10	-20	-60	0	0	+60	+60	+45	+40
20	-10	-25	-50	-10	-30	+60	-10	+50	+40
21	-10	-30	-50	-10	-10	+50	+60	+40	+40
37	-75	+40	-50	+40	-10	-15	-60	+60	+50
38	-	+40	-40	0	+10	+10	+80	+10	+50
Range of True Azimuths									
	-35	-26	-13	1	15	26	+36	+45	+52
	-52	-42	-36	-26	-15	-1	13	26	35
Average of Estimates									
	-8.6	1.1	-53	2	13	17.3	11	39	36

6.4 CORRELATION ANALYSIS

The location method based upon relative time differences between mortar recoil and impact requires a time measurement between signals which are recorded by the same sensor. Likeness between these signals because of similarity of wave path suggests use of cross correlation.

A processing program was written for the PDP-8 computer which could determine the lag corresponding to maximum correlation.

To provide the necessary input to the location program correlations were made between each explosion event of the cluster which surrounded each mortar firing position. Correlations were made over windows which expand the entire seismic signature. Each correlation function is represented by 128 lags of one sample each. Since the largest signals are due to surface waves and represent the majority of seismic energy the correlation is essentially one of surface (Rayleigh) waves. The similarities between signals was found to be reflected as similarity between correlation functions. Superposition of correlation functions indicates the path-time differences to each sensor. Figure 31 shows the overlay of two correlation functions for sensor positions 2 through 7. The corresponding differences in path length (meters) for the respective sensors are -12.0, -8.0, -3.0, 2.0, 7.0, 11.0, and 15.0. These shots were separated by only 25 meters. The step out corresponding to change in path length is clearly evident for each channel and demonstrates inherent capability of the system. Figures 32 through 34 show further examples of correlation overlay for the Twenty Nine Palm data. Figure 32 contains the autocorrelation of shot 22 which was detonated at the 1.5 kilometer firing position and the cross correlation with the recoil seismics. Figure 33 shows the relative comparison of three events separated by 125 meters. The dash lines point to the changes in alignment with corresponding changes in path length. These shifts all amount to less than a one cycle change. Figure 34 shows a similar case, but

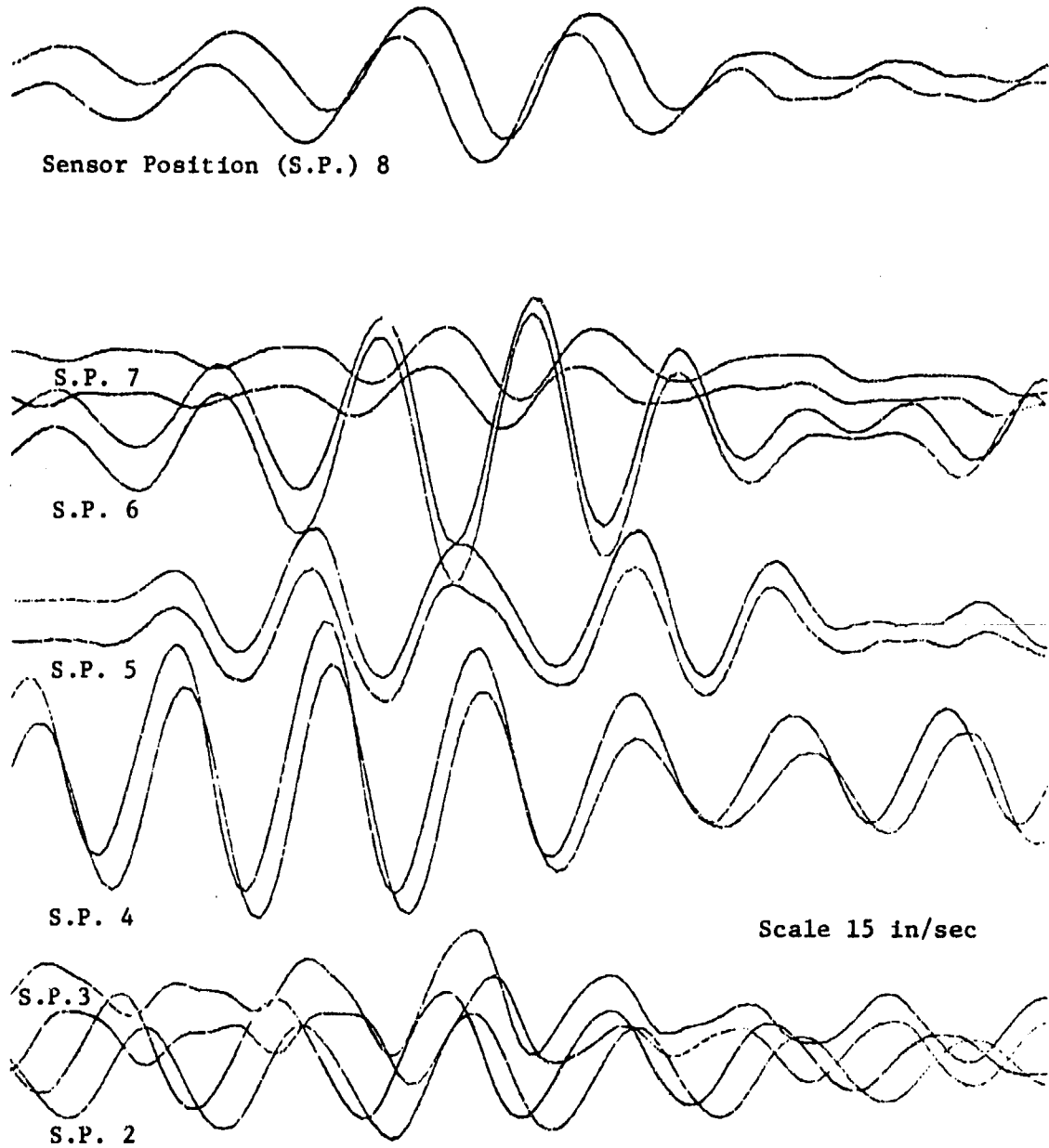


FIGURE 31. OVERLAY OF SEISMIC CORRELATION FUNCTIONS SHOWING CHANGES IN ALIGNMENT FOR SELECTED SENSOR POSITIONS. TOP TRACE EV. 22 WITH EV. 64. BOTTOM TRACE EV. 22 WITH EV. 65. SEPARATION OF EV. 65 and EV. 64 APPROXIMATELY 25 METERS.

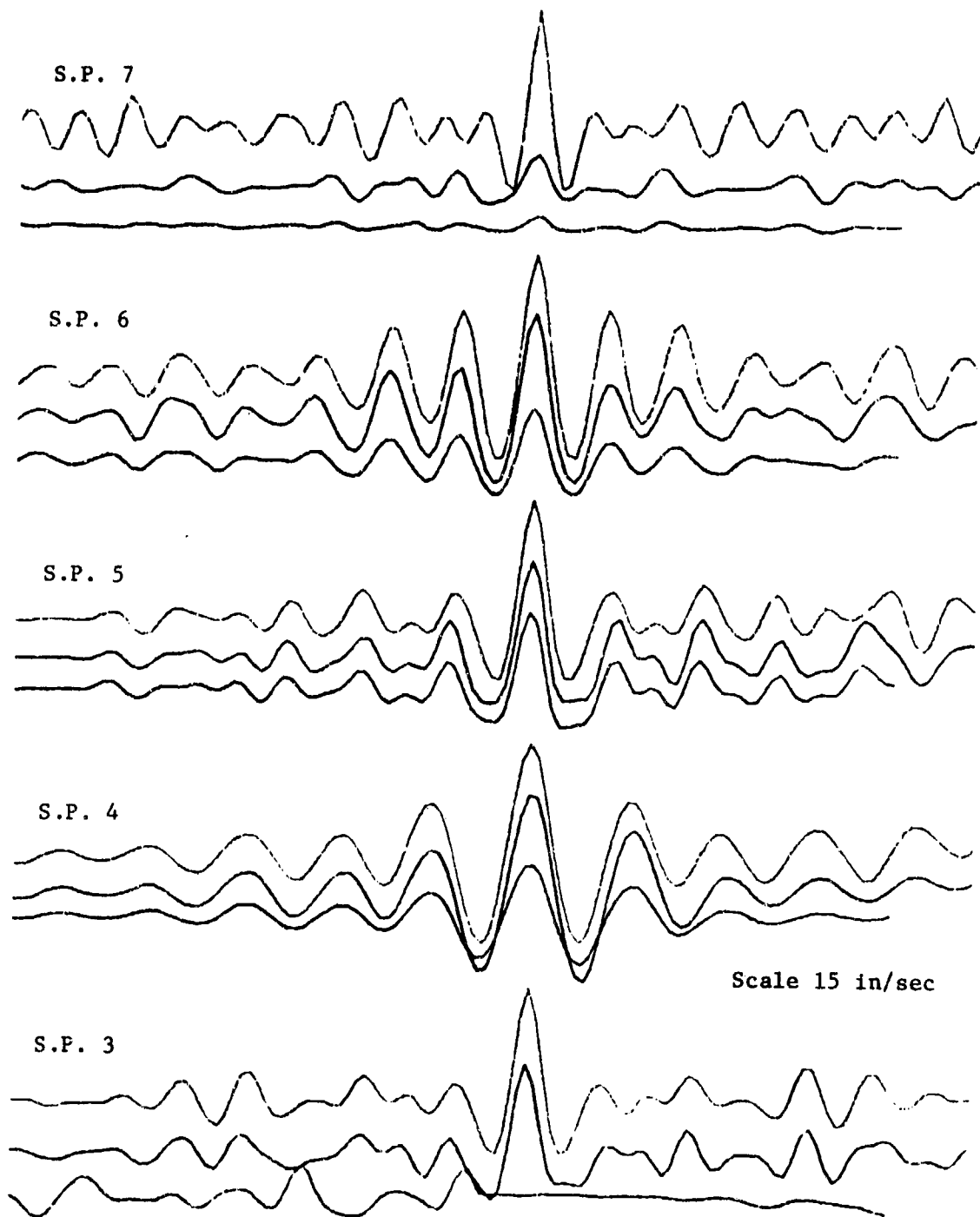


FIGURE 32. OVERLAY OF SEISMIC CORRELATION FUNCTIONS FROM RECOIL AND EXPLOSION EVENTS RECORDED AT THE SAME POSITION. TOP TRACE EV. 11 (EXPLOSION) WITH EV. 11, MIDDLE EV. 38 (RECOIL) WITH EV. 11. BOTTOM EV. 37 (RECOIL) WITH EV. 11.

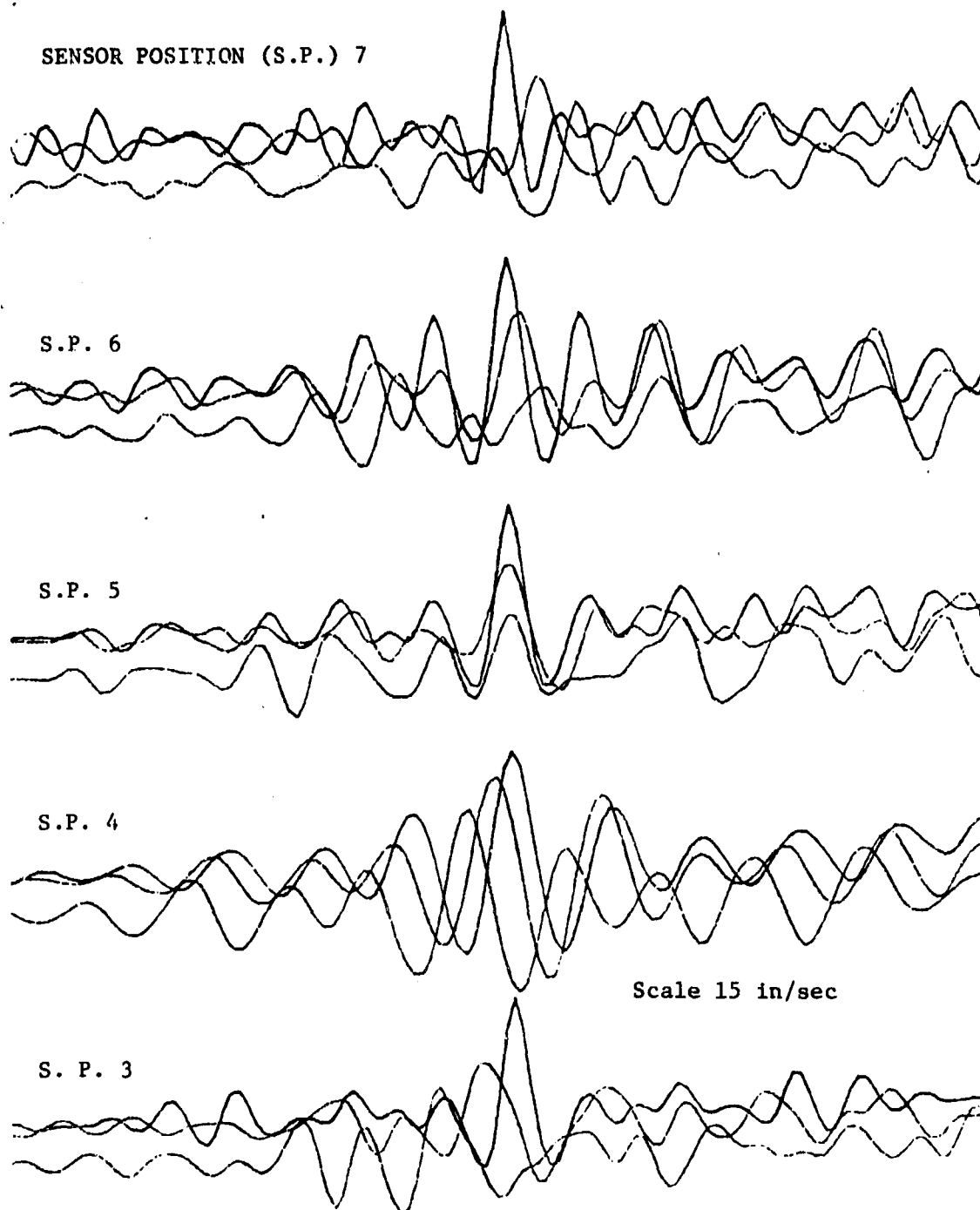


FIGURE 33. OVERLAY OF SEISMIC CORRELATION FUNCTIONS SHOWING CHANGES IN ALIGNMENT FOR SELECTED SENSOR POSITIONS. TOP TRACE EV. 11 WITH EV. 11, MIDDLE TRACE EV. 10 WITH EV. 11, BOTTOM EV. 9 WITH EV. 11, SEPARATIONS 0, 50, 125 METER, RESPECTIVELY.

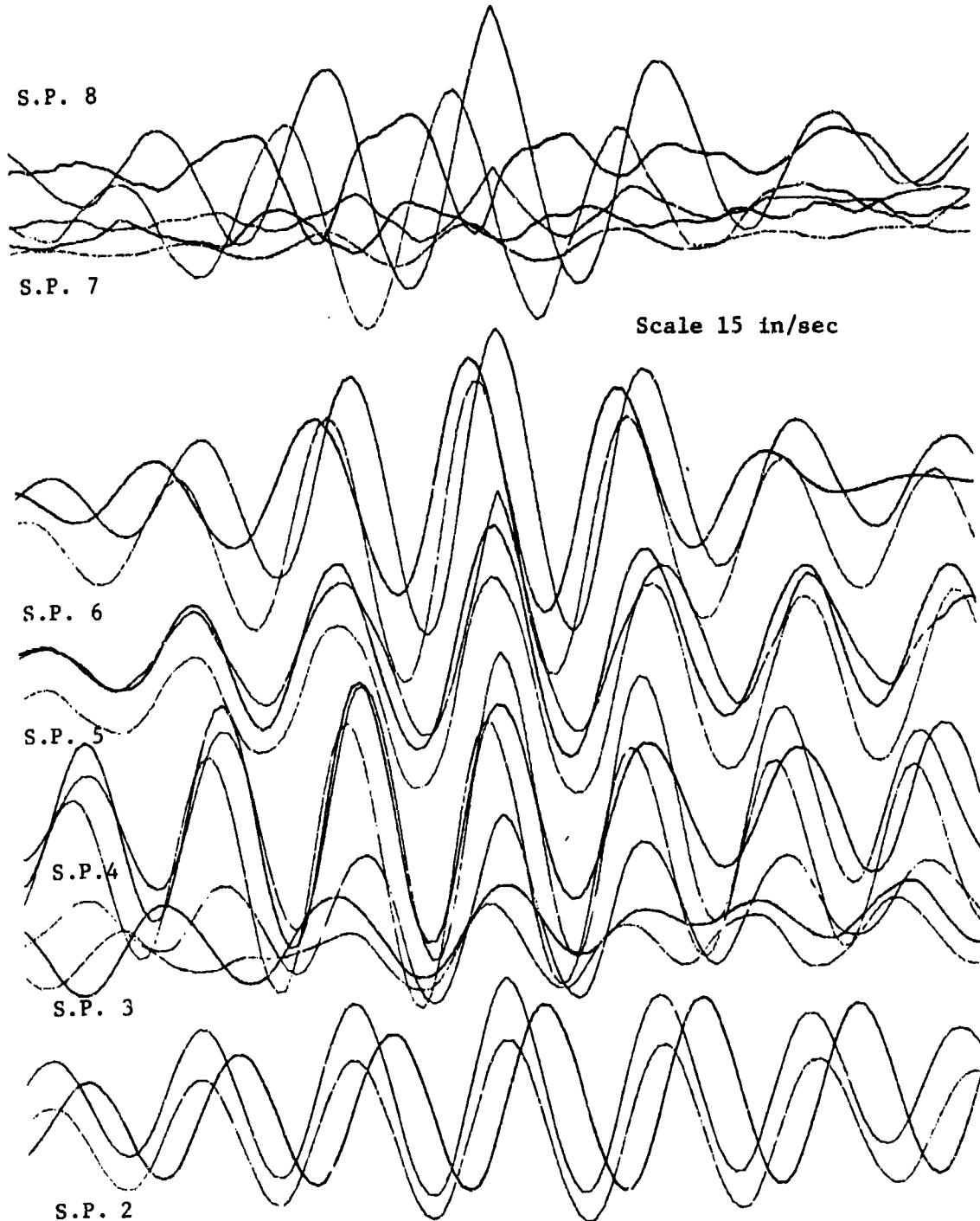


FIGURE 34. OVERLAY OF SEISMIC CORRELATION FUNCTIONS SHOWING CHANGES IN ALIGNMENT FOR SELECTED SENSOR POSITIONS. TOP TRACE EV. 22 WITH EV. 22, MIDDLE EV. 24 WITH EV. 22. BOTTOM EV. 23 WITH EV. 22, SEPARATIONS 0, 125, 50 METERS RESPECTIVELY.

with greater path differences. Note that the proper alignment does not always involve the peak of each trace, that is the peak correlation cannot be used exclusively for purposes of obtaining event time difference. Examination of the computer selected peak confirmed it to be an unreliable method. In order to obtain the estimated relative lag times between recoil and impact we were forced to make visual examination of correlation function sets. While such analysis would not lend itself easily to auto processing it may be possible to develop suitable programs.

Seismic correlation functions and signature data are given in Appendix B.

6.5 CALCULATION OF LOCATION ESTIMATES

The method of differences algorithms (seismics on seismics) was modified to accept the processed field data rather than simulated times. The program continued to allow for sensor position and return fire errors. Location estimates were made sequentially but without any dependent adaptive structure.

Location estimates were obtained for each mortar firing position using the individual explosion (calibrating) data. Estimates were calculated using relative times based on acoustic and seismics arrival picks and correlation alignment and were averaged over the sensor array. Computer output is summarized in Tables 6 through 10 which give event number, separation distances, and location error. The seismic times from correlation in general, produced very poor results probably due to picking the incorrect correlation peak. Outside of path velocity variants, the correlation time differences should smoothly increase or decrease from sensor to sensor. When analyzed, these times were found to be often erratic which could easily increase the measurement error. Times were smoothed to principal trends independent of actual path distances. Location errors resulting from rerunning this data are listed in Tables 11 and

TABLE 5
 LOCATION ESTIMATES FROM SEISMIC AND ACOUSTIC DATA
 TWENTY NINE PALMS, 1.0 km SITE*

Event	Separation Distance (m)	Location Estimate Based on First Seismic Arrival (x,y)	Error (m)	Location Estimate Based on Seismic Times from Correlation (x,y)	Error (m)	Location Estimate Based on Acoustic Arrival (x,y)	Error (m)
1	250	989,897	104	1085,1262	275	1086,1253	267
3	125	774,488	559	987,1022	25.8	996,963	37.6
5	250	1027,1079	83	559,1145	464	921,1184	201
7	125	732,1418	497	1152,651	380	1004,961	39.0
8	125	1368,598	545	1221,721	356	1003,1022	22.4
9	125	1560,643	664	845,495	528	1019,911	90.7
10	50	1007,1025	25.7	759,413	634	1014,1022	26.1
13	125	1190,894	217	1008,1422	422	1070,1298	306
15	50	1208,792	294	1058,1004	51.7	981,1004	19.5
16	125	1109,794	233	733,1701	750	989,1014	17.7
19	125	1549,386	824	993,1296	296	952,1192	198
20	125	1219,350	266	471,1790	951	975,1112	114
21	250	1144,728	307	1176,618	421	933,990	67.8

*Calculations made with no sensor and return fire errors.

TABLE 6
 LOCATION ESTIMATE FOR TWENTY NINE PALMS DATA
 1.5 km Site

Event	Separation Distance (m)	Location Estimate From First Seismic Arrival		Location Estimate From Correlation		Location Estimate From Acoustic Wave	
		(x,y)	Error (m)	(x,y)	Error (m)	(x,y)	Error (m)
23	64	--,--	--	1076,1508	82.2	999,1521	18.8
24	131	1407,2113	703	228,1787	336	1018,1557	24.4
63	253	681,701	898	858,1242	330	974,1696	158
64	131	870,1161	401	1056,1349	199	994,1654	114
65	103	942,1584	73	1029,1397	146	1006,1601	60.9
66	156	883,1558	119	1422,1324	474	988,1604	65.2
67	156	816,926	641	1188,1695	244	990,1547	12.6
68	101	850,993	567	1095,1828	303	1007,1600	60.0
69	253	1806,2506	1258	1264,1867	420	1030,1643	108
70	165	838,1123	447	1149,1618	165	998,1588	48.2
71	290	793,1239	366	967,1292	250	1000,1498	42.1
72	290	862,702	903	--,--	--	1009,1521	20.9
73	133	1181,1792	310	929,1712	186	980,1118	423
74	85	1318,2209	741	857,1537	143	1013,1556	20.6
75	210	3009,7247	6050	791,1652	237	1001,1633	93.2
76	327	1002,1566	26.3	1273,1890	444	--,--	--
77	327	1353,3722	2211	1041,1751	215	968,1640	106
42	0.0	--,--	--	984,1425	116	1015,1614	75.5
44	0.0	--,--	--	1000,1540	0	1013,1573	36.0
46	0.0	--,--	--	987,1483	58.9	968,1533	33.1

TABLE 7
LOCATION ESTIMATED FROM SEISMIC AND ACOUSTIC DATA - CAMP PENDLETON 108, 108A SITES*

Event	Separation Distance (M)	Location Estimate Based on First Seismic Arrival (x,y)	Location Estimate Based on First Seismic Arrival (x,y)	Error (M)	Error (M)	Location Estimate Based on First Seismic Arrival (x,y)	Error (M)
104	50	4849, 7150	1847, 11472	2378		1847, 11472	2919
105	125	811, 10233	-1080, 16002	2776		-1080, 16002	8308
109	462	4262, 8446	-14099, 26632	1112		-14099, 26632	24800
114	125	4069, 8153	2270, 10823	1114		2270, 10823	2148
115	248	4788, 7848	1268, 12279	1868		1268, 12279	3907
117	125	3087, 8903	-1293, 16304	167		-1293, 16304	8678
124	50	4304, 7962	3983, 7377	1417		3983, 7377	1700
127	125	3977, 8297	3814, 7747	950		3814, 7747	1294
128	375	3014, 9313	-9878, 24862	467		-9878, 24862	20659
129	350	3529, 8758	-10133, 25083	316		-10133, 25083	20992
130	279	4092, 8397	-7742, 23303	985		-7742, 23303	18110
131	255	3754, 8636	-6850, 22770	572		-6850, 22770	17149
132	217	4507, 7864	-5275, 21136	1635		-5275, 21136	14904
133	184		-4410, 20072			-4410, 20072	13537
134	125	3221, 8988	-2468, 18477	81.7		-2468, 18477	11145
137	300	4560, 7970	-7378, 23029	1611		-7378, 23029	17671
155	0.0		3258, 8949			3258, 8949	36.2
156	0.0		3193, 8940			3193, 8940	66.0
159	0.0		3205, 8943			3205, 8943	56.7
164	250		3162, 9005			3162, 9005	129
176	690	3220, 8448	2988, 8506	470		2988, 8506	486
177	561	3272, 8279	2872, 7852	634		2872, 7852	1128
178	430		3421, 8594			3421, 8594	361

*Calculations made with no sensor position and return fine errors.
Since No. seismic mortar signals from these sites were very poor. An explosion (103) at 108A was used to simulate the mortar signature.

TABLE 8
 COMPARISON OF LOCATION ERRORS WITH AND WITHOUT SIMULATED SENSOR POSITION AND
 RETURN FIRE ERRORS. Twenty Nine Palms Data, 1.5 km Site*

Event	Separation Distance (m)	Location Error Using 1st Arrival (m)		Location Error Using Correlations		Location Error Using Acoustic Data	
		With	Without	With	Without	With	Without
23	64	--	--	86.3	82.2	64.2	18.8
24	131	3717	703	356	336	24.2	24.4
63	253	933	898	318	330	166	158
64	131	5297	401	207	199	141	114
65	103	85	73	156	146	37.9	60.9
66	156	126	119	470	474	80.2	65.2
67	156	684	641	324	244	8.8	12.6
68	101	617	567	377	303	99.2	60.0
69	253	1296	1258	431	420	96.9	107.5
70	165	467	447	163	168	38.8	48.2
71	290	357	366	254	250	29.8	42.1
72	290	901	903	--	--	22.2	20.9
73	133	298	310	121	186	413	423
74	85	773	741	145	143	41.8	20.6
75	210	6203	6050	217	237	91.6	93.2
76	327	23.2	26.3	394	444	--	--
77	327	2328	2211	256	215	113	106
42	0.0	--	--	139	116	93.1	75.5
44	0.0	--	--	34.9	0.0	70.1	36.0
46	0.0	--	--	62.1	58.9	57.5	33.1

*Sensor position error $\sigma_S = 10m$, return fire errors $\sigma_D = 7.2$, $\sigma_R = 22.7$

TABLE 9
 LOCATION ERRORS USING CORRELATION DATA WHICH HAS BEEN PERTURBATED,
 TWENTY NINE PALMS, 1.5 km SITE*

<u>Event</u>	<u>Location Error With Perturbated Data (m)</u>	<u>Location Error As in Table 7 (m)</u>
23	112	82.2
24	370	336
63	246	330
64	66	199
65	38	146
66	430	474
67	322	244
68	332	303
69	526	420
70	231	168
71	117	250
72	---	---
73	310	186
74	265	143
75	423	237
76	577	444
77	358	215
42	16.1	116
44	---	0
46	---	58.9

*Perturbation sequence Pos. 2 + 3ms., Pos. 4 - 3ms, Pos. 6 + 3ms,
 Pos. 7 - 3ms

TABLE 10
 LOCATION ESTIMATES FROM SEISMIC DATA WITH SMOOTHING
 TWENTY NINE PALMS SITE (1.0 km site)

<u>Event</u>	<u>Separation Distance (m)</u>	<u>Location Estimate (x,y)</u>	<u>Error (m)</u>
1	250	1086,1253	267
3	125	996,963	37.6
5	250	921,1185	201
7	125	1004,961	39.0
8	125	1003,1022	22.4
9	125	1019,911	90.7
10	50	1014,1022	26.1
13	125	1031,1537	538
15	50	981,1004	19.5
16	125	706,1697	757
19	125	952,1192	198
20	125	975,1112	114
21	250	1182,632	411

TABLE 11

 LOCATION ESTIMATES FROM SEISMIC DATA WITH SMOOTHING
 TWENTY NINE PALMS SITE (1.5 km site)

<u>Event</u>	<u>Separation Distance (m)</u>	<u>Location Estimate (x,y)</u>	<u>Error (m)</u>
23	64	1075,1508	81.7
24	131	1228,1787	33.6
63	253	857,1242	330.5
64	131	952,1760	225
65	103	933,2131	594
66	156	1138,2189	664
67	156	1194,2025	523
68	101	975,1614	78.1
69	258	1277,1870	431
70	165	1168,1666	210
71	290	958,1716	180
73	133	928,1712	188
74	85	868,1399	193
75	210	979,1098	443
76	327	1234,2334	827
77	327	842,2683	1154

12. Results were improved especially at the 1.0 km site at Twenty Nine Palms.

6.6 DISCUSSION OF RESULTS

While the location errors presented in this analysis are not encouraging, they help point out some of the problems in using a seismic approach. The basic difficulty is finding a technique to make accurate measurements of the time difference. Using simulated sensor position and return fire errors did not greatly affect the results. It seems reasonable to conclude that the prime reason for large location errors was due to inaccuracies in timing the seismic signals and perhaps variations in seismic velocity within the near region around each mortar firing position as defined by the star cluster of explosion sites.

The location algorithm was simulated as discussed in section 3 under the assumptions of constant near velocity and a timing measurement error σ_T which was proportional to the separation distance between the enemy mortar and return fire impact.

In the simulation process as improved location estimates were made, the measurement errors for the next return shot were reduced allowing convergences to the desired position. As values of σ_T were increased the convergence process required an additional number of return rounds and more frequently did not converge at all. A value of $\sigma_T = 10$ ms. was found to be necessary to have acceptable results. Since the actual velocities were about twice those used for purposes of simulation, the acceptable value of σ_T could be nearer to 5 ms. When simulations were made without the latter assumption, changes of convergence were greatly reduced. In this case the multiple shot advantage is reduced to statistical improvement of an average location estimate. Convergence is by improvement of an average rather than by error reduction.

Examination of the tables of location errors seems to indicate that the measurement error is not related to separation. The measurement error which occurs with real data is a combination of both error in technique and error due to variations as a result of the local geology. In particular the signal may show slight changes in frequency, amplitude, and phase velocity which would contribute to the error in measuring time differences.

Using the first seismic arrival as a means of measuring relative time difference gave generally poorer results than using correlation. The actual first arrival is difficult to identify because of low signal levels. The calculated first arrival travel times when combined with known surface path lengths did not yield constant velocities. First arrival velocities for the Twenty Nine Palms data were about 1800 m/sec and exhibited several percent variation in travel time to the same sensor as between shots with corresponding minor changes in path length.

The acoustic time delays produced superior location estimates to those based on seismic first arrivals mainly because acoustic arrivals could be easily identified to within one or two samples (3 to 6 ms). Acoustic velocities while affected by met conditions, are perhaps fairly uniform at these short ranges. Acoustic time differences were six times larger than the seismic and therefore less sensitive to measurement error in determining location estimates.

Cross correlation of the seismic signature is considered to be better than using first arrivals but is not without problems and limitation which require further study. The seismic surface waves were observed to have a principal frequency content between 20 and 30 hertz. At greater ranges principal frequencies would be expected to be lower due to selective absorption and dispersions. The signals and their correlation are largely sinusoidal. For this reason it is difficult to pick the proper correlation peak for best signal alignment. Use

of the maximum peak was found to be completely unreliable since such peaks had often only slightly greater amplitude than other lags. A single cycle error in alignment can represent a 30 to 50 ms error which is unacceptable. If proper alignment could be achieved a measurement error of 3 to 10 ms could be expected at a sampling rate of 300 samples per second. A higher rate would tend to reduce this error.

This improvement in location accuracy that was achieved by smoothing the time differences for the 1.0 kilometer site at Twenty Nine Palms shows that some method is needed which collectively aligns all sensor signals simultaneously. The poor results achieved otherwise indicates that correlation by itself is not adequate. While it is now known why the same smoothing process did not improve results at the 1.5 kilometer site it is recognized that the time differences were much less and therefore were sensitive to alignment errors. In this case, a greater sensor spacing (base) may be required to achieve the same degree of location accuracy.

It should also be mentioned that location estimates were based upon an average of all possible sensor solutions and therefore if certain time differences were in great error they would tend to throw off the entire estimate. Some improvement might result if a weighted geometric average rather than an arithmetic average were used to make the estimate. Missing sensor data are indicated in the tables of Appendix B.

While the field data was not processed to be used with the hyperbolic location algorithm, the results of using this location techniques would not likely be an improvement over those estimates reported above. The basis for this conclusion is mainly due to the fact that greater correlation of seismics was observed between shots than between sensors.

In summary, it is felt that significant advances must be made in the methods of observing seismic time delays before the advantages of a seismic location system can be realized.

CONCLUSIONS AND RECOMMENDATIONS

The following conclusions and recommendations are made after completing this study of seismic mortar location.

7.1 GENERAL CONCLUSION

While this study found some promising characteristics of a seismic mortar location concept sufficient limitations at this point of development will require further exploratory development to resolve before beginning any advance development work.

7.2 SPECIFIC CONCLUSIONS

Range Limitations - Under quiet background conditions at Twenty Nine Palms seismic signals with low noise levels were observed from 81 mm mortar recoil to a range of about 1800 meters. Events at greater ranges were planned for the field measurements program but were not completed because of time and windy conditions. It is felt that seismic signals from recoil could be observed to ranges of 3000 meters under quiet conditions. The use of signal enhancement techniques could double this range. At Camp Pendleton under high background noise conditions generated by base activities reliable seismic signals from mortar recoil could not be observed at 500 meters range. While loss of signal could be due in part to path effects and energy coupling problems, low signal levels were likely due to the high noise levels. Required field gains were 20 dB greater at Camp Pendleton than at Twenty Nine Palms.

System Design Problems - Although only a cursory examination of system design was made no serious problems could be identified which would not allow building a system with off the shelf technology.

Basic Information Requirements - The essential input information needed to establish mortar locations using seismics includes positions, impact positions of directed fire, and the seismic signature. Of primary importance is the use of directed fire for calibration and ranging. Thus, this study could not find any practical means of obtaining necessary calibration information covertly.

Signal Characteristics - Seismic surface waves (Rayleigh waves) as observed on a vertical axis seismometer were found to have the largest amplitudes. These surface wave signals were identical for recoil and explosion events. Also shots fired in the vicinity of a mortar position showed a great deal of similarity as did the corresponding cross correlation functions.

Algorithms - Of the two algorithms investigated the method of relative differences (seismics on seismics) appears to be the most promising for a small light-weight system concept.

Location Accuracies - Location accuracies produced by utilization of field data were generally disappointing for the seismic data. The acoustic data appears at the short ranges under consideration to produce superior location estimates. Such differences could be attributable to the fact that the seismic velocities were five to six times faster than the velocity of sound. The higher velocity media implies a greater sensitivity to timing errors. Some difficulty was found in timing the seismic waves. The use of peak correlation was found to be an unreliable means. Location errors obtained from timing seismic waves were not related to the separation distance between a known impact and location of an enemy recoil. The timing error was apparently not related directly to the separation distance between recoils and impacts as expected.

The location estimates made using acoustical and seismic data recorded at Camp Pendleton were not useful. The poor quality of these estimates may be attributable in part to the high noise levels and frequent interfering sources from base activities.

7.3 GENERAL RECOMMENDATION

It is recommended that further exploratory work be considered for development of a light weight man packed seismic system. The system concept should be expanded to targets other than mortars and should fully exploit the use of acoustic signals as well as the seismic.

7.4 SPECIFIC RECOMMENDATIONS

1. Investigate and evaluate using existing data methods of signal enhancement which would be applicable to this system concept. Project maximum effective range for various targets.
2. Determine surveillance capabilities of the seismic-acoustic location system against such battlefield targets as trucks, tanks and a walking man.
3. Investigate and evaluate means of signal processing which will produce accurate signal timing information.
4. Investigate methods of improving the signal to noise of the seismics by analyzing the collected data in the frequency domain.
5. Investigate the use of acoustics for location as well as the advantages of seismic for identification or discrimination of a mortar recoil from a shell impact.

REFERENCES

1. Hemdal, J. F., An Investigation of Factors Affecting Sound Ranging: Literature Search and Analysis, Final Report 6400-209-T, University of Michigan, Geophysics Laboratory, Willow Run Laboratories, June 1970.
2. Haskell, N. A., The Dispersion of Surface Waves on Multilayered Media, Bull. Seism. Soc. Amer., Vol. 43, No. 17, 1953.
3. Clark, S. P., Jr., Editor, Handbook of Physical Constants, Revised Edition, The Geological Society of America, Inc., 1966.
4. Sorenson, H. W., Kalman Filtering Techniques, Advances in Control Systems, Vol. 3, C. T. Leondes, Editor, Academic Press, 1966.



APPENDIX A

FORTRAN Listing of Simulation Algorithms:

1. Hyperbolic Location with Kalman filter.
2. Subprograms to the Hyperbolic Location Algorithm.
3. Location Algorithm using the Seismics or Seismic technique (subroutine k4).
4. Histogram: Same location simulation as (3) but designed to make many iterations and printout a histogram of location errors.



```
C
C PROGRAM TO LOCATE TARGET MORTAR FIRE POSITION THROUGH A SUCCESSION OF
C APPROXIMATIONS UTILIZING TARGET FIRE AND N SENSOR LOCATIONS
C
C      VARIABLES USED BY PROGRAM
C
C ISW      SWITCH=1 FOR FIXED SENSORS,=1 FOR FIRE SENSORS AROUND POINT
C X(J),Y(I) ACTUAL SENSOR LOCATION COORDINATES RELATIVE TO COMPUTER POSITION
C XA,YA    APPROXIMATION OF FIRING POINT
C XP,YP    ACTUAL FIRING LOCATION
C XR,YR    RETURN FIRE SOURCE
C SS      STANDARD DEVIATION FOR ERRORS IN DISTANCE MEASUREMENTS
C ST      STD DEV FOR TIME MEASUREMENTS
C SD      STD DEV FOR DEFLECTION IN RETURN FIRE
C SR      STD DEV FOR RANGE IN RETURN FIRE
C
C VE(I)    ESTIMATED PATH VELOCITIES
C VR(I)    ACTUAL PATH VELOCITIES
C XE(J),YE(I) MEASURED SENSOR LOCATIONS
C DT(I)    DIFFERENCE IN ARRIVAL TIME BETWEEN SENSORS I & I-1
C DTP(I)   DIFFERENCE WITH ERROR TERM
C XI,YT    IMPACT POINT OF RETURN FIRE
C ER      RANGE ERROR
C EP      DEFLECTION ERROR
C TR      ADJUSTED TIME TO SENSOR FROM IMPACT
C KMAX     ITERATION LIMIT
C DJM,W(I) WORK AREAS
C K        ITERATION COUNTER
C H(I,J)   BASIC KALMAN MATRIX
C Z(I)     KALMAN MEASUREMENT VECTOR
C V(I)     KALMAN STATE VECTOR
C R(T)     DIAGONAL SCALAR COVARIANT ERROR MATRIX
C
C
C
C      D(A,B,W,Z)=SQRT((A-W)*(A-W)+(B-Z)*(B-Z))
C      DIMENSION X(20),Y(20),XE(20),YE(20),DT(20),DTE(20),VE(20),VR(20),
C      $,W(20),V1(20),H(20,20),R(20,20),V(20),Z(20),PINV(20,20),P(20,20)
C      $,DT(20),DP(20),T(20),AA(3),BB(3),CC(3),DD(2)
C      $,XT(17),YT(17)
C      COMMON PINV
C      DATA PJ,R,H/3.1415926535,600*0./
C      DT(1)=.
C      DTE(1)=0.
C
C INITIALIZE NORMALIZED RANDOM NUMBER GENERATOR
C
```

```

CALL TIME(7,0,INIT)
INIT=INIT*2+1
CALL GRAND1(INIT)

C
C INPUT VELOCITIES AND STANDARD DEVIATIONS
C
  READ (5,450) N,KMAX,IMP,ISK
  IF (N.GT.8) GOTO 900
  READ (5,400) (V1(I),I=1,N)
C PROVIDE FOR 1 ESTIMATE OF ALL PATH VELOCITIES
  IF (V1(2).NE.0.) GOTO 15
  DO 16 IT=2,N
16 V1(IT)=V1(1)
15 READ (5,400) (VP(I),I=1,N)
17 READ (5,400) SS,ST,XP,YF,XA,YA,SR,SD,RR,DEL
  READ (5,400) XP,YR
  DO 11 J=1,N
11 READ (5,400) (PINV(I,J),I=1,N)
  IF (ISK.EQ.0) GOTO 5

C
C FIRE SENSORS IN PATTERN AROUND ESTIMATED FIRING LOCATION
C
  READ (5,400) SDFI
  Y(1)=XA+SDFI
  Y(1)=YA
  Y(2)=X(1)
  Y(2)=YA+SDFI
  X(3)=XA
  Y(3)=Y(2)
  X(4)=XA-SDFI
  Y(4)=Y(2)
  X(5)=X(4)
  Y(5)=YA
  X(6)=Y(4)
  Y(6)=YA-SDFI
  X(7)=XA
  Y(7)=Y(6)
  X(8)=X(1)
  Y(8)=Y(6)

C
C FIND ACTUAL SENSOR LOCATIONS
C
  DO 4 I=1,N
  ER=GRAND(SR,0.)
  ED=GRAND(SD,0.)
  PHT=ATAN((X(I)-XP)/(Y(I)-YR))

```

Reproduced From
Best Available Copy

```

IF (PHI.LT. . .) PHI=PI+PHI
PP=PT/2.-PHI
XF(I)=PI*SIN(PHI)+PD*SIN(PP)+X(I)
4 YF(I)=PD*COS(PHI)+PD*CCS(PP)+Y(I)
GOTO 6
C
C READ IN FIXED SENSOR LOCATIONS
C
C
5 READ (5,400) ((X(I),Y(I)),I=1,5)
IF (N.GT.5) READ (5,400) ((X(I),Y(I)),I=6,N)
DO 10 I=1,N
VF(I)=GRAND(SS,X(I))
10 YF(I)=GRAND(SS,Y(I))
C
C SET UP CONSTANTS
C
6 N=N-1
COV=1./PS
DO 12 I=1,PS
12 Z(I,I)=COV
C
C GENERATE ARRAY OF TARGET POINTS FOR INITIAL RETURN FIRE
C
003 XT(1)=XA
YT(1)=YA
STEP=DEL
DO 110 I=1,2
XT(I+1)=XA+STEP
YT(I+1)=YA
XT(I+2)=XT(1)
YT(I+2)=YA+STEP
XT(I+3)=XA
YT(I+3)=YT(1)
XT(I+4)=XA-STEP
YT(I+4)=YT(1)
XT(I+5)=XT(1)
YT(I+5)=YA
XT(I+6)=XT(1)
YT(I+6)=YA-STEP
XT(I+7)=XA
YT(I+7)=YT(1)
XT(I+8)=XT(1)
YT(I+8)=YT(1)
STEP=STEP+DEL
IF (TMP.LT. 10) GOTO 120
110 CONTINUE
    
```

```

12) CONTINUE
C
C CALC DELTA T'S FOR INITIAL RECOIL DATA
C
      W(1)=D(X(1),Y(1),XF,YF)
      T(1)=W(1)/VR(1)
      DO 20 I=2,N
      W(I)=D(X(I),Y(I),XF,YF)
      T(I)=W(I)/VR(I)
20  DT(I)=T(I-1)-T(I)
      DT(1)=T(N)-T(1)
      DO 13 I=1,N
      V(I)=1./V1(I)
13  VR(I)=V1(I)
      K=0
      WPITP(6,100) XF,YF,XA,YA,SS,ST,SR,SD
      WRITP(6,150) ((I,X(I),Y(I),XE(I),YE(I),VR(I),V1(I),DT(I)),I=1,N)
      DO 21 I=1,N
21  DTE(I)=DT(I)+GRAND(ST,C.)
      WRITE(6,250) ((I,DTE(I)),I=1,N)
C
C IMPROVE VELOCITY ESTIMATES THROUGH MULTIPLE IMPACTS
C
      I=0
      DO 131 I=2,IMP,2
      ER=GRAND(SR,C.)
      ED=GRAND(SD,C.)
      PHI=ATAN((XT(I)-XR)/(YT(I)-YR))
      IF (PHI.LT.C.) PHI=PHI+PI
      PP=PI/2.-PHI
      XI=ER*SIN(PHI)+ED*SIN(PP)+XT(I)
YI=ER*COS(PHI)+ED*COS(PP)+YT(I)
C
160 ER=GRAND(SR,C.)
      ED=GRAND(SD,C.)
      PHI=ATAN((XT(I-1)-XR)/(YT(I-1)-YR))
      IF (PHI.LT.C.) PHI=PHI+PI
      PP=PI/2.-PHI
      XII=ER*SIN(PHI)+ED*SIN(PP)+XT(I-1)
      YII=ER*COS(PHI)+ED*COS(PP)+YT(I-1)
      IF (XI.EQ.XII.AND.YI.EQ.YII) GOTO 160
C
C FIND TRAVEL TIMES AND VELOCITIES FROM EACH IMPACT TO EACH SENSOR
C
      DI(1)=D(X(1),Y(1),XI,YI)
      DP(1)=D(X(1),Y(1),XII,YII)
    
```

Reproduced From
Best Available Copy

```

DO 140 J=2,N
DT(J)=D(X(J),Y(J),XI,YI)
DP(J)=D(X(J),Y(J),XTT,YTT)
Z(J-1)=DP(J-1)/VF(J-1)-DT(J)/VR(J)+GRAND(ST,2.)
Z(N+J-1)=DP(J-1)/VR(J-1)-DP(J)/VF(J)+GRAND(ST,2.)
H(J-1,J-1)=D(XT(J-1),YF(J-1),XT(I),YT(I))
H(J-1,J)=D(XF(J),YF(J),XT(I),YT(I))
H(N+J-1,J-1)=D(XF(J-1),YF(J-1),XT(I-1),YT(I-1))
H(N+J-1,J)=D(XF(J),YF(J),XT(I-1),YT(I-1))
140 CONTINUE
CALL KALMAN(T,V,Z,D,R,2*N,N)
L=L+2
DO 130 J=1,N
130 VF(J)=1./V(J)
WRITE(6,600) L
WRITE(6,350)((J,VF(J)),J=1,N)
131 CONTINUE
C
C USE BETTER VELOCITIES AND RECOLL INFO FOR NEW POINT ESTIMATE
C
25 K=K+1
IF(K.GT.KMAX) GOTO 900
C
C GET APPROXIMATION OF TARGET POSITION
C USING EACH PAIR OF POINTS GET ESTIMATE FOR AVERAGING
C
L=L+1
VR=L
YR=L
YR=L
DO 30 I=2,N
CALL HLOC(XF(I-1),YF(I-1),VF(I-1),DDE(I),XA,YA,XL,YL,83)
YR=YR+YL
YR=YR+YL
L=L+1
30 CONTINUE
C
C 2 SPECIAL CASES
C
AA(1)=XF(N-1)
AA(2)=XF(N)
AA(3)=XF(1)
BB(1)=YF(N-1)
BB(2)=YF(N)
BB(3)=YF(1)
CC(1)=VF(N-1)
CC(2)=VF(N)

```

Reproduced From
Best Available Copy

```

        CC(3) =VF (1)
        DD(1) =DTE (N)
        DD(2) =DTI (1)
        CALL HLOC(AA,BB,CC,DD,XA,YA,XL,YL,&B1)
        XB=XB+XL
        YB=YB+YL
        L=L+1
    C
31  AA(1) =VF (N)
    AA(2) =VF (1)
    AA(3) =VF (2)
    BB(1) =VF (N)
    BB(2) =VF (1)
    BB(3) =VF (2)
    CC(1) =VF (N)
    CC(2) =VF (1)
    CC(3) =VF (2)
    DD(1) =DTE (1)
    DD(2) =DTI (2)
    CALL HLOC(AA,BB,CC,DD,XA,YA,XL,YL,&B2)
    XB=XB+XL
    YB=YB+YL
    L=L+1
32  IF (L.EQ.0) GOTO 980
    XA=XB/L
    YA=YB/L
    C
    C DISPLAY NEW ESTIMATE
    C
        DUM=D(XA,YA,YF,YF)
        WRITE (6,200) K,L,XA,YA,DUM
    C
    C RANDOMLY DECIDE WHETHER NEW RECOIL DATA OR GET IMPACT DATA
    C
25  DUM=GRAND(1.,0.)
    IF (DUM.GT.0.) GOTO 36
    C
    C GENERATE IMPACT DATA FOR (XA,YA)-GET IMPACT POINT
    C
80  K=K+1
    IF (K.GT.KMAX) GOTO 900
    SP=GRAND(SR,0.)
    SD=GRAND(SD,0.)
    PHI=ATAN((XA-XP)/(YA-YP))
    IF (PHI.LT.0.) PHI=PHI+PI
    DP=PI/2.-PHI
    
```

Reproduced From
Best Available Copy

```

        XI=ER*SIN(PHI)+ED*SIN(PD)+XA
        YI=ER*COS(PHI)+ED*COS(PD)+YA
    C
    C GENERATE IMPACT POINT FOR (XA+DEL,YA+DEL)
    C
        YB=YA+DEL
        YB=YB+DEL
        60 ER=GRAND(SD,1.)
        ED=GRAND(SD,1.)
        PHI=ATAN((XE-YE)/(YB-YE))
        IF (PHI.LT.0.) PHI=PHI+PI
        PD=PI/2.-PHI
        XII=ER*SIN(PHI)+ED*SIN(PD)+XB
        YII=ER*COS(PHI)+ED*COS(PD)+YB
        IF (XJ.EQ.XII.AND.YI.EQ.YII) GOTO 60
    C
    C FIND TRAVEL TIMES AND VELOCITIES FROM EACH IMPACT TO EACH SENSOR
    C
        DI(1)=D(X(1),Y(1),XI,YI)
        DP(1)=D(X(1),Y(1),XII,YII)
        DO 40 I=2,N
            DI(I)=D(X(I),Y(I),XI,YI)
            DP(I)=D(X(I),Y(I),XII,YII)
            Z(I-1)=DI(I-1)/VR(I-1)-DI(I)/VR(I)+GRAND(ST,1.)
            Z(N+I-1)=DP(I-1)/VR(I-1)-DP(I)/VR(I)+GRAND(ST,1.)
            H(I-1,I-1)=D(XE(I-1),YE(I-1),XA,YA)
            H(I-1,I)=-D(XE(I),YE(I),XA,YA)
            H(N+I-1,I-1)=D(XE(I-1),YE(I-1),XB,YB)
            H(N+I-1,I)=-D(XE(I),YE(I),XB,YB)
        40 CONTINUE
        CALL KALMAN(H,V,E,P,R,2*N,N)
        DO 50 I=1,N
            50 VE(I)=1./V(I)
            WRITE (6,300) N
            WRITE (6,350) ((I,VE(I)),I=1,N)
    C
    C GET NEW POINT ESTIMATE
    C
        L=0
        XB=0.
        YB=0.
        DO 70 I=2,N
            CALL HLOC(YE(I-1),YE(I-1),VE(I-1),DPE(I),XA,YA,XL,YL,870)
            YB=XB+YI
            YB=YB+YL
            L=L+1
        70 CONTINUE
    
```

C
C 2 SPECIAL CASES
C

```

AA(1) =XF(N-1)
AA(2) =XE(N)
AA(3) =XF(1)
BB(1) =YF(N-1)
BB(2) =YF(N)
BB(3) =YE(1)
CC(1) =VF(N-1)
CC(2) =VE(N)
CC(3) =VF(1)
DD(1) =DTE(N)
DD(2) =DTF(1)
CALL HLOC(AA, BB, CC, DD, XA, YA, XL, YL, &71)
XP =XB +YL
YF =YB +YL
L =I +1
    
```

C

```

71 AA(1) =XF(N)
AA(2) =XE(1)
AA(3) =XF(2)
BB(1) =YF(N)
BB(2) =YF(1)
BB(3) =YE(2)
CC(1) =VE(N)
CC(2) =VE(1)
CC(3) =VF(2)
DD(1) =DTE(1)
DD(2) =DTF(2)
CALL HLOC(AA, BB, CC, DD, XA, YA, XL, YL, &72)
XB =XB +XL
YB =YB +YL
L =L +1
    
```

```

72 IF (L.FO.) GOTO 981
XA =XB /L
YA =YB /L
    
```

C DISPLAY NEW APPROXIMATION

```

DUM =D(XA, YA, XF, YF)
WRITE (6, 210) L, XA, YA, DUM
GOTO 25
900 WRITE (6, 500)
909 CONTINUE
STOP 0
980 STOP 1
981 STOP 2
    
```

```

100 FORMAT ('ACTUAL SOURCE=',F8.1,',',F8.1,' FIRST ESTIMATE=',F8.1
$,',',F8.1/' SIGMA S=',F8.3,' SIGMA T=',F8.3,' SIGMA R=',F8.3
$,',',F8.3/' SIGMA D=',F8.3/'-',22X,' ACTUAL SENSOR   MEASURED SENSOR'
$,2X,'ACTUAL VELOCITY   INITIAL VEL. FST. DELTA T (RECOIL)')/
150 FORMAT (1X,I3,13X,F8.1,',',F8.1,4X,F8.1,',',F8.1,8X,F8.1,11X,F8.1
$,3X,F8.4)
200 FORMAT ('O ',I3,' RECOIL DATA--NEW ESTIMATE BASED ON ',I3
$,',',F8.1,5X
I,'DISTANCE TO SOURCE=',F8.2)
210 FORMAT ('O NEW ESTIMATE BASED ON ',I3
$,',',F8.1,5X
I,'DISTANCE TO SOURCE=',F8.2)
250 FORMAT ('O RECOIL DELTA W/ ERROR:'
$,/ (25X,I3,F12.4))
300 FORMAT ('O ',I3,' IMPACT DATA--NEW PATH VELOCITIES=')
350 FORMAT (25X,I3,F12.4)
400 FORMAT (10F8.2)
450 FORMAT (3I3)
500 FORMAT ('O STOP 0')
550 FORMAT ('I FUN # ',I2/)
600 FORMAT ('O INITIAL RESPONSE OF ',I3,' IMPACTS GIVING NEW PATH'
$,',',F8.1,5X
I,'DISTANCE TO SOURCE=',F8.2)
END
    
```

C
C
C
C

J

```

PROGRAM NO LOCATE POINT USING HYPERBOLIC FUNCTIONS WITH
METHOD OF STEEPEST DESCENT
    
```

```

SUBROUTINE HLOC(X,Y,V,T,XA,YA,XL,YL,*)
REAL*4 K
DIMENSION X(3),Y(3),V(3),T(2),DP(3),FX(2),FY(2),F(2)
XP=XA
YP=YA
K=10.
FACTK=2.
30 DP(1)=D(X(1),Y(1),XP,YP)
   DP(2)=D(X(2),Y(2),XP,YP)
   DP(3)=D(X(3),Y(3),XP,YP)
   DO 10 I=1,2
      G=V(I)/(V(I+1)*DP(I+1))
      FX(I)=(XP-X(I))/DP(I)-G*(XP-X(I+1))
      FY(I)=(YP-Y(I))/DP(I)-G*(YP-Y(I+1))
10  F(I)=DP(I)-V(I)*DP(I+1)/V(I+1)-T(I)*V(I)
      GX=2.*F(1)*FX(1)+2.*F(2)*FX(2)
      GY=2.*F(1)*FY(1)+2.*F(2)*FY(2)
      DF=D(GX,GY,0.,0.)
      XL=XP-K*GX/DF
      YL=YP-K*GY/DF
      FP=F(1)*F(1)+F(2)*F(2)
40  F(1)=D(X(1),Y(1),XL,YL)-V(1)*D(X(2),Y(2),XL,YL)/V(2)-T(1)*V(1)
      F(2)=D(X(2),Y(2),XL,YL)-V(2)*D(X(3),Y(3),XL,YL)/V(3)-T(2)*V(2)
      GL=F(1)*F(1)+F(2)*F(2)
      IF (GL.GE.GP) GOTO 20
      CALL STEP(XP,YP,XL,YL,XN,YN,K)
      XP=XL
      YP=YL
      XL=XN
      YL=YN
      GP=GL
      K=FACTK*K
      GOTO 40
20  K=K/2.
      FACTK=1.
      IF (K.GT..01) GOTO 30
      IF (GL.GT.5.) GOTO 90
      RETURN
90  RETURN 1
      END
    
```

Reproduced From
Best Available Copy

FIND END POINT OF DIRECTED VECTOR FROM (X1,Y1) THROUGH (X2,Y2)
WHICH IS DISTANCE K FROM (X2,Y2)

C

```

SUBROUTINE STEP(X1,Y1,X2,Y2,X3,Y3,K)
IMPLICIT REAL*4 (A-Z)
IF (X1.EQ.X2) GOTO 10
M=(Y2-Y1)/(X2-X1)
D=SQRT(K*K/(M**2+1))
X3=X2+D
IF (D*(Y2-X1).LT.0.) X3=X2-D
Y3=M*D+Y2
RETURN
10 X3=X2
   XK=K
   Y3=Y2+SIGN(XK,(Y2-Y1))
RETURN
END
    
```

C

C USE KALMAN FILTER TO FIND NEW VELOCITIES

C

```

SUBROUTINE KALMAN(H,V,Z,P,R,M,N)
COMMON PINV(20,20)
REAL*8 D1,D2
REAL*4 K
DIMENSION H(20,20),TP(20),V(20),Z(20),P(20,20),R(20,20),K(20,20)
$,HT(20,20),W1(20,20),W2(20,20),D1(20,20),D2(20,20)
CALL TRANS(H,HT,M,N)
CALL MULT(HT,P,W1,N,M,M)
CALL MULT(W1,H,W2,N,M,N)
DO 10 I=1,N
DO 10 J=1,N
PINV(I,J)=PINV(I,J)+W2(I,J)
10 D1(I,J)=PINV(I,J)
CALL MULT(H,V,W2,M,N,1)
CALL INV(N,20,D1,TP,20,D2)
DO 20 I=1,N
DO 20 J=1,N
20 P(I,J)=D2(I,J)
DO 30 I=1,N
30 W2(I,1)=Z(I)-W2(I,1)
CALL MULT(P,W1,K,N,M,M)
CALL MULT(K,W2,W1,N,M,1)
DO 40 I=1,N
40 V(I)=V(I)+W1(I,1)
RETURN
    
```

```

C
C SUBROUTINE TO MULTIPLY MATRICES
C
      SUBROUTINE MULT (A,B,C,L,M,N)
      DIMENSION A (20,20), B (20,20), C (20,20)
      DO 10 I=1,L
      DO 10 J=1,N
      C (I,J)=0.
      DO 10 K=1,M
      S=A (I,K) *B (K,J)
10  C (I,J)=C (I,J)+S
      RETURN
      END

C
C SUBROUTINE TO TRANSPOSE MATRICES
C
      SUBROUTINE TRANS (A,P,M,N)
      DIMENSION A (20,20), B (20,20)
      DO 10 I=1,N
      DO 10 J=1,M
10  B (I,J)=A (J,I)

      RETURN
      END

C
C SUBROUTINE TO SETUP ARRAYS FOR KALMAN FILTER OF RECOIL DATA
C
      SUBROUTINE KRESET (X,Y,H,XA,YA,XB,YB,N)
      DIMENSION X (10), Y (10), H (10,10)
      M=N-1
      DO 20 I=1,M
      A1=D (X (I), Y (I), XA, YA)
      A2=D (X (I+1), Y (I+1), XA, YA)
      X11= (XA-X (I)) /A1
      X22= (XA-X (I+1)) /A2
      Y11= (YA-Y (I)) /A1
      Y22= (YA-Y (I+1)) /A2
      H (I, I)=X11* (XB-XA) +Y11* (YB-YA) +A1
20  H (I, I+1)=X22* (XA-XB) +Y22* (YA-YB) -A2
      RETURN
      END

C
C HANDY DISTANCE FUNCTION
C
      FUNCTION D (A,B,W,Z)
      D=SQRT ((A-W) * (A-W) + (B-Z) * (B-Z))
      RETURN
      END
    
```

```

1      SUBROUTINE K4
2      D(A,B,W,Z)=SQRT((A-W)*(A-W)+(B-Z)*(B-Z))
3      REAL K
4      DIMENSION X(10),Y(10),XF(10),YF(10),TR(10),TI(10),CY(10)
5      S,S(10),C(10),SM(10),X2(2),Y2(2),K(2),X1(2),Y1(2),R(10,2)
6      DATA PI/3.1415926535/
7      READ (5,100) N,IKMAX
8      READ (5,150) ((X(I),Y(I)),I=1,5)
9      M=N-1
10     MI=M-1
11     IF (N.GT.5) READ (5,150) ((X(I),Y(I)),I=6,N)
12     READ (5,150) SS,ST,SR,SD,XA,YA,YF,YF,VR,VF,DEL,RO
13     IK=0
14     C
15     C INITIALIZE NORMALIZED RANDOM NUMBER GENERATOR
16     C
17     CALL TIME(7,0,INIT)
18     INIT=INIT*2+1
19     CALL GRAND1(INIT)
20     C
21     C GET RECOIL TIMES
22     C
23     DO 10 I=1,N
24     TR(I)=D(X(I),Y(I),XF,YF)/VR
25     XF(I)=X(I)+GRAND(SS,0.)
26     YF(I)=Y(I)+GRAND(SS,0.)
27     10 CONTINUE
28     MI=0
29     C
30     C RETURN FIRE TO (XA,YA)
31     C
32     50 IK=IK+1
33     IF (IK.GT.IKMAX) GOTO 90
34     IS=0
35     XT=XA+DEL
36     YT=YA+DFL
37     ER=GRAND(SR,0.)
38     ED=GRAND(SD,0.)
39     PHI=ATAN(YT/YX)
40     IF (PHI.LT.0.) PHI=PHI+PI
41     PP=PI/2.-PHI
42     XI=ER*SIN(PHI)+ED*SIN(PP)+XT
43     YI=ER*COS(PHI)+ED*COS(PP)+YT
44     DUMI=D(XF,YF,XI,YI)
45     XR=0.
46     YR=0.

```



```

1      SUBROUTINE HIST
2      D(A,B,W,Z)=SQRT((A-W)*(A-W)+(B-Z)*(B-Z))
3      REAL K
4      DIMENSION X(10),Y(10),XF(10),YF(10),TR(10),DT(10),DF(10)
5      F,S(10),C(10),SM(10),X2(2),Y2(2),K(2),XI(2),YI(2),B(10,2)
6      THIST(26)
7      DATA PI/3.1415926535/
8      READ (5,100) N
9      READ (5,150) ((X(I),Y(I)),I=1,5)
10     M=N-1
11     Y1=M-1
12     IF (N.GT.5) READ (5,150) ((X(I),Y(I)),I=6,N)
13     READ (5,150) SS,ST,SR,SD,XX,YY,XF,YF,VL,VR,DEL,DT
14     WRITE (6,250) XF,YF,XX,YY,SS,ST,SR,SD,VR,VE,DEL
14.25  WRITE (6,450) ((X(I),Y(I)),I=1,N)
15     DO 5 I=1,25
16     5 THIST(I)=0
17     DC 90 I0OP=1,200
18     XA=XX
19     YA=YY
20     IK=0
21     C
22     C INITIALIZE NORMALIZED RANDOM NUMBER GENERATOR
23     C
24     CALL TIME(7,0,INIT)
25     INT=INIT*2+1
26     CALL GRAND1(INIT)
27     C
28     C GET RECOIL TIMES
29     C
30     DC 10 I=1,N
31     TR(I)=D(X(I),Y(I),XF,YF)/VR
32     XF(I)=X(I)+GRAND(SS,0.)
33     YF(I)=Y(I)+GRAND(SS,0.)
34     10 CONTINUE
35     ML=0
36     C
37     C RETURN FIFF TO (XA,YA)
38     C
39     50 IK=IK+1
40     IF (IK.GT.25) GOTO 90
41     TS=0
42     XT=XA+DEL
43     YT=YA+DEL
44     FR=GRAND(SF,0.)
45     FD=GRAND(SD,0.)
46     PHT=ATAN(XT/YT)
    
```

```

47     IF (PHI.LT.0.) PHI=PHI+PI
48     PP=PI/2.-PHI
49     XI=PP*SIN (PHI) + PD*SIN (PP) + XT
50     YI=PP*COS (PHI) + PD*COS (PP) + YT
51     DUM1=D(XF,YF,XI,YI)
52     XR=0.
53     YB=0.
54
55     C   CCF IMPACT TRAVEL TIMES
56     C
57     DO 30 J=1,N
58     TI (J) =D (X (J) , Y (J) , XI , YI) /VS
59     SM (J) = (YT-YF (J)) / (XT-XF (J))
60     TH=ATAN (SM (J))
61     IF (TH.LT.0.) TH=TH+PI
62     C (J) =COS (TH)
63     S (J) =SIN (TH)
64     SM (J) =-1./SM (J)
65     30 CONTINUE
66     K (1) =TI (1) -TR (1)
67     K (2) =TI (2) -TR (2)
68     DO 20 I=3, N
69     DO 20 L=1, 2
70     T=TI (I) -TP (I) +DUM1*GRAND (CF,C.) /V+K (L)
71     20 B (T,L) =YT-T*VS*S (I) -SM (T) *X+SM (T) *T*AVE*C (T)
72     DO 60 I=4, M
73     DO 70 I=1, 2
74     X1 (L) = (B (I,L) -B (I-1, L)) / (SM (I-1) -SM (I))
75     Y1 (L) =SM (I-1) *X1 (L) +B (I-1, L)
76     X2 (L) = (B (I+1, L) -B (I, L)) / (SM (I) -SM (I+1))
77     Y2 (L) =SM (I) *X2 (L) +B (I, L)
78     70 CONTINUE
79     IF (X1 (2) .EQ. X1 (1)) GOTO 80
80     SMI = (Y1 (2) -Y1 (1)) / (X1 (2) -X1 (1))
81     IF (X2 (2) .EQ. X2 (1)) GOTO 40
82     SMIT = (Y2 (2) -Y2 (1)) / (X2 (2) -X2 (1))
83     XTEM = (Y1 (1) -SMI*X1 (1) -Y2 (1) +SMIT*X2 (1)) / (SMIT-SMI)
84     YTEM =SMI*XTEM+Y1 (1) -SMI*X1 (1)
85     GOTO 55
86     80 XTEM=X1 (2)
87     IF (X2 (2) .EQ. X2 (1)) GOTO 90
88     SMIT = (Y2 (2) -Y2 (1)) / (X2 (2) -X2 (1))
89     YTEM =SMIT*XTEM+Y2 (1) -SMIT*X2 (1)
90     GOTO 55
91     40 XTEM=X1 (2)
92     IF (X1 (2) .EQ. X1 (1)) GOTO 90
93     SMI = (Y1 (2) -Y1 (1)) / (X1 (2) -X1 (1))
    
```

```

94      YTFM=SMI*XTFM+V1(1)-SMY*X1(1)
95      55 XB=XB+XTFM
96      60 YB=YB+YTEM
97      XR=XB/(M-3)
98      YR=YB/(M-3)
99      YA=(XA*(IK-1)+XR)/IK
100     YA=(YA*(IK-1)+YR)/IK
101     DUM2=D(XF,YF,XA,YA)
102     IF (DUM2.LT.50.) GOTO 90
103     IF (DUM2.IT.1.85) GOTO 50
104     TK=26
105     90 THIST(IF)=THIST(IK)+1
106     WRITE (6,200) ((I,THIST(I)),I=1,26)
107     RETURN
108     900 STOP 1
109     100 FORMAT (I3)
110     150 FORMAT (12F10.4)
111     200 FORMAT (2I6)
112     250 FORMAT ('ACTUAL SOURCE=',F8.1,',',F8.1,', FIRST ESTIMATE=',F8.1
113     $,',',F8.1/' SIGMA S=',F8.3,', SIGMA T=',F8.3,', SIGMA R=',F8.3
114     $,', SIGMA D=',F8.3/' ACTUAL VELOCITY=',F8.3,', VELOCITY ESTIMATE='
115     $, F8.3)
115.25  450 FORMAT (2F10.3)
116     END
    
```

APPENDIX B

TABLE B.1
Coordinates (x,y) Acoustic/Seismic Travel Times. Sensors 1 through 9.

Event	Coordinates (x,y)	Acoustic/Seismic Travel Times. Sensors 1 through 9.								
128	2883,8856	897 112	937 113	944 113	1127 116	1282 136	1454 160	1645 175	1820	1992
129	2932,8774	876 135	909 135	923 135	1072 131	1222 139	1391 153	1575 207	1748 192	1919
130	3025,8752	804 124	833 124	820 124	995 132	1145 142	1316 202	1507 184	1681	1854
131	3014,8826	796 124	832 125	833 125	1018 133	1176 148	1351	1548	1726	1902
132	3046,8846	761 126	800 120	807 118	996 132	1158 141	1337	1539	1721	1898
133	3107,8801	770	802	797	983	1172	1319	1521	1701	1877
<u>Mortar Firings</u>										
134	3130,8894	680 121	721 118	745 119	937 130	1109	1292	1503	1690	1876
137	2957,8867	836 131	876 130	887 130	1022 142	1232 152	1407	1604	1781	1956
155	3253,8913	585	645	698	906	1090				
156	3253,8913	587	647	700	907	1090				
159	3253,8913	585	644	696	904	1088				
164	3006,8875	792	833	846	1036	1201				

TABLE B.1

Event	Mortar Firings Coordinates (x,y)	Acoustic, Seismic Travel Times. Sensors 1 through 9.					
		1066	1033	933	1057	1141	172
176	2779,8412	155	149	141	146	155	175
177	3147,8366	619	777	717	615	841	988
		137	122	113	122	131	119
178	3230,8484	931	885	790	914	1006	1140

TABLE B.2
 SHOT COORDINATES, ACOUSTIC TRAVEL TIMES, AND SFISMIC TRAVEL TIMES.
 Twenty Nine Palms, 1.5km Site. Travel times given in
 number of samples with sampling rate equal to 300 samples/second

Event	Coordinates (x,y)	Acoustic/Seismic Travel Times. Sensors 1 through 9.																	
		1672	1564	1481	1427	1405	1421	1469	1549	N/A	1652	1539	1448	1386	1357	1369	1411	1487	1588
22	1000,1540	1672	1564	1481	1427	1405	1421	1469	1549	N/A	358	325	309	308	316	316	337	343	352
23	1050,1500	1652	1539	1448	1386	1357	1369	1411	1487	1588	1620	1499	1400	1330	1292	1291	1325	1393	1486
24	1125,1500	299	254	234	237	239	238	251	272	274	299	254	234	237	239	238	251	272	274
63	750,1500	N/A	1414	1358	1338	1356	1409	1492	1607	1738	N/A	259	246	241	243	243	256	256	281
64	875,1500	N/A	1437	1367	1331	1331	1363	1436	1540	N/A	N/A	228	222	222	237	242	264	267	297
65	905,1500	N/A	1449	1376	1334	1329	1362	1428	1526	N/A	N/A	216	205	204	219	219	232	246	297
66	911.6,1411.6	N/A	1361	1281	1234	1227	1259	1326	1328	N/A	N/A	240	228	226	244	234	254	267	297
67	1088.4,1411.6	N/A	1494	1393	1319	1281	1282	1319	1394	N/A	N/A	209	198	191	209	203	223	226	297
68	1088.4,1588.4	N/A	1589	1497	1432	1400	1404	1441	1512	N/A	N/A	245	233	227	240	227	235	236	297
69	1250,1500	N/A	1595	1482	1394	1333	1318	1335	1389	N/A	N/A	257	236	236	251	252	242	257	297
70	1000,1375	N/A	1380	1287	1227	1204	1222	1278	1372	N/A	N/A	231	219	213	231	219	234	240	297
71	1000,1250	N/A	1196	1100	1034	1012	1034	1094	1193	N/A	N/A	238	218	208	232	213	238	241	297

Coordinates		Acoustic/Seismic Travel Times. Sensors 1 through 9.											
Event	(x,y)												
72	1000,1250	N/A	1193	1094	1029	1007	1007	1007	1089	1188	N/A		
		N/A	230	205	193	196	197	197	223	236	N/A		
73	911.6,1638.4	N/A	1547	1477	1438	1433	1459	1517	1605	N/A			
		N/A	252	243	246	252	266	258	277	N/A			
74	1000,1625	N/A	1558	1480	1428	1411	1428	1476	1555	N/A			
		N/A	256	241	244	253	256	253	268	N/A			
75	1000,1750	N/A	1678	1601	1553	1536	1549	1592	1669	N/A			
		N/A	297	262	303	279	273	276	288	N/A			
76	1250,1750	N/A	294	288	288	300	255	276	285	N/A			
77	750,1750	N/A	1614	1560	1536	1545	1581	1647	1742	N/A			
		N/A	269	260	281	281	284	290	302	N/A			
<u>Mortar Firings</u>													
42	1000,1540	1616	1506	1423	1368	1349	1367	1419	1505	1613			
44	1000,1540	1613	1506	1423	1371	1353	1372	1423	1508	1620			
46	1000,1540	1597	1495	1413	1358	1336	1350	1397	1481	N/A			

TABLE B.3
SENSOR COORDINATES
SENSOR POSITIONS 1 THROUGH 9
(x,y)
TWENTY NINE PALMS

(0,0)
(250,0)
(500,0)
(750,0)
(1000,0)
(1250,0)
(1500,0)
(1750,0)
(2000,0)

TABLE B.4
SENSOR COORDINATES
SENSOR POSITIONS 1 THROUGH 9
(x,y)
CAMP PENDLETON

(3906,8862)

(3911,8609)

(3817,8380)

(3946,7905)

(3967,7656)

(3909,7386)

(3882,7037)

(3831,6793)

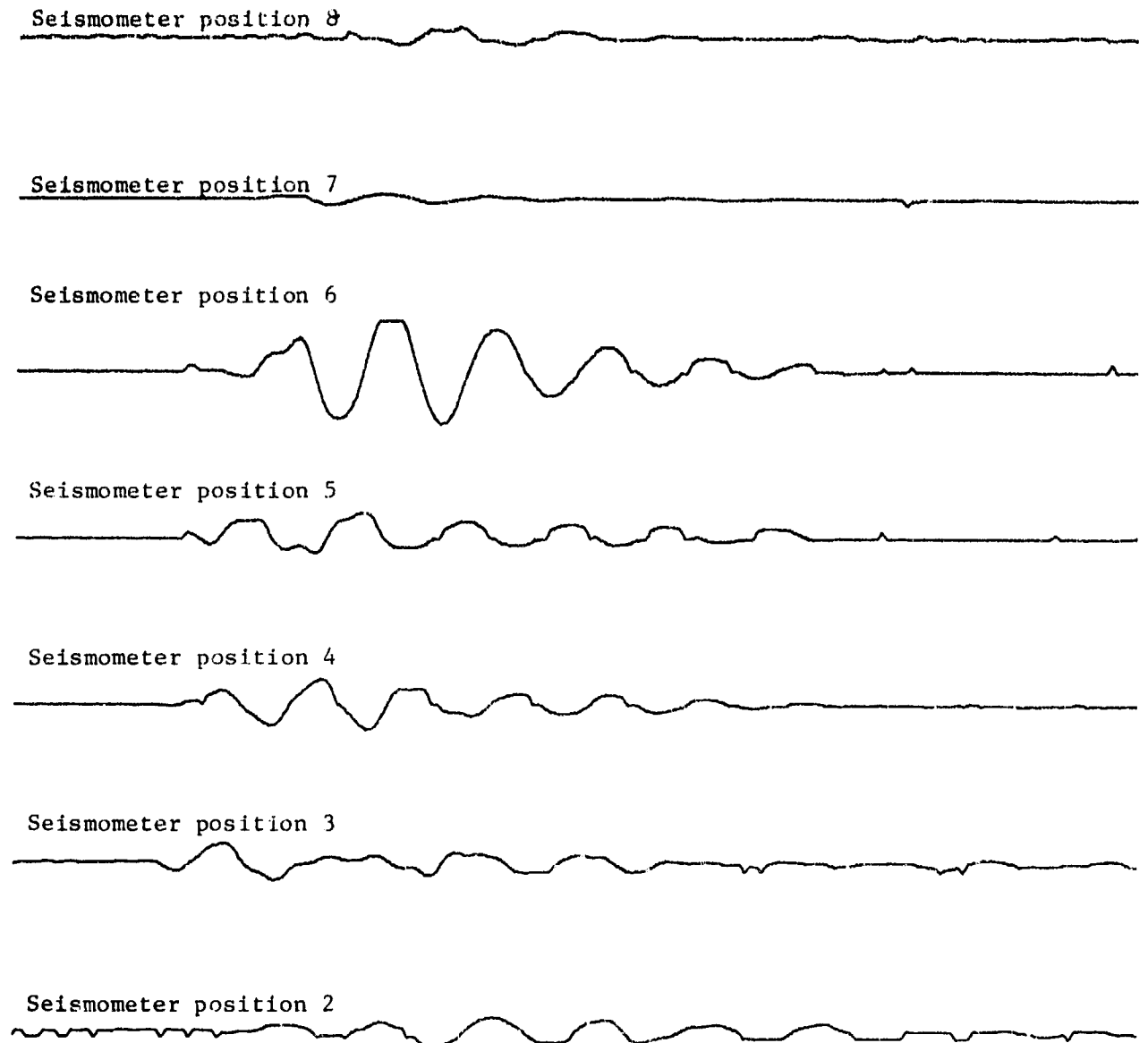


FIGURE B.1. VERTICAL AXIS SEISMOGRAMS FROM EXPLOSION EVENT 23
TWENTY NINE PALMS, 1.5 km Site, Scale 10 in/sec

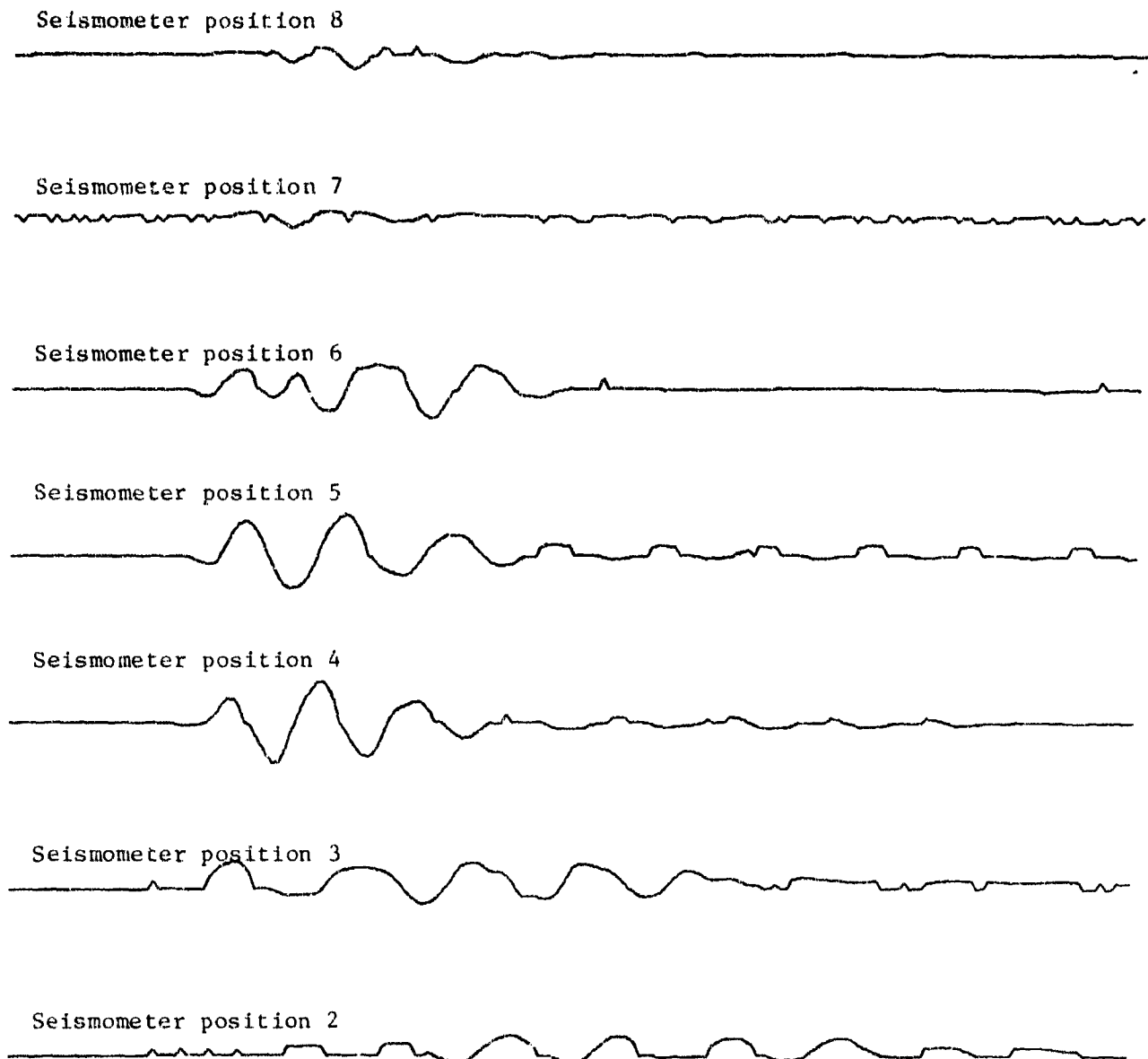


FIGURE B.2. VERTICAL AXIS SEISMOGRAMS FROM EXPLOSION EVENT 24,
 TWENTY NINE PALMS, 1.5 km Site, Scale 10 in/sec

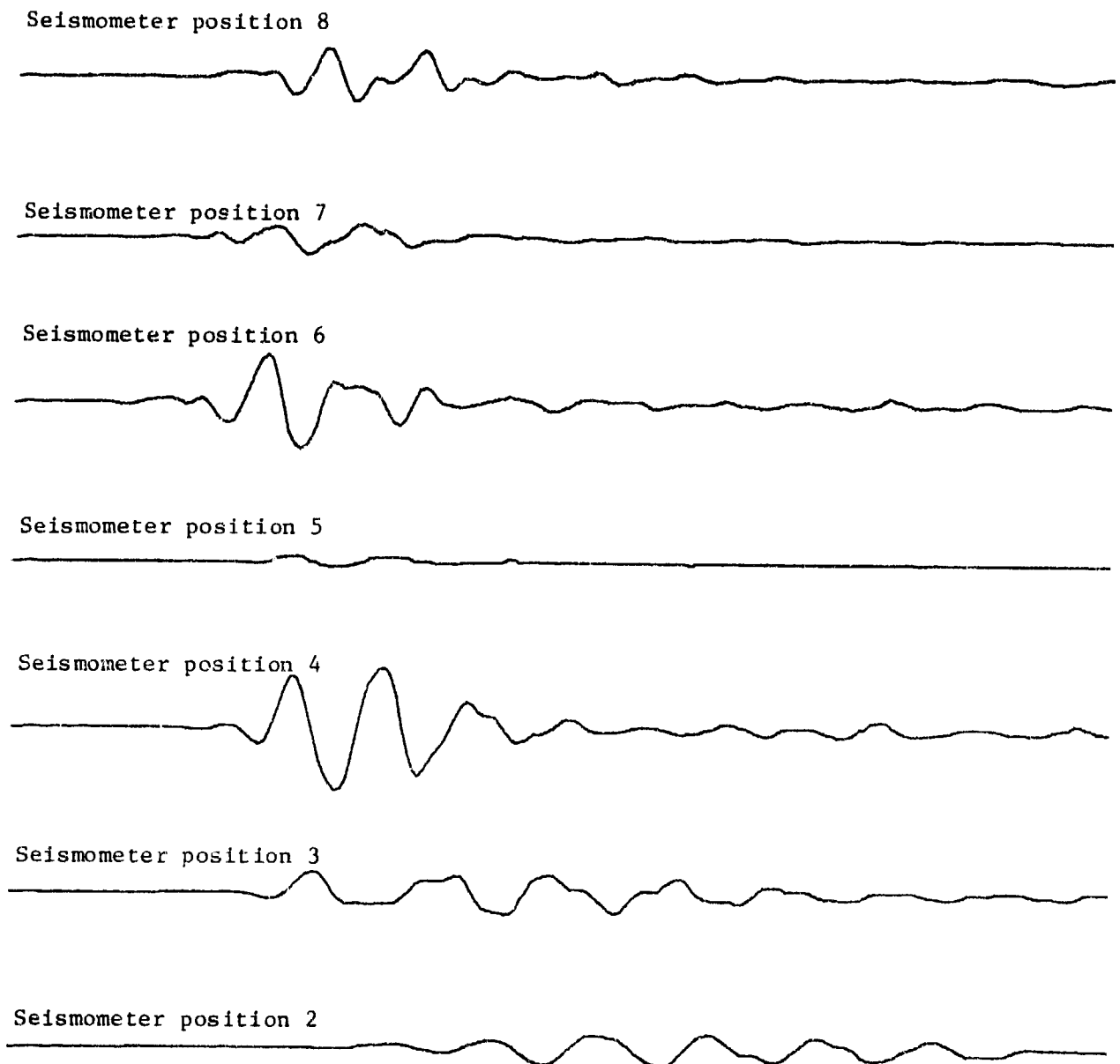


FIGURE B.3. VERTICAL AXIS SEISMOGRAMS FROM EXPLOSION EVENT 69,
TWENTY NINE PALMS, 1.5 km Site, Scale 10 in/sec

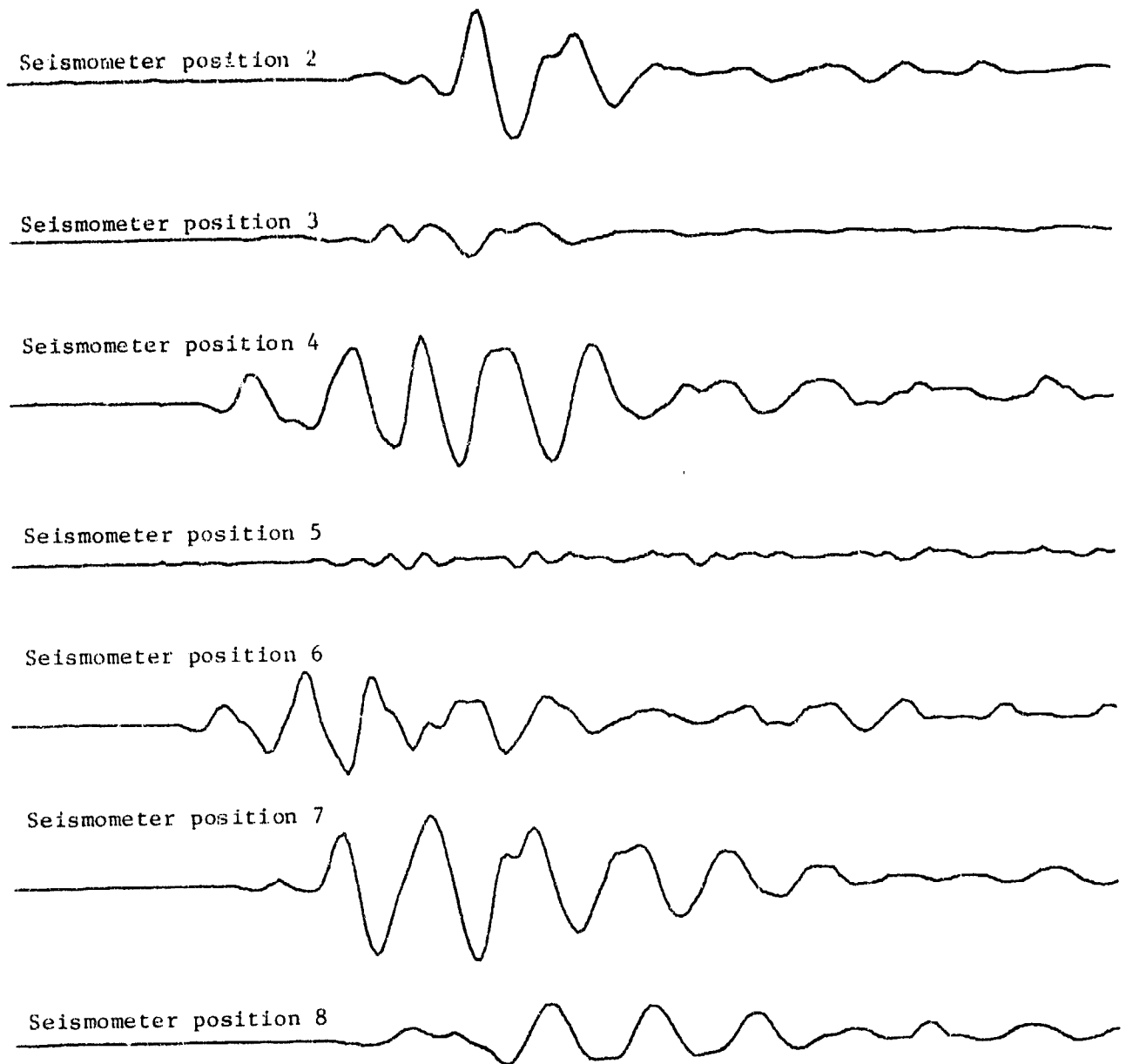


FIGURE B.4. VERTICAL AXIS SEISMOGRAMS FROM EXPLOSION EVENT 71
 TWENTY NINE PALMS, 1.5 km Site, Scale 10 in/sec

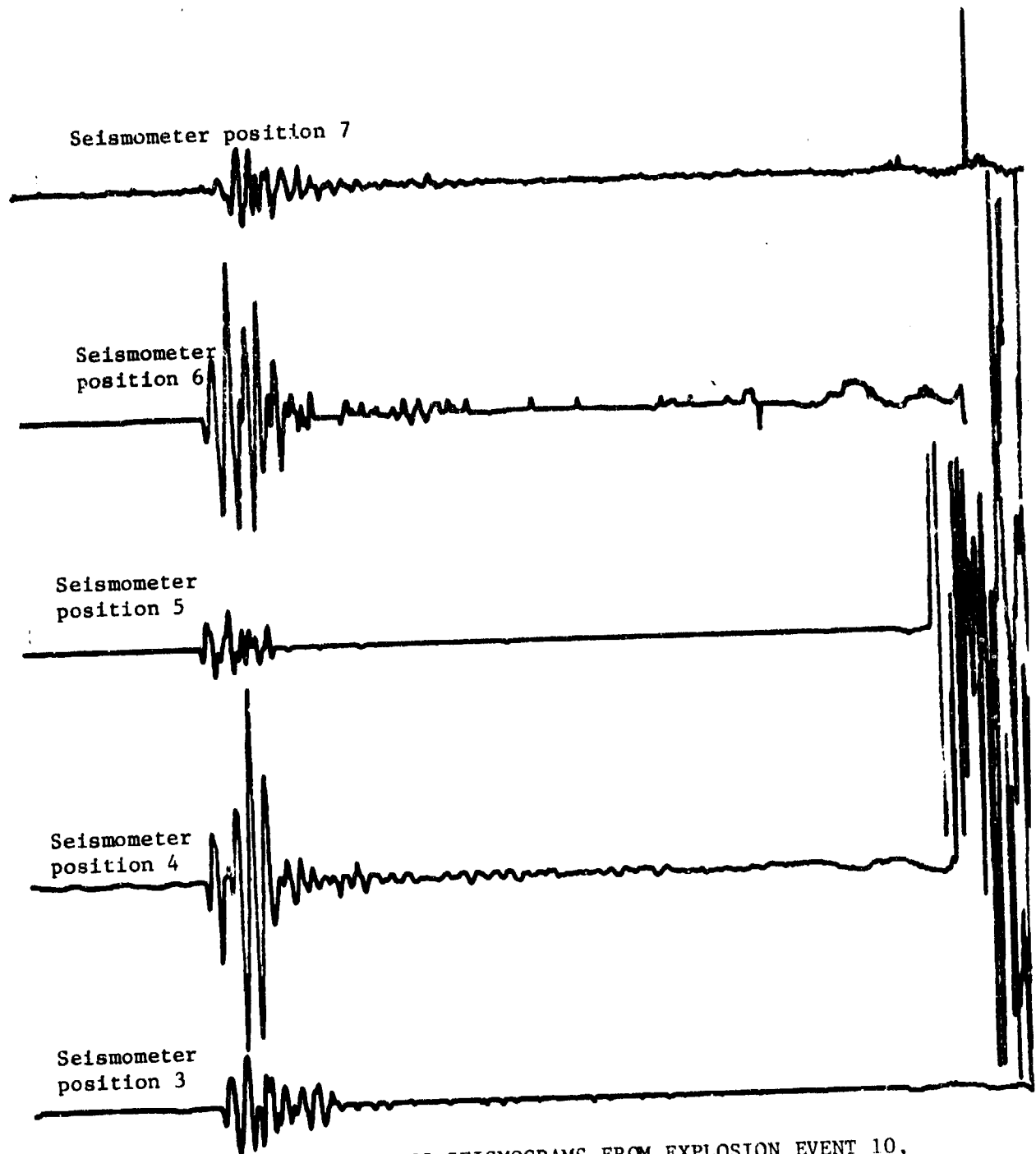


FIGURE B.5. VERTICAL AXIS SEISMOGRAMS FROM EXPLOSION EVENT 10, TWENTY NINE PALMS, 1.0 km Site, Scale 2 in/sec

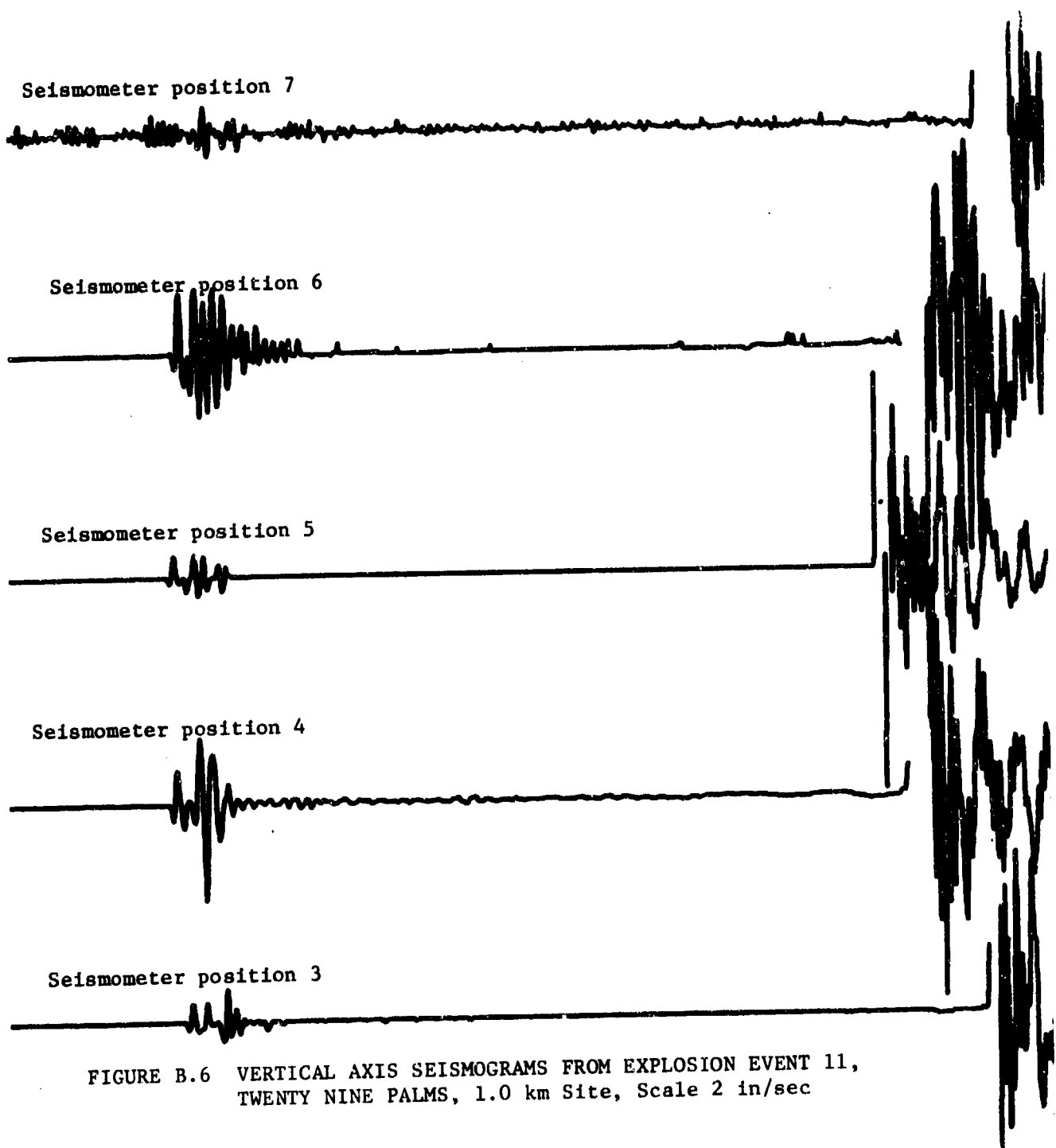
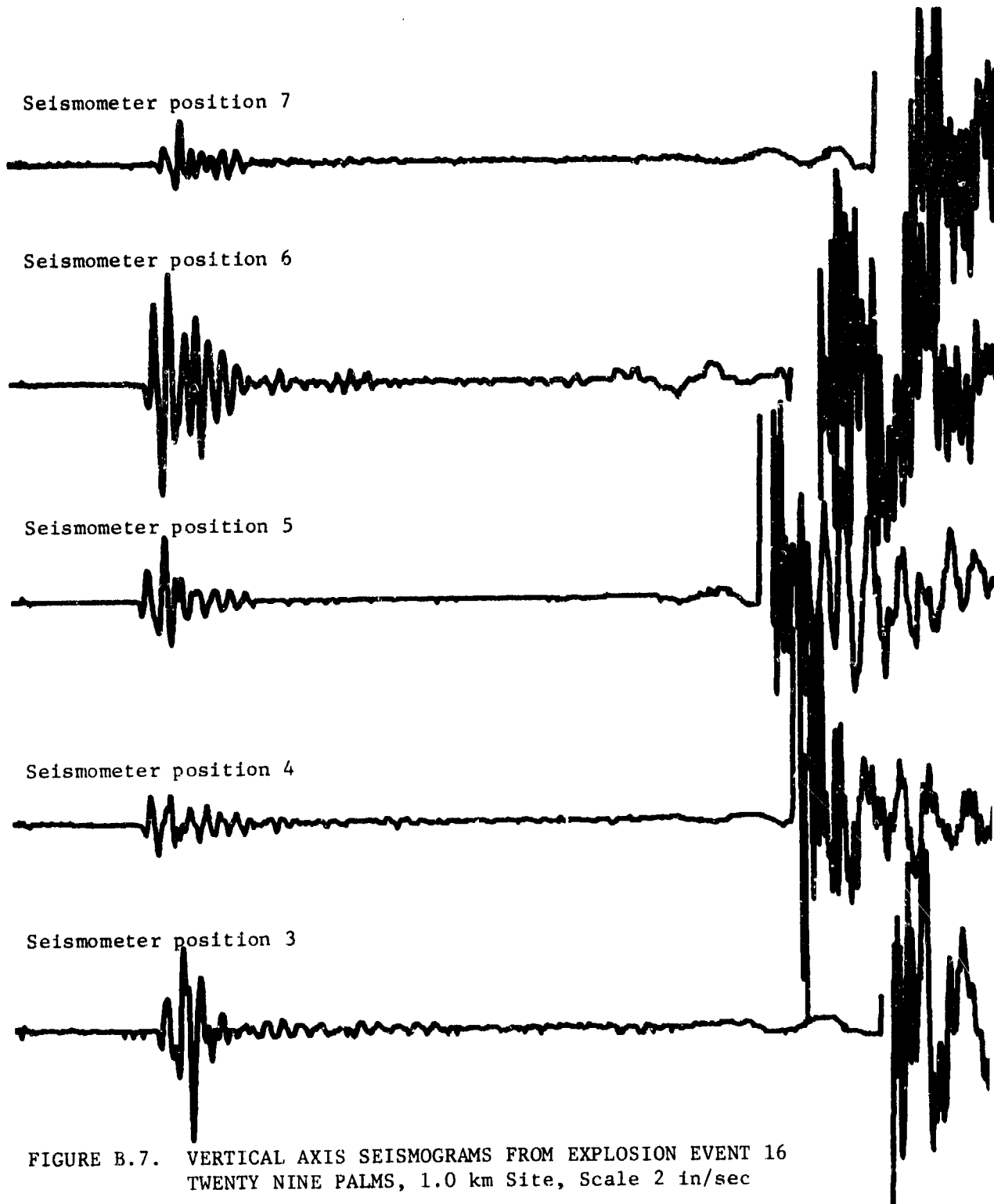


FIGURE B.6 VERTICAL AXIS SEISMOGRAMS FROM EXPLOSION EVENT 11,
TWENTY NINE PALMS, 1.0 km Site, Scale 2 in/sec



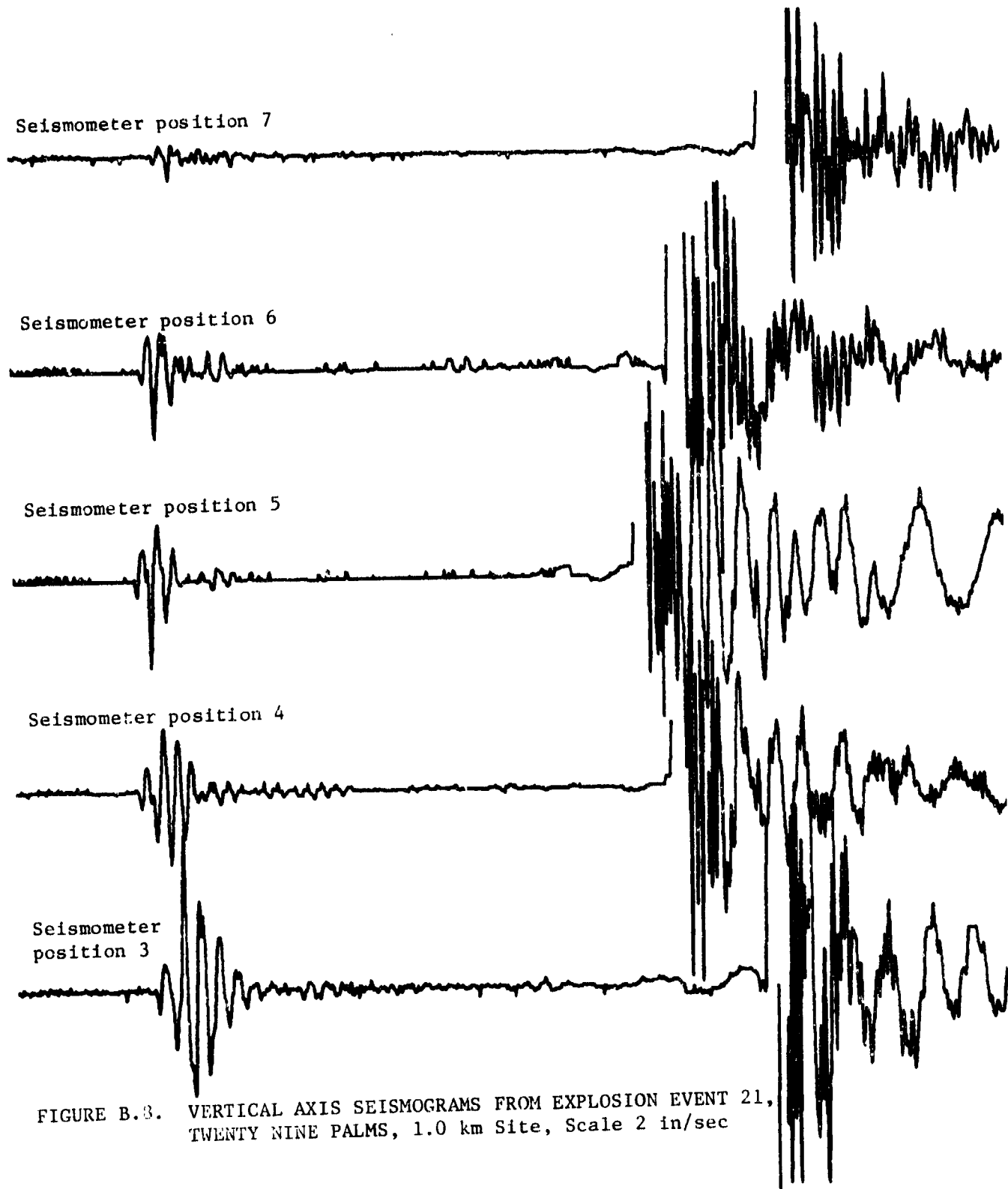


FIGURE B.3. VERTICAL AXIS SEISMOGRAMS FROM EXPLOSION EVENT 21, TWENTY NINE PALMS, 1.0 km Site, Scale 2 in/sec

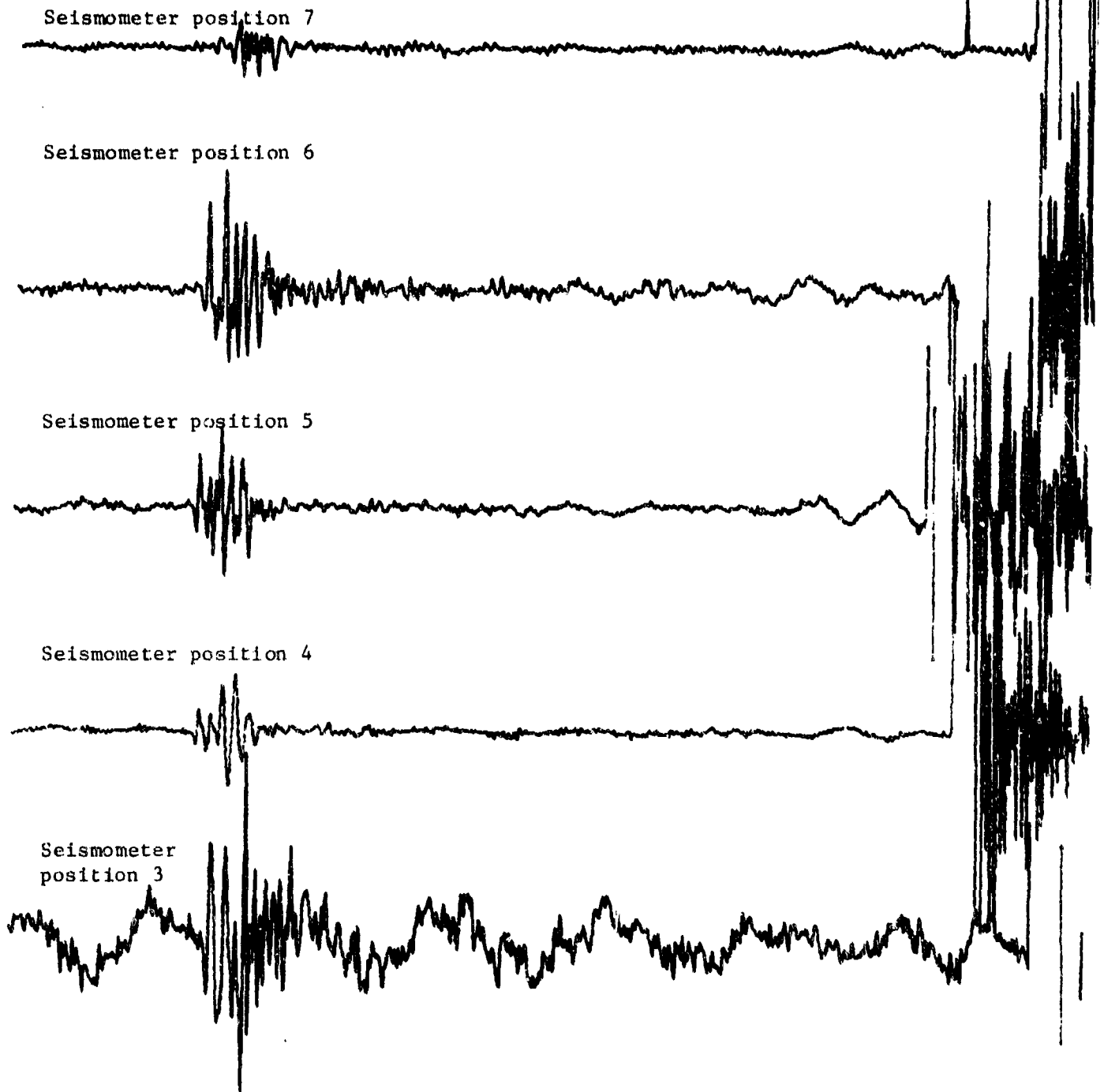


FIGURE B.9. VERTICAL AXIS SEISMOGRAMS FROM MORTAR RECOIL EVENT 38,
 TWENTY NINE PALMS, 1.0 km Site, Scale 2 in/sec

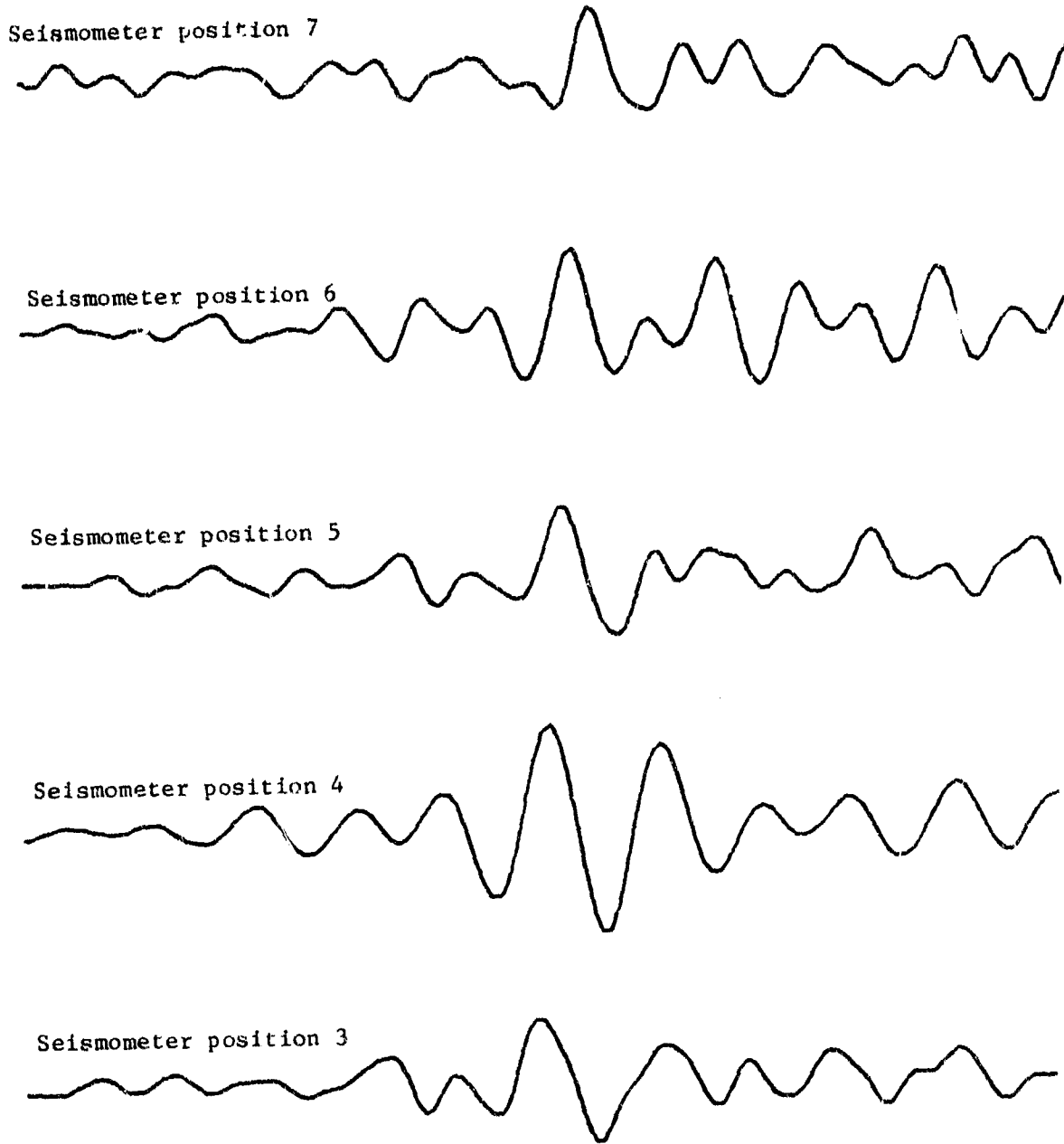


FIGURE B.10. CORRELATION FUNCTIONS, EVENT 11 VERSUS EVENT 10,
 TWENTY NINE PALMS, 1.0 km Site, Scale 15 in/sec

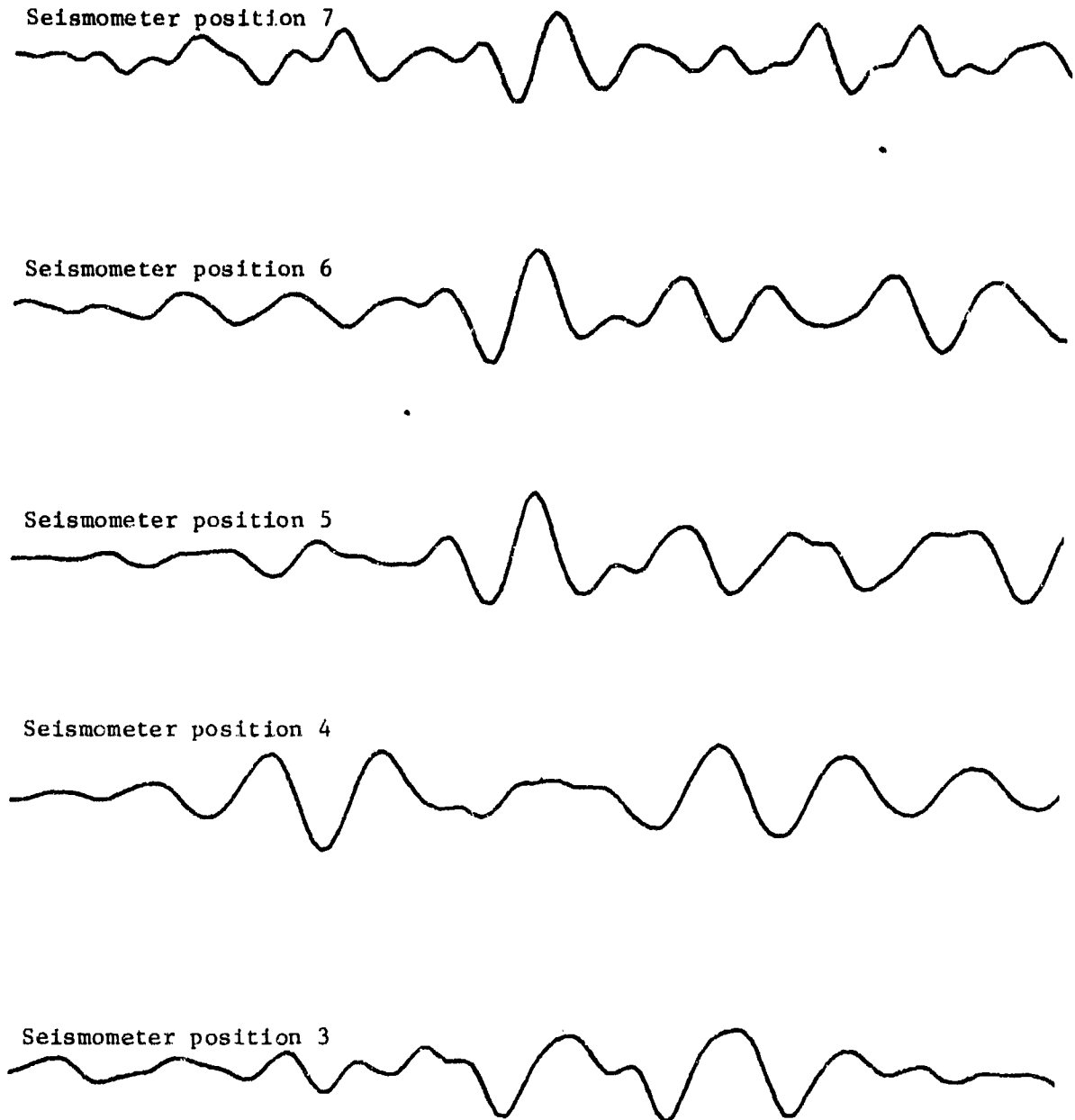


FIGURE B.11. CORRELATION FUNCTIONS, EVENT 11 VERSUS EVENT 16,
TWENTY NINE PALMS, 1.0 km Site, Scale 15 in/sec

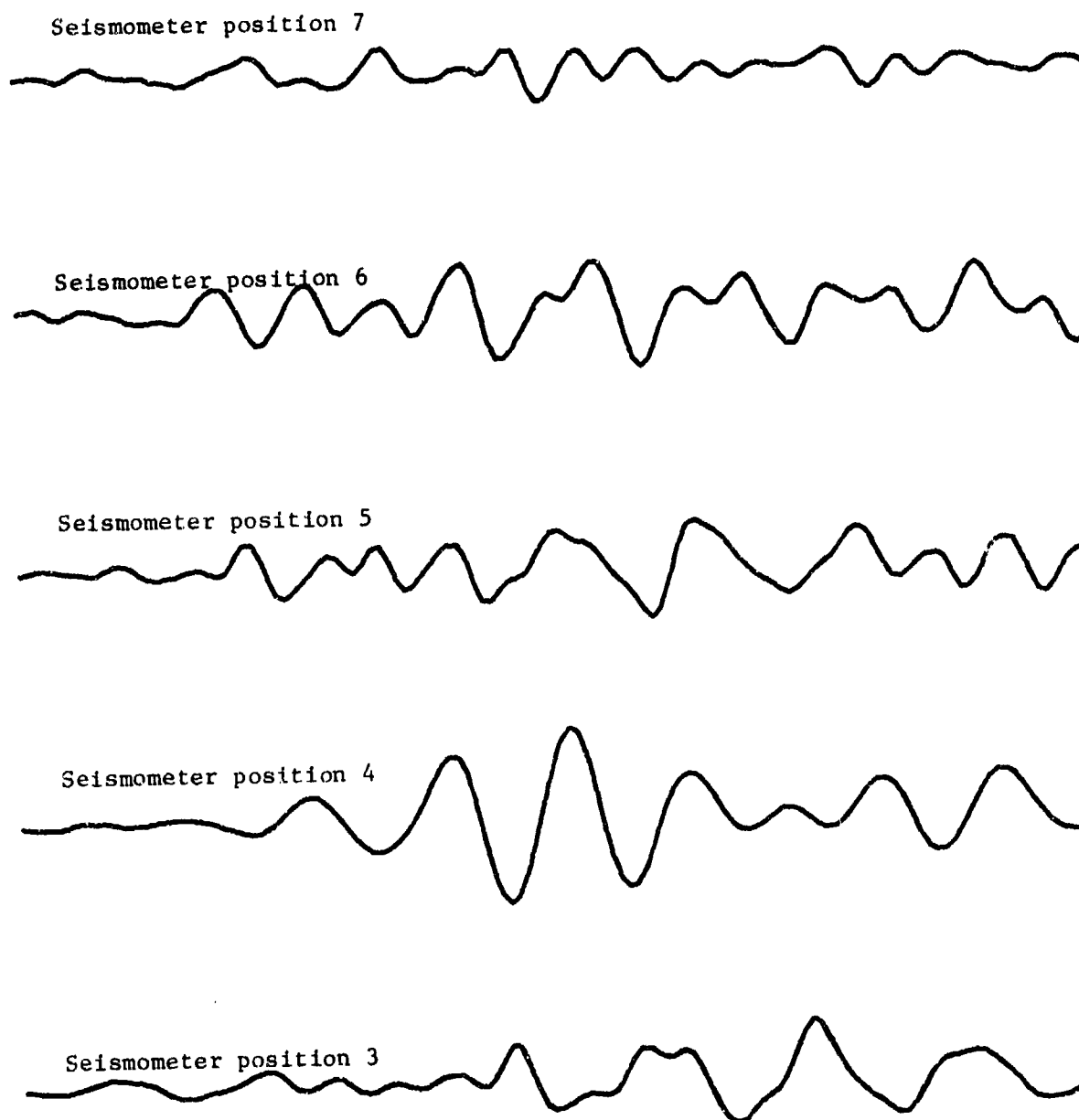


FIGURE B.12. CORRELATION FUNCTIONS, EVENT 11 VERSUS EVENT 21,
 TWENTY NINE PLAMS, 1.0 km Site, Scale 15 in/sec

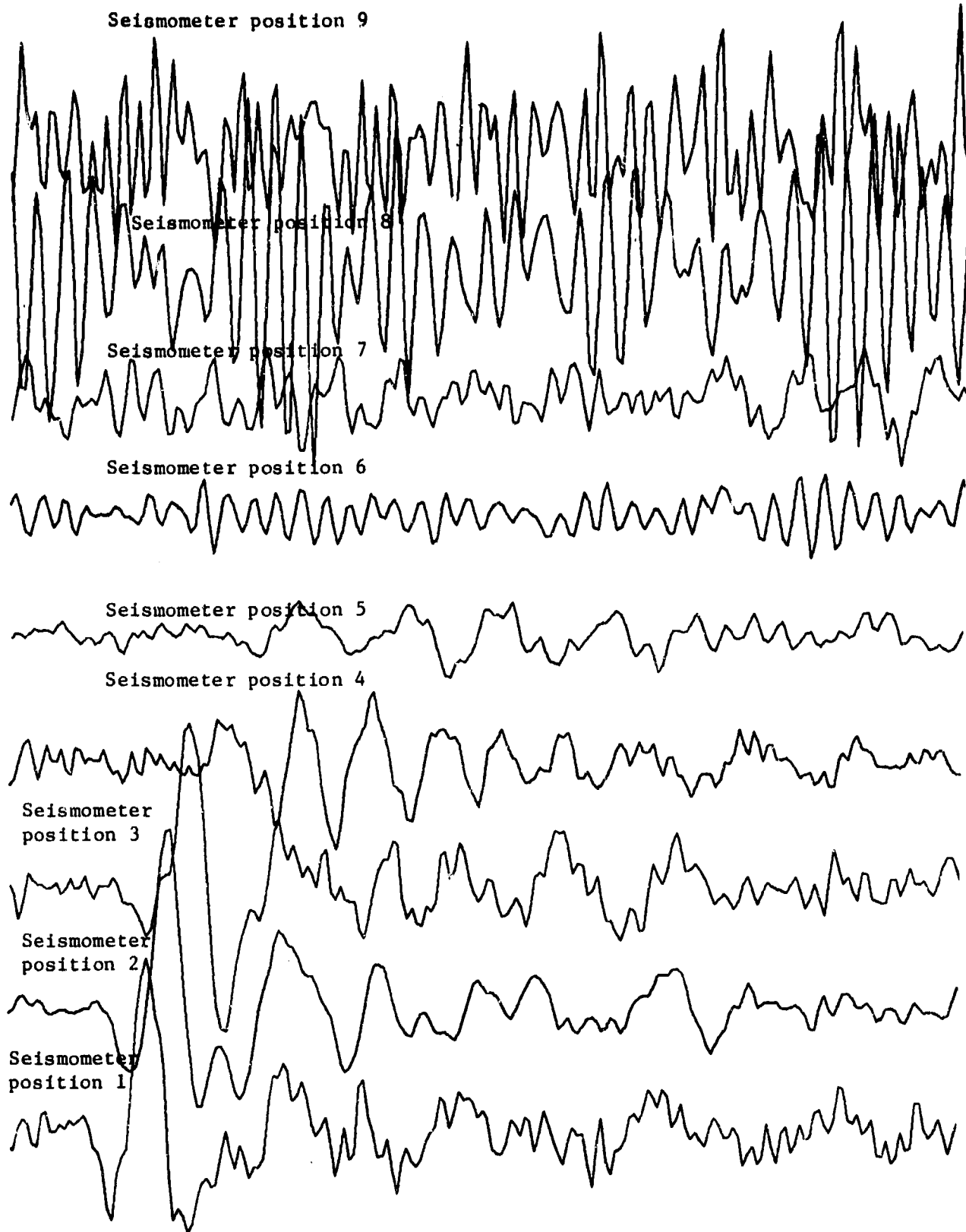


FIGURE B.13. VERTICAL AXIS SEISMOGRAMS FROM EXPLOSION EVENT 104, CAMP PENDLETON, SCALE 10 in/sec

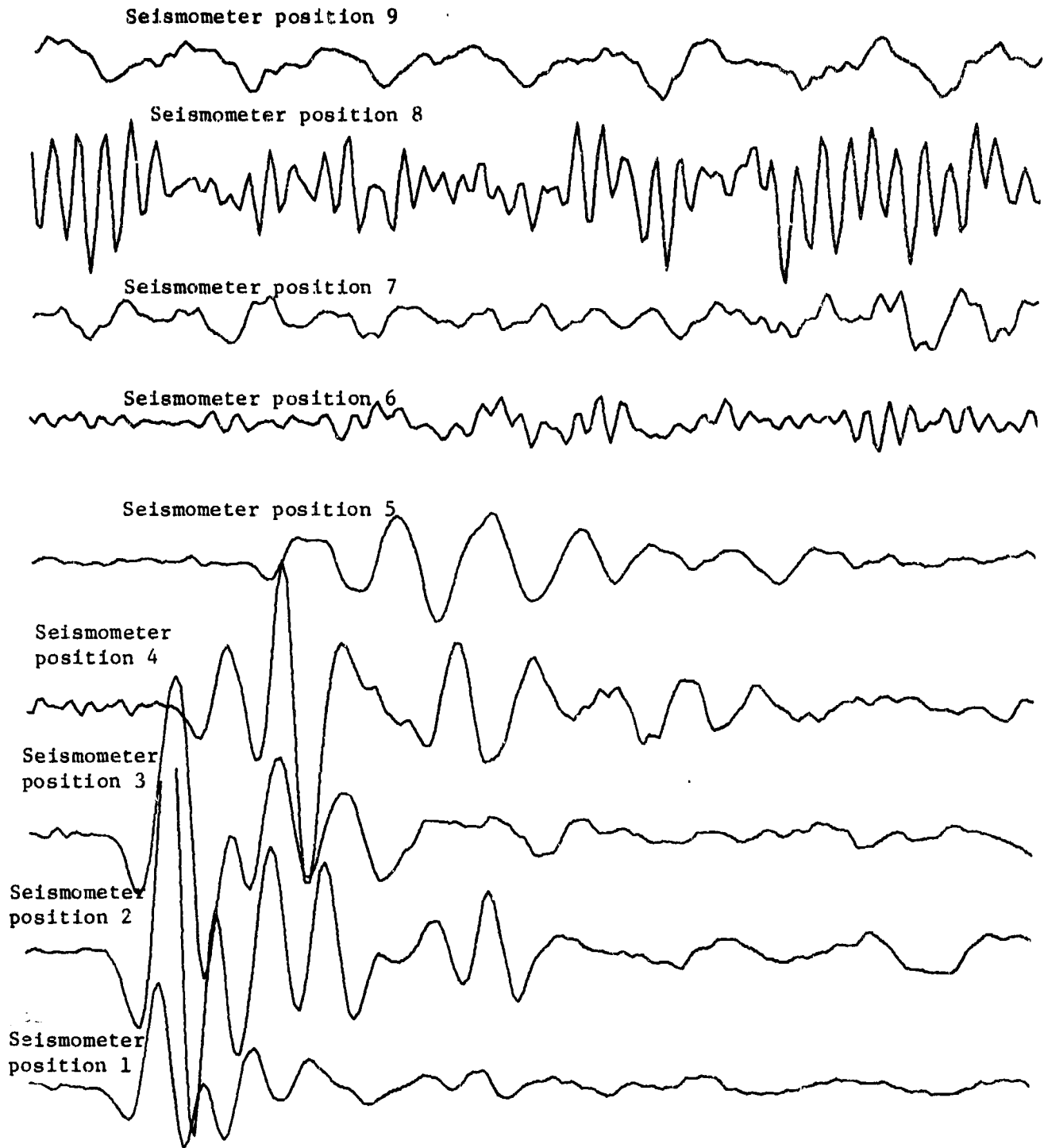


FIGURE B.14. VERTICAL AXIS SEISMOGRAMS FROM EXPLOSION EVENT 114, CAMP PENDLETON, SCALE 10 in/sec

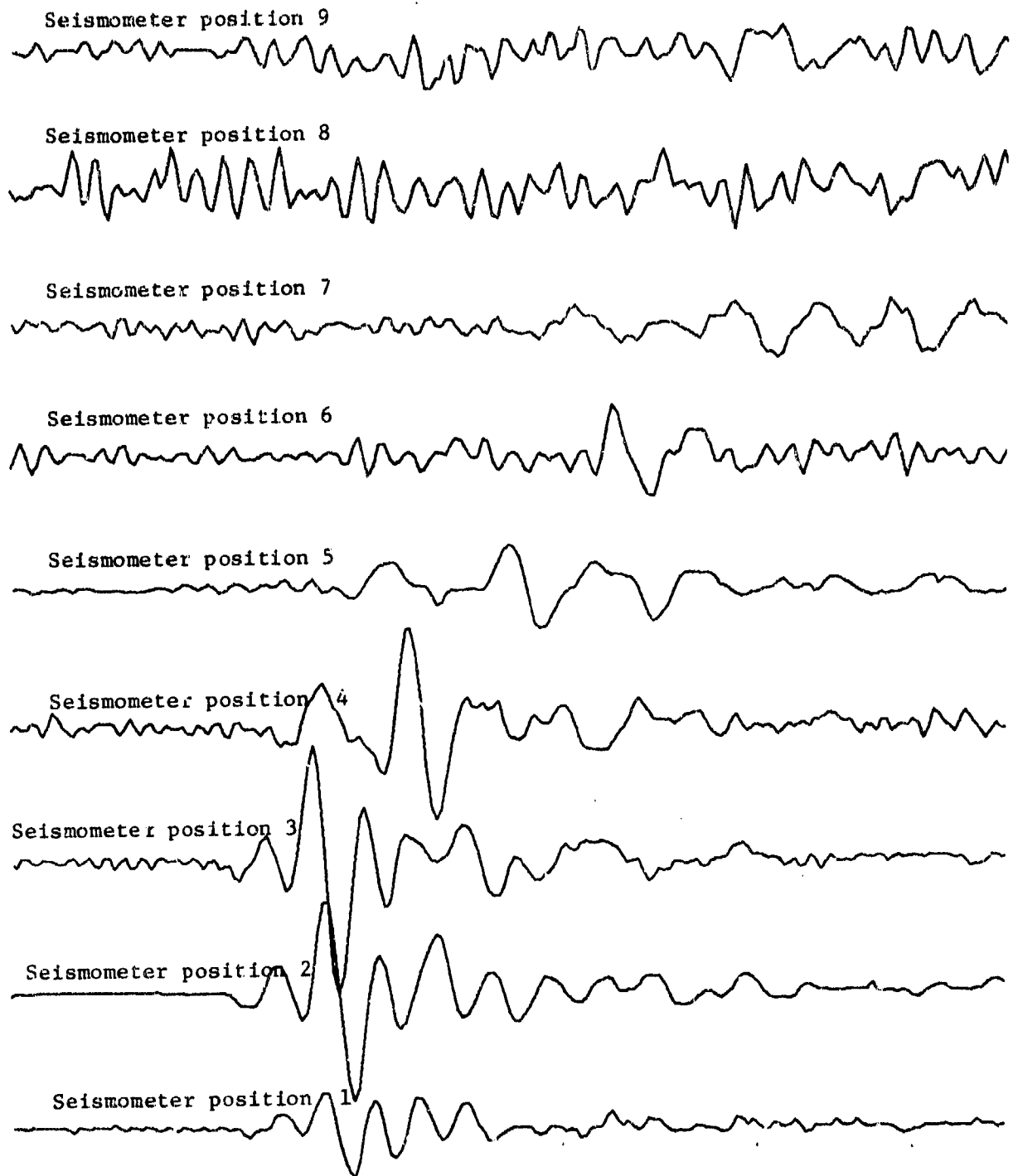


FIGURE B.15. VERTICAL AXIS SEISMOGRAMS FROM EXPLOSION EVENT 130, CAMP PENDLETON, SCALE 10 in/sec

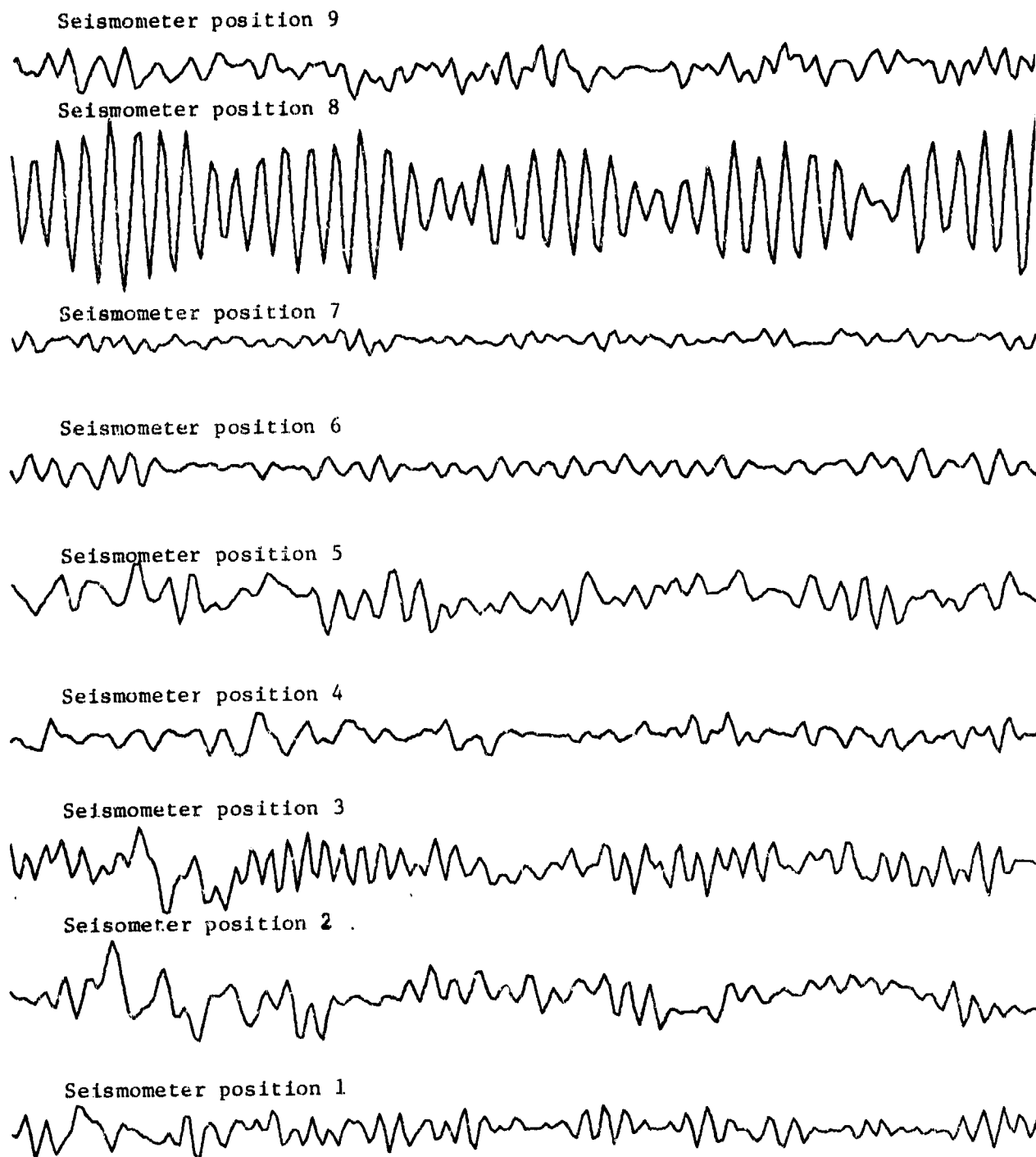


FIGURE B.16. VERTICAL AXIS SEISMOGRAMS FROM MORTAR RECOIL EVENT 155, CAMP PENDLETON, SCALE 10 in/sec

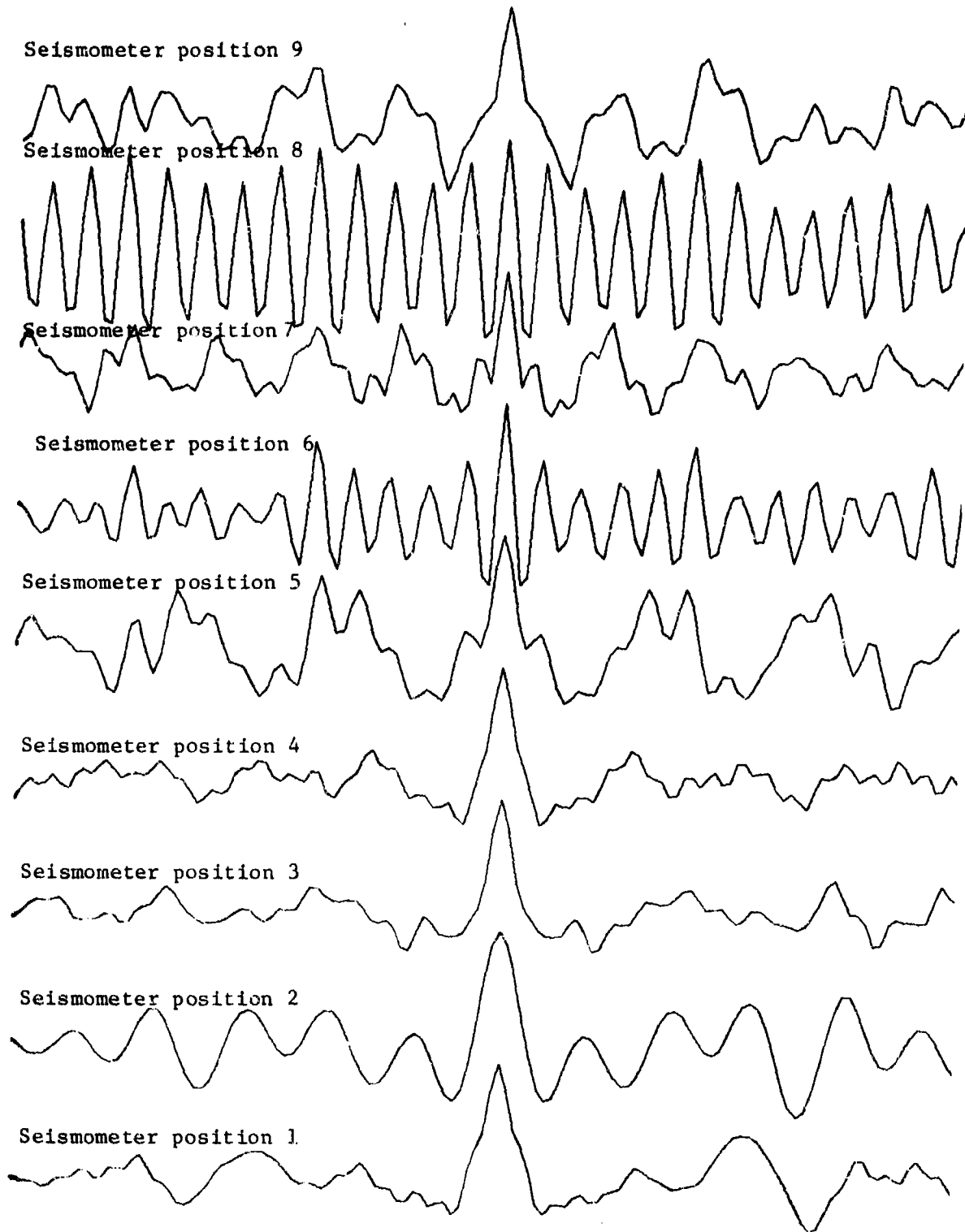


FIGURE B.17. AUTO-CORRELATION FUNCTIONS, EXPLOSION EVENT 103, CAMP PENDLETON, SCALE 15 in/sec

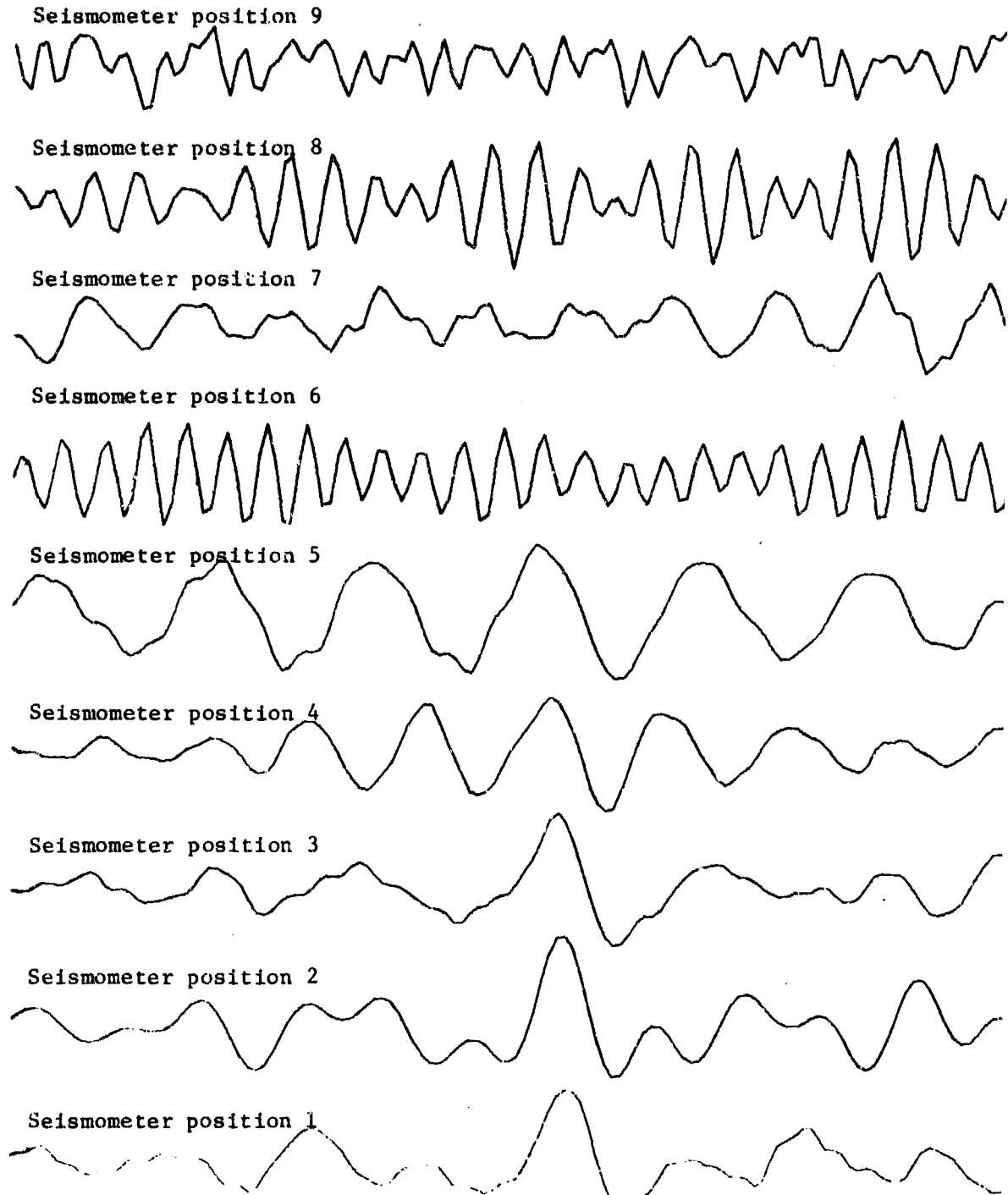
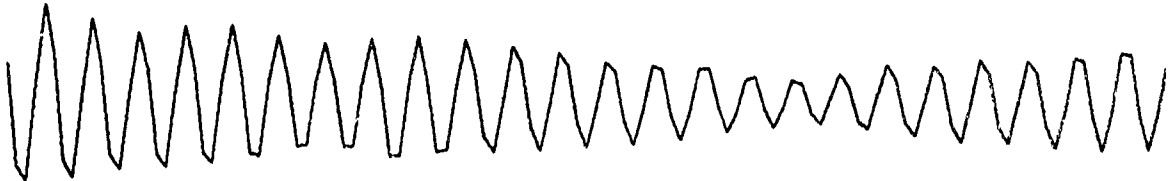


FIGURE B.18. CORRELATION FUNCTIONS, EVENT 103 VERSUS EVENT 104
CAMP PENDLETON, SCALE 15 in/sec

Seismometer position 9



Seismometer position 8



Seismometer position 7



Seismometer position 6



Seismometer position 5



Seismometer position 4



Seismometer position 3



Seismometer position 2



Seismometer position 1



FIGURE B.19. CORRELATION FUNCTIONS, EVENT 103 VERSUS EVENT 114
CAMP PENDLETON, SCALE 15 in/sec

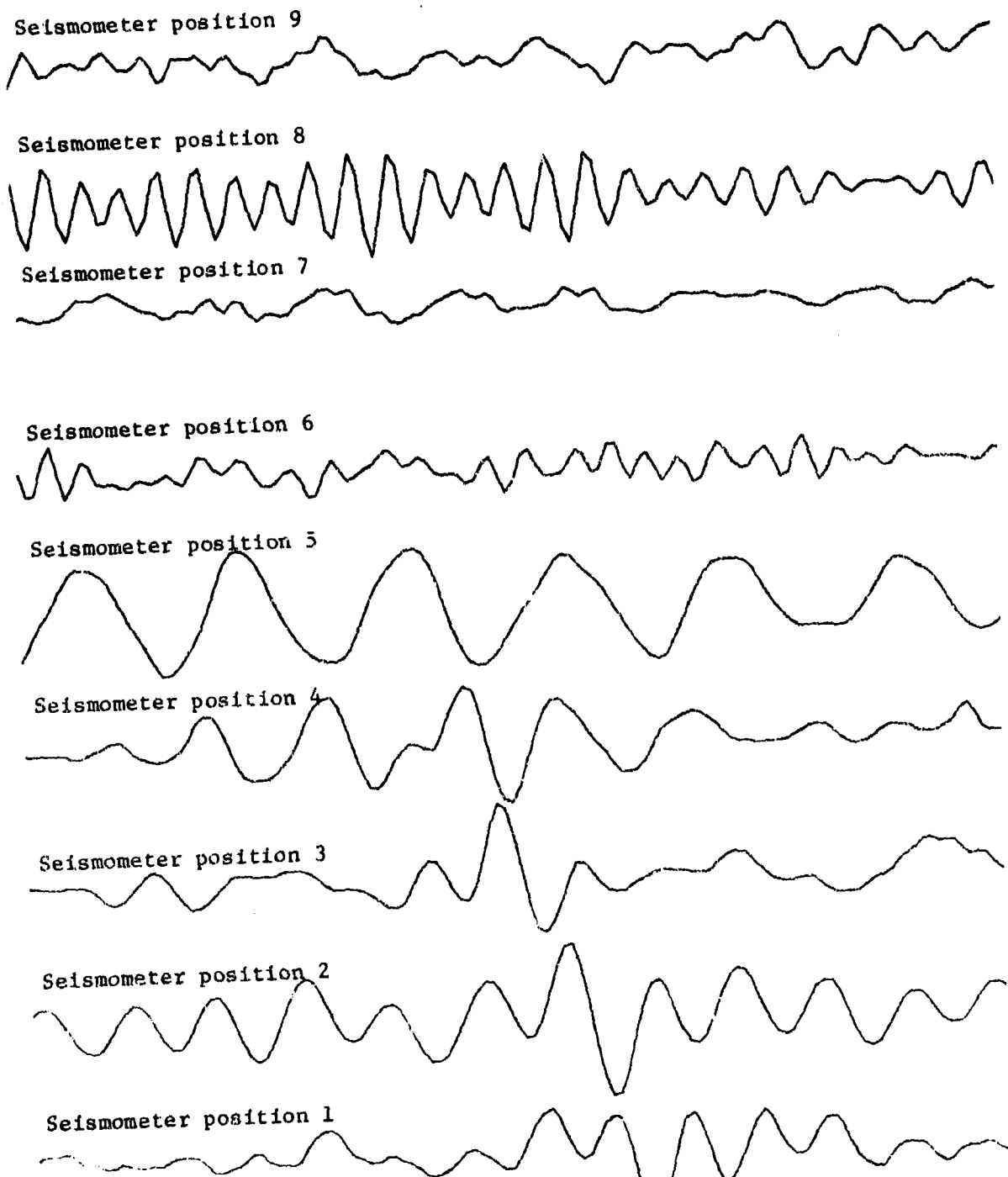


FIGURE B.20. CORRELATION FUNCTIONS, EVENT 103 VERSUS EVENT 130
CAMP PENDLETON, SCALE 15 in/sec